Biomechanics and Biaxial Mechanical Stimulation of Self-Assembly Tissue Engineered Blood Vessels

A Thesis
Presented to
The Academic Faculty

by

Michael T. Zaucha

In Partial Fulfillment
of the Requirements for the Degree
Doctor of Philosophy in the
School of Mechanical Engineering

Georgia Institute of Technology
May 2011

Biomechanics and Biaxial Mechanical Stimulation of Self-Assembly Tissue Engineered Blood Vessels

Approved by:

Dr. Rudolph L. Gleason, Jr., Advisor
School of Mechanical Engineering
School of Biomedical Engineering
Georgia Institute of Technology

Dr. J. Brandon Dixon
School of Mechanical Engineering
Georgia Institute of Technology

Dr. Alexander Rachev
School of Mechanical Engineering
Georgia Institute of Technology

Dr. Chrysanthi Williams
Electroforce Systems Group
Bose Corporation

Dr. W. Robert Taylor
School of Medicine
Emory University

Date Approved: March 23, 2011

To my parents, Tom and Cathy,

the rest of my family,

and all of my friends

ACKNOWLEDGEMENTS

There are numerous people who I would like to thank for their support in achieving this milestone. First, I would like to thank my advisor, Dr. Rudolph Gleason, Jr. for his support over the past several years. Without his guidance and passion, none of this work would have been possible. Additionally, I would like to Dr. Alexander Rachev for continuing to challenge me and help in refining my technical skills. I must also thank the other members of my thesis committee for reviewing my work, providing critical feedback and providing invaluable guidance in the completion of this work: Dr. Robert Taylor, Dr. Sandy Williams and Dr. J. Brandon Dixon.

To my collaborators from Laboratoire d'Organogénèse Expérimentale in Quebec City, Canada, thank you for working with me and being able to provide materials which are the central focus of this work. Special thanks must go to Dr. Robert Gauvin for working closely with me to develop methodologies and results. Our friendship that has developed will be forever cherished.

I would also like to thank many people who provided technical assistance along the way. Thank you to all of the other members of the Gleason lab who have challenged me to critically review my work and provided valuable insights. To John Graham and Louis Boulanger at the machine shop, thank you for spending time to make and re-make much of the hardware which were critical in this work.

My deep appreciation goes out to my family. To my parents, Tom and Cathy, thank you for always being there to listen and continuing to believe in me. You have provided me every opportunity for which I could have ever asked and for this I am

forever grateful. To my extended family, thank you for listening and helping me keep life in perspective.

Lastly, I would like to thank all my friends who provided a support structure over the past few years. I cannot thank you all enough for helping me to maintain my morale and reason during difficult times.

TABLE OF CONTENTS

LIST OF TABLES

LIST OF FIGURES

LIST OF SYMBOLS AND ABBREVIATIONS

a	Lumen Radius
AI	Alignment Index
ANOVA	Analysis of Variance
BVS	Biological Vascular Substitute
C	Compliance
CVD	Cardiovascular Disease
DAPI	4',6-diamidino-2-phenylindole
DMEM	Dulbecco's modified Eagle's medium
EC	Endothelial Cell
ECM	Extracellular Matrix
ePTFE	Expanded Polytetrafluoroethylene
$E_{\theta\theta}$	Circumferential Green Strain
f	Axial Force
FBS	Fetal Bovine Serum
FFT	Fast Fourier Transform
h	Wall Thickness
hDF	Human Dermal Fibroblast
hUSMC	Human Umbilical Smooth Muscle Cell
hVSMC	Human Vascular Smooth Muscle Cell
IH	Intimal Hyperplasia
IMA	Internal Mammary Artery
LCA	Left Coronary Artery

LOEX	Laboratoire d'Organogénèse Expérimentale
mmHg	Millimeters of Mercury
MTT	Methylthiazol Tetrazolium
P	Transmural Pressure
RCA	Right Coronary Artery
SA-	Self Assembly-
SMC	Smooth Muscle Cell
ssTEVMA	Single Step Assemble Tissue Engineered Vascular Media/Adventitia
TEBV	Tissue Engineered Blood Vessel
TEVA	Tissue Engineered Vascular Adventitia
TEVM	Tissue Engineered Vascular Media
TEVMA	Tissue Engineered Vascular Media/Adventitia
W	Strain Energy Function
λ	Stretch Ratio
σ	Cauchy Stress

SUMMARY

Despite efforts by clinicians and scientists world-wide, coronary artery disease remains to be the leading cause of morbidity and mortality in industrialized nations. Development of a tissue engineered coronary by-pass graft with low thrombogenicity and immune responses, suitable mechanical properties, and a capacity to remodel to their environment could have a significant impact on the treatment of coronary artery disease. While many methods for the tissue engineering of blood vessels have been developed, one promising approach is the self-assembly method. Using autologous cells that produce an endogenous extracellular matrix (ECM), the potential for therapeutic success is high due to biocompatibility. However, despite these advantages, improvements can be made which will give the grafts an even higher rate of patency. This dissertation presents a study of the characterization of the biaxial mechanical properties of self-assembly tissue engineered blood vessels (SA-TEBV), as well as developing a framework for fabrication strategies of SA-TEBV.

Native arteries are exposed to multiaxial mechanical loads, including (a pulsatile) blood pressure that causes the vessel to cyclically distend circumferentially, blood flow that induces a shearing load along the luminal surface, and an axial extending load; the latter is relieved upon excision, causing the vessel to retract. These mechanical loads introduce intramural wall stresses and flow induced wall shear stresses that play a key role in mechano-biological signaling and tissue homeostasis. Until now, the mechanical properties of SA-TEBV have only been characterized in the circumferential direction (i.e. burst pressure and circumferential elastic modulus). The objective of this work is to

characterize the biaxial mechanical properties of SA-TEBV to quantify their mechanical behavior and local intramural stresses under physiological loading. The work will show that while the global mechanical response of the SA-TEBV is similar to that of native arteries (and potentially sufficient), the local intramural stresses (using the current fabrication techniques) differ greatly from native coronary arteries. Therefore, a novel approach to fabricate the self-assembly derived tissue sheets is developed and tested which utilizes biaxial mechanical stimulation to alter the microstructure, thereby controlling their mechanical response.

CHAPTER I

INTRODUCTION

1.1 Motivation

Cardiovascular disease (CVD) is the leading cause of death in the US; more specifically, coronary artery disease accounts for 54% of all CVD and 20% of mortality in the US, with an estimated economic cost of $142.5 billion.[1] Over half a million coronary by-pass procedures are performed in the United States each year, however, it is estimated that 30% to 50% of all coronary by-pass grafts will result in restenosis, requiring additional clinical intervention.[1] One often cited cause for restenosis is a "compliance mismatch" between the native and grafted tissues. In addition, for many patients, suitable autologous grafting tissues are not available.

1.1.1 Artery Structure.

Arteries primarily function to transmit blood, rich in oxygen and other nutrients, from the heart to other tissues throughout the body. As blood is ejected from the heart, it travels through the aorta and subsequently through various arteries with decreasing diameter. As the blood reaches the peripheral tissue, it is transported through the capillaries where most of the oxygen and nutrient exchange occurs. The depleted blood is then returned to the heart through veins of increasing diameter. As the blood leaves the heart, the pressure driving the flow is high and decreases as the blood reaches the periphery. Therefore, different vessels throughout the cardiovascular system are subjected to different mechanical loads. In addition, the ejected blood is inherently

pulsatile due to the pumping action of the heart. The vasculature acts to dampen this pulsatile flow pattern mainly through the compliance of the vessel. For these vessels to properly transport the blood throughout the body they must maintain not only proper biochemical homeostasis, but also suitable mechanical properties.

From the preceding description of the systemic architecture of the cardiovascular system, it would be correct to speculate that the microstructure of blood vessels varies depending upon wherein the body the vessel is found. Nevertheless, all arteries are composed of three distinct layers: the intima, media and adventitia. A schematic diagram of an artery is seen in Figure 1.1. The intima is composed of a single layer of endothelial cells which regulate the transport of nutrients across the vessel wall. These cells also possess anti-coagulant properties which allow blood to flow unrestricted throughout the vasculature. The basal lamina is an important feature of the intima. Composed of mostly of a thin layer of collagen type IV, this web-like structure provides a location for the endothelial cells to attach, grow and function. Separating the intima and media is the internal elastic lamina, a fenestrated sheet of elastin.[2]

The central layer of an artery, the media, is primarily composed of smooth muscle cells (SMC), collagen (primarily types I, III, V), elastin and proteoglycans. SMCs are aligned nearly circumferentially and have contractile properties which act to regulate vascular tone as well as luminal diameter. These cells are paired with elastin and collagen fibers to form functional units and are arranged in concentric sheets. While the size of the functional unit remains nearly equal across different vessel geometries, the number of sheets varies depending on diameter. The external elastic lamina separates the media and adventitia and is very similar in structure to the internal elastic lamina.[2]

The outermost layer of an artery is the adventitia. This layer is primarily composed of fibroblasts and collagen type I. Additionally, this layer contains the vaso vasorum, the network of microvasculature which provides blood to the vessel wall. It is believed that the adventitia primarily functions to prevent acute over distention of the artery [2], however, recent studies suggest it also plays a role in maintaining vascular tone.[3-5] The fibroblasts regulate and maintain the collagen within this layer. It is clear from this description that the microstructure of the artery is a complex hierarchy of cells, connective tissue and other molecules (i.e. proteoglycans, fibronectin and laminin) which are arranged in different mass/volume fractions, orientations or distributions. Alterations in the content and organization of cells and extracellular matrix would result in alterations of the mechanical properties of the artery. While homeostasis is maintained in healthy individuals, CVD can alter the structure of the artery and render these vessels ineffective, necessitating clinical intervention.

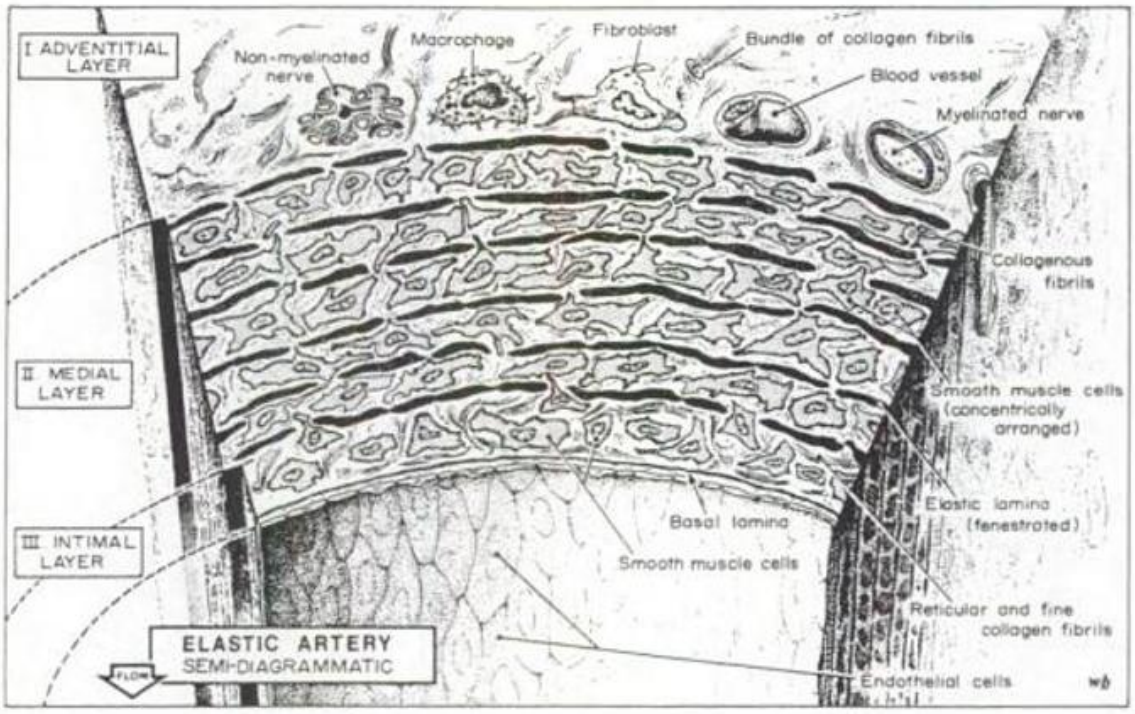

Figure 1.1. Schematic representation of a typical native elastic artery showing the three primary layers, the intima, media and adventitia, and their primary constituents (from Rhodin 1979 [6])

1.1.2. Biomechanics and Bypass Grafting

Traditionally, saphenous veins have been used for coronary by-pass grafting; in their native environment, these veins experience an order-of-magnitude lower shear stresses, much lower mean and cyclic pressures, and higher radius to thickness ratio when compared to coronary arteries. Thus, following implantation of the saphenous vein into the arterial system, the shear stress increases along with the circumferential stress, while the cyclic pressure and cyclic strain dramatically increase. Typically, veins are implanted at a fairly low axial stretch, thus the axial stress likely decreases. These altered loads can induce significant remodeling in the graft vessel. Grafts derived from the arterial system (e.g., internal mammary artery (IMA) or radial artery) experience less dramatic, but still

significantly, altered loading following implant. Thus the IMA often grows in a tortuous fashion, indicating maladaptive remodeling due to insufficient axial loading.[7]

In addition to graft remodeling, the host vessel experiences significant changes in the local loads near the anastomosis, including altered cyclic strains due to compliance mismatch between the host and graft and altered hemodynamics due to diameter and compliance mismatch. Host tissues experience oscillatory shear stress and a significant reduction in cyclic strain; both mechanical stimuli are associated with intimal hyperplasia and plaque formation. To date, synthetic small diameter grafts have proven ineffective as a replacement for autologous grafts; this is mainly as a result of thrombogenicity and compliance mismatch. Comparing autologous (compliant) to synthetic (non-compliant) grafts, it was found that the two year patency rate of compliant grafts was more than two times superior than the patency rate of non-compliant grafts.[8] The previous result however brings into question the resulting effect of synthetic graft biocompatibility. To eliminate synthetic materials from the experiment, Abbott *et al.* chemically cross-linked arterial autografts with glutaraldehyde to decrease the compliance of the grafts prior to implantation.[9] It was found that the 3 month patency was significantly greater in compliant (not cross-linked) grafts.

Specific mechanisms of failure as a result of compliance mismatch have been investigated. Intimal hyperplasia (IH) at and around the suturing point has been shown to cause significant intimal thickening with synthetic grafts (ePTFE) whereas IH with autologous grafts result in significantly less thickening.[10] To eliminate blood-synthetic material contact, Trubel *et al*. used autologous vein autografts externally stiffened with Dacron mesh to force compliance mismatch.[11] It was found that significant IH

occurred in compliance mismatched vessels while very little IH was observed in diameter mismatched vessels. Ballyk *et al*. mathematically investigated compliance mismatch and found that significantly increased transmural stresses develop near the vasculature-graft junction [12]. This mathematical finding, along with experimental results of Matsumoto and Hayashi [13], further suggest a localized cellular response to an increased stress. These studies, and others, indicate a pressing need for a novel clinical therapy which could be met by development of a small diameter tissue engineered blood vessels (TEBVs) with low thrombogenicity and immune responses, suitable mechanical properties, and a capacity to remodel to their local environment.[14-16]

1.1.3. Tissue Engineered Blood Vessels

Since the first TEBV was reported by Weinberg and Bell in 1986 [17], tremendous advances have been made towards the development of a clinically useful small diameter TEBV, including short term patency *in vivo*.[18-20] These advances have relied on tools and techniques from a wide variety of disciplines, ranging from molecular and cell biology and biochemistry to material science and biomechanics. With regard to the latter, biomechanical stimuli have been shown to stimulate remodeling of TEBVs to greatly improve their mechanical behavior.[19, 21] These studies demonstrate the central role that mechanical cues play in the growth and remodeling of TEBVs. There is a critical need, however, to develop theoretical and experimental frameworks that can be used to characterize these mechanisms. Such frameworks can be used to motivate strategies to improve mechanical and functional properties and reduce requisite culture times for TEBV development.

Different platforms for developing a suitable TEBV graft have shown great promise; these include gel-derived [17, 22], polymeric biodegradable scaffold-derived [19], and self-assembly derived-TEBVs.[18] Collagen-based TEBVs were first proposed by Weinberg and Bell in 1986.[17] These models use reconstituted collagen as the scaffold material for the cells. The process of fabrication involves initially suspending cells (fibroblasts or SMCs) in a soluble form of the collagen. Through neutralization, the soluble collagen gels entrapping the cells within the solid matrix. Upon culture, remodeling occurs where the cells degrade and reorient the existing matrix and lay-down neo-synthesized collagen. A layer of endothelial cells can be seeded in the lumen to generate an intima-like layer.

Polymeric scaffold-derived TEBVs can be made from many materials; examples include poly(methyl methacrylate) PMMA, poly(glycerol-sebacate) (PGS), polyglycolic acid (PGA), among others.[19, 23-27] The idea behind this tissue engineering model relies on the ability of the cells to generate matrix while the scaffold is resorbed. Resorbtion rates are be controlled by manipulating the structural architecture such as porosity and density. With sufficient culture time, these TEBVs have been shown to attain high burst pressures along with short term *in vivo* patency.

TEBVs constructed by self-assembly (SA-TEBVs) have shown superior mechanical strength (burst pressure >1,000 mmHg), morphology, structural organization, and vasomotor response compared to other TEBVs.[3, 28-34] The fabrication technique for the self-assembly approach can be seen in Figure 1.2.

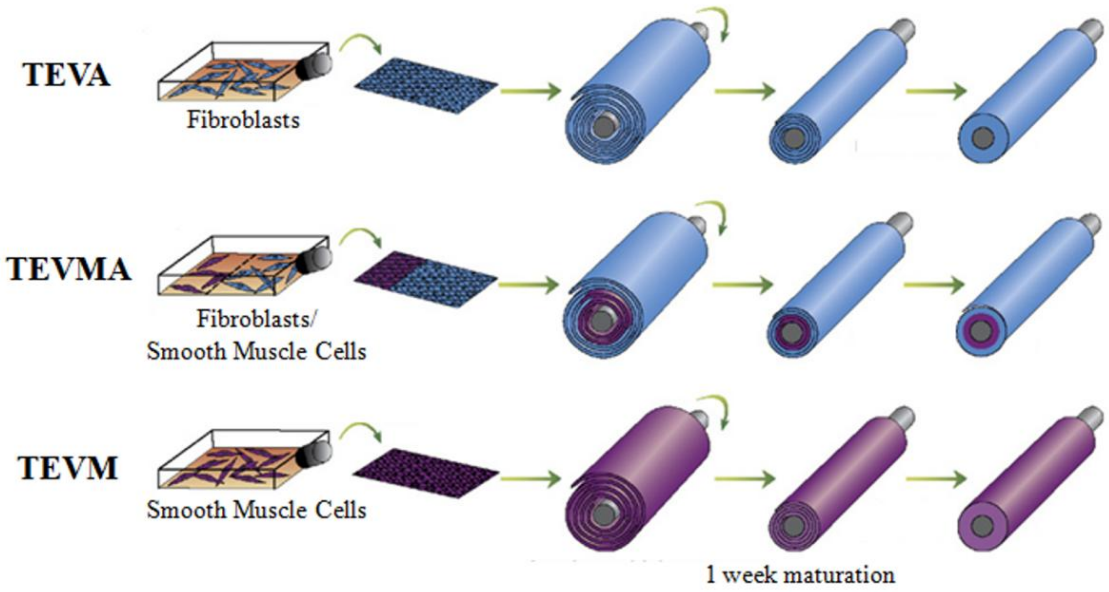

Figure 1.2: Schematic representation for the fabrication of the three vascular constructs. (Adapted from Auger *et al*. [35]).

Generating single layer correlates consists of culturing either human umbilical smooth muscle cells (hUSMC) or dermal fibroblasts (hDF) in supplemented culture media to ultimately produce tissue engineered vascular media (TEVM) or tissue engineered vascular adventitia (TEVA), respectively. After several weeks of static culture, the cells form a thick living tissue sheet that can be rolled around a mandrel and cultured to form a TEBV with layers similar to the media and adventitia of native vessels. Producing a bi-layer tissue engineered vascular adventitia/media (TEVMA) consists of beginning with a co-culture of hUSMC and hDF to produce the tissue sheet. Endothelial cells can be seeded on the luminal surface to form a functioning endothelium.[36]

This work seeks to combine theoretical and experimental techniques to better understand the role that biaxial mechanical stimuli play in growth and remodeling

mechanisms of SA-TEBV. An aid to help better understand this process is seen in Figure 1.3.

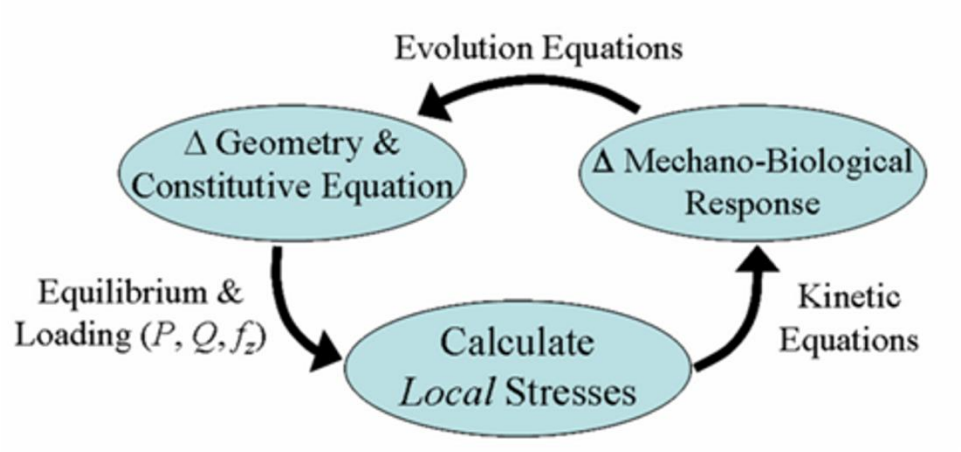

Figure 1.3: Illustration of a theoretical approach to studying and understanding the underlying mechanisms of growth and remodeling of vascular tissue engineering

Performing standard biaxial biomechanical testing to understand the tissue level response will allow us to use constitutive laws to describe the material response of the TEBV. The same set of equations will allow us to understand the local stresses throughout the vascular wall under specific loading conditions. By culturing under defined mechanical loads and monitoring tissue level vascular geometry, kinetic equations can be developed to understand the interactions between loading and TEBV evolution. Lastly, performing mid- and end-point biaxial biomechanical tests will allow new constitutive models to be developed which in turn will be used to develop a better understanding of how the local stresses evolve.

1.2 Thesis Organization

The goal of this dissertation is to study, experimentally and theoretically, the mechanical properties and investigate innovative fabrication strategies of SA-TEBV.

Novel experimental methods will be required to characterize the initial mechanical properties of SA-TEBV, as well as subject the vessels to multiaxial mechanical loading during culture. Previous techniques, along with their limitations, will be discussed and used as a baseline to develop a novel bioreactor. Theoretical approaches have been developed to characterize the mechanical properties of native vessels. Similar strategies will be employed to describe the mechanical behavior of SA-TEBV, as well as generating a predictive two-layer model to understand how different fabrication techniques may alter the mechanical response of the tissue. The results and limitations of this model will be discussed. Lastly, novel experimental approaches laying the groundwork for original fabrication strategies of TEVA utilizing multiaxial mechanical stimuli will be investigated.

Chapter 2 defines the specific goals to be met in order to complete this body of work. Chapter 3 introduces existing bioreactor systems (as well as their limitations) which are required to experimentally perform this work. This chapter also describes the design and validation of a novel bioreactor and examples of its capabilities and limitations. Chapter 4 outlines the theoretical framework that will be used to characterize the biaxial material response of SA-TEBV, as well as report experimental results of biaxial biomechanical testing. This chapter also describes the development and implementation of a predictive two-layer model for the response of a TEVMA. Chapter 5 begins with a review of the effects of uniaxial mechanical stretching on 2 dimensional cell cultures and 3 dimensional tissue structures. Results are then shown from human dermal fibroblasts that were subjected to biaxial mechanical stimulation to investigate the effects on cell alignment and orientation. Lastly, Chapter 6 provides a brief summary of

the results and implications, as well as potential future directions for this body of research.

CHAPTER II

OBJECTIVES

Despite efforts by many clinicians and scientists world-wide, coronary artery disease remains to be the leading cause of morbidity and mortality in industrialized nations. As a result, there is a critical need for small diameter vascular substitutes to be used as bypass grafts. Current synthetic materials are not suitable as small diameter grafts due to their high thrombogenic potential. Therefore, a central focus of this research is to develop vascular substitutes that induce low thrombogenicity and immune response, possess suitable mechanical properties, and have a capacity to remodel to their local mechanical and biologic environments. Tissue engineered blood vessels (TEBV) have shown promise in meeting these critical needs.

Numerous techniques have been developed to create TEBVs. To date, self assembly-derived TEBVs have shown superior mechanical strength [33], morphology, structural organization, and functional vasomotor response compared to other TEBVs. While self-assembly derived TEBVs have shown superior quality, there are still major deficiencies with this approach; namely, length of time required to develop the TEBV, and lack of appropriate mechanical properties.

We have developed a collaboration with Dr. Francois Auger who pioneered the self-assembly method. This collaboration was developed with the desire to advance the understanding of how these vessels are capable of growing and remodeling. To make these vessels a clinically and economically viable alternative to autologous grafting procedures, the length of time required to develop these vessels must be reduced. It is our

ultimate goal to utilize biaxial mechanical stimulation to shorten the required culture time and induce changes in the mechanical properties of the vasculature to better mimic native vessels.

Specific Aim 1: *Develop a novel bioreactor capable of performing cylindrical biaxial biomechanical tests and culturing tissue engineered blood vessels (TEBV).*

To fully characterize biomechanical properties and culture TEBV subjected to mechanical loading, independently controlled pressure, axial extension and flow are required while simultaneously monitoring vascular geometry.

Specific Aim 2: *Characterize the cylindrical biaxial biomechanical properties of statically cultured tissue engineered vascular adventitia (TEVA) and tissue engineered vascular media (TEVM).*

Our working hypothesis is that TEVA and TEVM can be accurately characterized using a phenomenological and structurally-motivated mathematical model and subsequently used to develop a validated two-layer predictive model for tissue engineered vascular media/adventitia (TEVMA).

Specific Aim 3: *To quantify the ability to control human dermal fibroblast alignment with biaxial mechanical stimulation.*

Our working hypothesis is that human dermal fibroblasts (hDF) grown on the inside of small diameter silicone tubes and subjected to biaxial dynamic stretching will aligned in the direction of principle shear.

Successful realization of these aims will lead to several technologies advancing the understanding of TEBV. First, we will develop and advance the design of a novel bioreactor with the capability to precisely control mechanical loading. Second, a validated two-layer model will enable us to perform parametric studies that will provide insights into TEVMA design parameters to tailor the biomechanical response of future generation TEBVs. Finally, we will advance our capabilities to develop multi-layer (heterogeneous) TEBV with morphology and microstructure similar to native vessels.

CHAPTER III

BIAXIAL BIOREACTOR SYSTEM

3.1 Introduction

In native blood vessels, remodeling mechanisms appear to be aimed towards maintaining the local, 3-D mechanical environment (i.e., the local stresses or strains). Specifically, experimental perturbations in mean or cyclic circumferential [13, 37] and axial [7, 38-40] stresses (or strains) as well as wall shear stress [41] induce changes in vessel geometry and material properties that appear to be aimed at restoring these stresses to 'target' levels. Tissue engineered constructs also adapt to altered mechanical loading. Seliktar *et al*. [21] demonstrated collagen fiber remodeling and increased mechanical strength in response to cyclic pressure stimulation, showing highly organized collagen lamellar assemblies and circumferential smooth muscle cell alignment throughout the thickness of the wall in dynamically conditioned constructs compared to statically conditioned constructs; circumferential alignment of SMCs has been shown to significantly increases functional properties in response to histamine, a known vasodilator.[30] Ng and Swartz [42] have shown cellular and ECM reorganization in response to fluid flow, with human dermal fibroblast and collagen fiber realigning perpendicular to the direction of flow in collagen gels. Whereas less is known about the role of axial extension on TEBV remodeling, axial stretch-induced remodeling in native arteries has been reported at rates that were 'unprecedented' compared to pressure- and flow-induced remodeling.[7, 43, 44] In addition to these three individual loading scenarios, it is now becoming evident that specific combinations of multidirectional loads

appear to have a synergistic effect on the remodeling and tissue formation.[45] Thus, to truly characterize mechanically-mediated remodeling in TEBVs, one must consider multiaxial loading.

Many groups have developed bioreactors capable of studying the individual and combined mechanical effects on a number of tissue types. Most bioreactors are designed to mimic *in vivo* conditions allowing engineering of functional tissue *in vitro.*[46] For example, Engelmayr *et al*. reported synergism for multidirectional loading was performed on a custom device capable of precisely controlling cyclic flexture, stretch and flow, mechanical stimuli commonly experienced by heart valve tissue.[47] Multiple bioreactors have been reported in the literature to culture vascular tissue under altered luminal flow and circumferential distension [21, 48-51], but fewer have developed one capable of precisely controlling axial distension.[50, 52, 53] Similar systems such as the LumeGen bioreactor from Tissue Growth Technologies and the ElectroForce system from Bose are now commercially available. None of these devices, however, offer the combined capabilities of (*i*) simultaneous independent control of pulsatile pressure, luminal flow, and axial load (or stretch) over long-term culture while monitoring vessel geometry, (*ii*) performing intermittent cylindrical biaxial mechanical testing on the same vessel at multiple time-points in culture, and (*iii*) performing intermittent multiphoton microscopy on a live vessels mounted within the bioreactor at multiple time-points in culture and under multiple loading scenarios. Towards this end, we have built and tested a novel bioreactor capable of long term culture of TEBV subjected to individual or combined external mechanical stimuli: mean and cyclic pressure, axial load (or length), and luminal flow; monitoring vascular geometry throughout culture. In addition, this device is

designed to perform intermittent cylindrical biaxial biomechanical tests and multi-photon confocal microscopy to quantify changes in the mechanical behavior and microstructural organization of the TEBVs, at multiple time-points in culture. Here we present the motivation for this experimental design and demonstrate the capabilities of the device to precisely and independently control the multiaxial mechanical loading during culture and perform intermittent mechanical testing and microscopy.

3.2 Experimental Bioreactor System

To increase throughput of experiments and decrease time requirements for studies, four identical bioreactors are setup in parallel in a dual, water-jacketed CO_2 incubators (NuAir model NU-S8500) and controlled using one computer. A single bioreactor is composed of 5 subsystems, as shown: (1) the culture chamber, (2) the flow control, (3) the pressure control, (4) axial motion control, (5) the geometry monitoring subsystem (Figure 3.1).

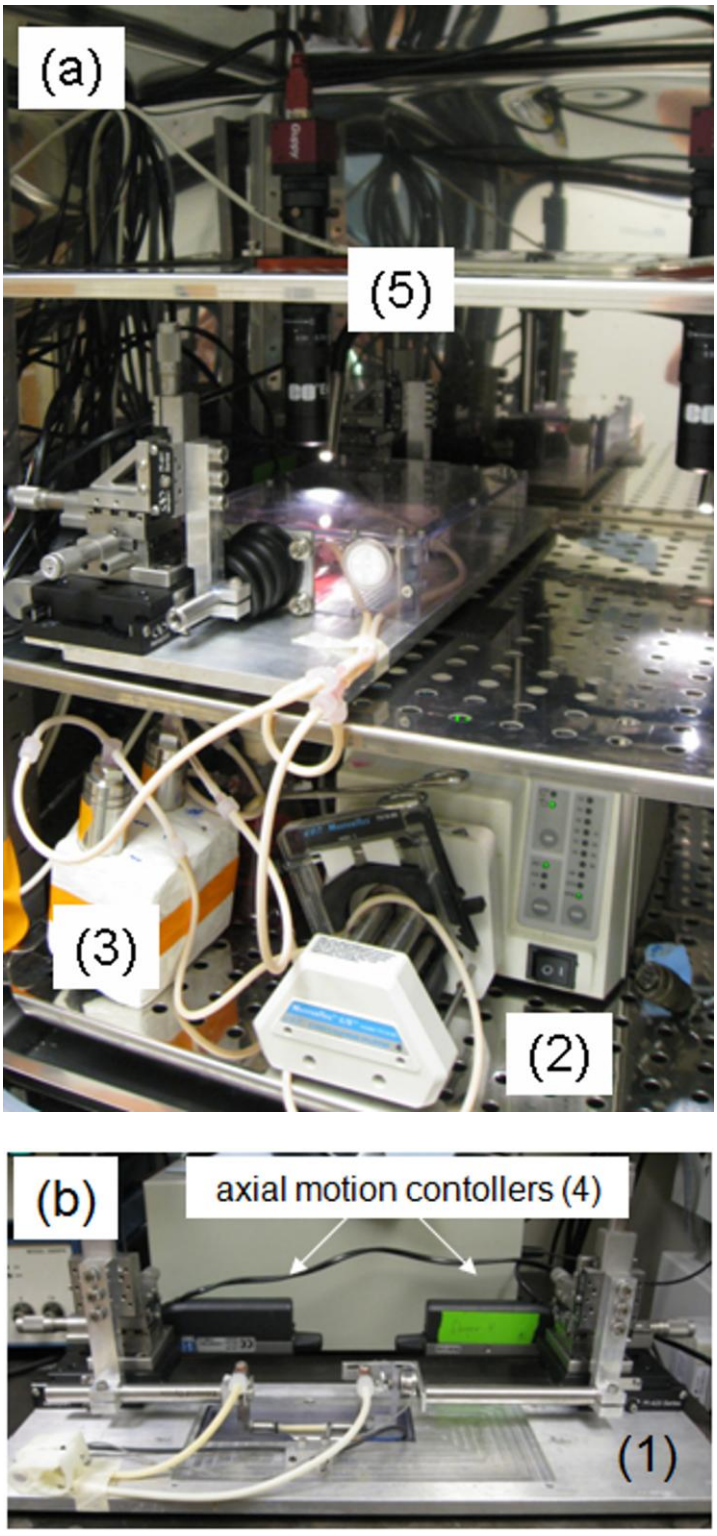

Figure 3.1. Bioreactor/biomechanical testing device for TEBVs with subsystems as noted in text. Fully assembled system shown in incubator (a). Image of culture chamber showing axial motion controllers as well as mounted BVS (b). Detailed image of BVS showing points of attachment to cannula, ultrasound transducer, and load cell (c).

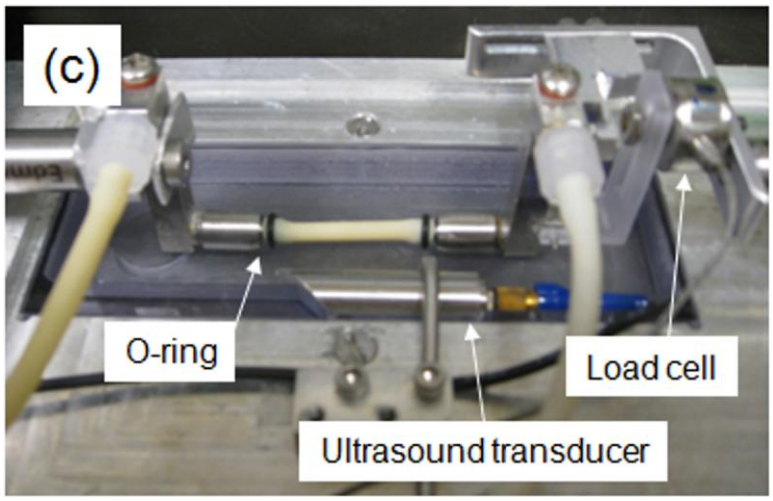

Figure 3.1 continued

3.2.1 Culture Chamber

The base of the bioreactor is machined from a solid aluminum plate. Two uniaxial spring actuated stages (Newport model M-423) with appropriate fittings for mounting linear actuators (Newport model LTA-HS) are mounted to the base. Atop both uniaxial stages are three axes manually adjustable stages (Newport model M461) with three manual micrometers to allow for alignment of cannula prior to TEBV mounting. Connected to these stages is a stainless steel rod and custom machined part to allowing mounting of "L" shaped cannula and a load cell (Delta Metrics Inc. model XLU68s) to measure axial force. The TEBVs are mounted on the cannula which allow for luminal perfusion. Because this system is capable of being used on a range of vessel sizes, the cannula can range in outer diameter from 1 mm to 5 mm. The ends of the cannula may be tapered to allow easier mounting of the vessel and given grooves to prevent sliding of the o-rings or sutures that hold the TEBV in place.

A custom polycarbonate top with gas exchange filters is used to prevent contamination during transport and culture. Rubber baffles allow for enclosure of the top around the stainless steel rod while not restricting linear motion. The bath in which the vessel is cultured is made from polycarbonate with a clear cover slip to allow for imaging on an inverted confocal microscope (Zeiss LSM 510, cameleon argon laser). A second flow loop allows for circulation and media exchange in the polycarbonate bath.

3.2.2 Flow Control

A peristaltic pump (Ismatec model IPC) is used to generate luminal flow with given rate and pattern. The pump communicates with the computer via a DAQ board allowing a prescribed flow waveform to be generated. The reservoir is a 5 port 250 mL Erlenmeyer flask with solid stopper. Medium is pumped out of this flask from a bottom port, travels through the pump prior to entering the first pressure transducer. Flow continues into the culture chamber and through the vessel before exiting the culture chamber and returning to the second pressure transducer. Once leaving the second transducer, flow reenters the reservoir. The flow loop contains one bypass prior to the vessel to allow for total removal of air bubbles from the tubing. The bypass is closed during culture to ensure all flow is through the vessel. Measurements of flow rates are obtain using an ultrasonic flow monitoring system (Transonic model T402) with appropriate probe size. The probe is located on the vessel to directly measure the flow rate through the vessel, but is large enough as to not impose any external traction on the vessel. Data was collected using an analog output from the flow monitoring unit and time-averaged over each second.

3.2.3 Pressure Controls

Pressure in the vessel is controlled by regulating static gas pressure in the reservoir. Static pressure in the reservoir is controlled using a custom designed syringe pump. A syringe is mounted onto a uniaxial stage whose position is controlled via a linear actuator. The syringe plunger is fixed allowing movement of the stage to move the syringe tube relative to the plunger. Tubing and a filter connect the syringe to the reservoir. As the plunger moves into the tube, pressure is increased in the reservoir. Likewise, as the plunger moves out of the tube, pressure is decreased. Because we are controlling static pressure in the reservoir, pressure at the reservoir inlet and outlet are equal thereby not inducing any pressure gradient or flow.

Pressure in the vessel is monitored using two pressure transducers (Honeywell model FGP) located on the bottom rack of the incubator properly calibrated to account for static pressure head. A feedback control was developed in LabView (National Instruments v7.1) to deliver periodic pressure curves with adjustable set-points for minimum and maximum pressure, and waveform period. Further development with a more sophisticated control algorithm could use a Fourier series approach to deliver a physiological pressure waveform at physiological rates. Due to the risk of vascular leakage or air leakage in the syringe, a three-way solenoid pinch valve is used to reload the piston once it reaches the end of its range of travel. Reloading of the syringe takes approximately ten seconds. Analog inputs from the pressure transducers and load cell, as well as analog outputs to the pump and digital outputs to the pinch valves are communicated with the computer via a data acquisition (DAQ) board (National Instruments model USB-6259).

3.2.4 Axial Motion Control

Uniaxial sliding stages on the culture device fit linear actuators which are controlled using a Newport motion controller (model XPS). This motion controller is capable of controlling eight linear actuators simultaneously. Two actuators are used per device to prevent translation of the vessel in the camera focus area. Therefore, one motion controller is capable of controlling all four parallel bioreactors. This motion controller is capable of monitoring actuator movement with 0.035μm resolution. LabView communicates with the motion controller via an Ethernet cable to precisely control movements of the actuators to prescribed spatial locations; hence axial extensions are referenced to the unloaded length of the vessel. Additionally, using a feedback loop in LabView, oscillatory axial distensions are capable at frequencies of ~1 Hz.

3.2.5 Vascular Geometry Monitoring

A digital camera (AVT Guppy IEEE 1394) is mounted above the vessel and combined with a fiber optic light source (Dolan-Jenner Fiber-Lite) for illumination. Real time processing of the digital image is accomplished using LabView vision software to measure outer diameter of the vessel. In addition, markers may be attached to the outer surface of the vessel and tracked in real time to quantify the displacements in a local region of the vessel, thereby eliminating end effects on the measurement of strain.

Wall thickness is measured using ultrasonic techniques. An ultrasonic pulse-receiver (Olympus NDT model 5900PR) is used in combination with a 25MHz transducer (Olympus NDT model V-324SM). At each vessel/media interface, there is a change in the speed of sound causing a reflection which is captured by the transducer. Because there are four interfaces, the output signal has four peaks. The signal is acquired

via a 250MS/s, 8 bit PCI digitizer (National Instruments model PCI-5114). Approximately 20 waveforms are averaged and manipulated using a Hilbert transform in combination with convolution to accentuate the peaks over the noise. A peak detection algorithm is then used to determine the location of the four peaks which correspond to the dimensions of the vessel. The specifications of the digitizer allow a theoretical resolution of 3 μm.

3.3 Experimental Methods

3.3.1 Preparation, Sterilization and Sterile Tissue Cannulation

Prior to sterilization, all components are washed in a soap bath and thoroughly rinsed with water. Pressure transducers are rinsed three times with 70% ethanol an allowed to evaporate overnight. Ethylene oxide (EO) is used to sterilize the fully assembled device (with chamber cover removed) so as not to damage the movable stages, pressure transducers and load cell. Sterilization of additional tubing segments and the reservoir is accomplished in an autoclave. The flow loop is created consisting of the reservoir, pressure transducers, pump and appropriate tubing. Cannulation of the vessel occurs in a biological safety cabinet. Once securely mounted using sterile sutures or O-rings, the chamber cover is attached. The flow loop is connected to the culture chamber and lastly the linear actuators are secured to the uniaxial stages. Typically, cannulating the vessel and setting up the bioreactor is accomplished in under 1 hour.

Long-term culture capabilities of this device are demonstrated using biological vascular substitutes (BVS) that were generously donated by Francois Auger's laboratory. These vessels were created using the self-assembly method as previously described.[33] Vessels were cultured and tested in Dulbecco's modified Eagles medium (DMEM,

Mediatec, Inc., with 4500mg/L of D-glucose and L-glutamine) supplemented with 10% fetal bovine serum (Mediatec, Inc.), antibiotic (P/S, Mediatec, Inc., 50 I.U./mL penicillin and 50 mg/mL streptomycin) and additional L-glutamine (Mediatec, Inc., 5000 g/L).

3.3.2 Biaxial Biomechanical Testing

The custom LabView program allows us to prescribe a variety of loading patterns for mechanical testing (e.g., pressure-diameter, force-length, or stress-relaxation tests). To demonstrate the device capabilities, pressure-diameter and force-length tests were performed. Biomechanical testing was performed in the bioreactor immediately following culture without any required handling of the TEBV. Prior to testing, the unloaded length of the vessel was measured. Under quasistatic conditions, pressure was varied from 0-120mmHg at fixed axial stretches of λ_z = 1.0, 1.15, 1.25, where $\lambda_z = \ell / L$ ℓ is the current length and L the unloaded length, at the time of interest. From this data, pressure-diameter (*P*-*d*) and axial force-pressure (*f*-*P*) curves were generated. Additionally, λ_z was cyclically varied up to 1.25 at pressures of 20mmHg, 40mmHg and 120mmHg. Axial force-length (*f*-*L*) curves were generated from this data.

A second set of mechanical testing data are shown using collagen gel based TEBVs (due to the ease and relative inexpensiveness of fabrication). The collagen gel derived TEBVs were developed following the methods of Stegemann *et al.* [54] Briefly, smooth muscle cells were isolated from rat aortas and combined with reconstituted bovine type I collagen. Controlling the environmental conditions of the collagen, gelation was induced around glass mandrels to form the TEBVs. Following 2 day static culture, the TEBVs were mounted on this device and cyclically inflated at λ_z = 1.00

from pressures of 0-10 mmHg for five cycles, then 0-20 mmHg for five cycle, then 0-30 mmHg for five cycles, and so forth until these freshly gelled vessels ruptured; pressure, diameter, and axial force where monitored at fixed axial length.

3.3.3 Confocal Imaging

Decellularized TEVA were used to image collagen content and organization via multi-photon microscopy. A Zeiss LSM 510 META inverted confocal microscope with Chameleon Ultra Ti:sapphire femtosecond laser (Coherent) was tuned to 800nm and used to excite and detect collagen. The laser reached the sample through either a 40x/1.3NA or 63x/1.4NA oil immersion objectives (Zeiss). The fields of view were 225 x 225 μm and 143 x 143 μm respectively. The META module of the microscope was configured as a 380-420 bandpass filter to detect backwards scattering second harmonic signal from collagen.[55] Imaris software (Bitplane) was used for 3D reconstruction of images.

3.4 Bioreactor Capabilities

3.4.1 Vascular Geometry monitoring

Camera calibration was performed using a glass slide with etched lines spaced at 500 μm. The camera was focused to achieve 20 μm per pixel, representing a field view of 8,500 x 11,400 μm on the digital camera. A representative image of a BVS and the outer diameter are shown for a vessel cultured at an axial extension $\lambda_z^* = \ell / L(0)$, where $L(0)$ is the unloaded axial length at the beginning of culture ($t = 0$), with cyclic pressure application (32.5mmHg ± 7.5mmHg, rate of one cycle per minute), and incremental flow (5 minutes at 3 mL/min once a day) for nutrient and metabolite exchange (Figure 3.2a & b). Notice that we have placed markers on the vessel to allow for measurements of local

displacement, in parallel to measurements of diameter and overall vessel length. Data were collected once per minute for 96 hours. As seen, there is little variation in the diameter measurements (less than 100 μm) between consecutive data points.

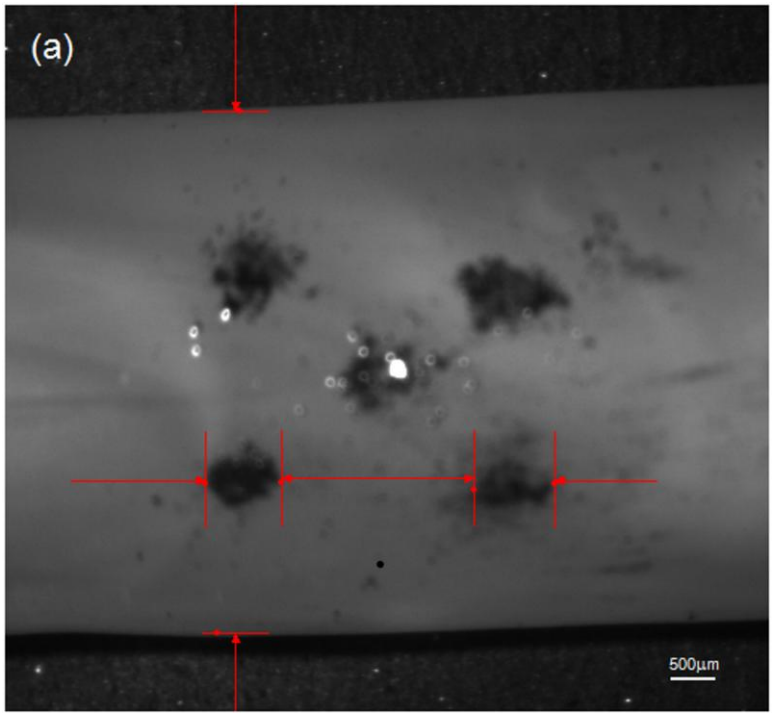

Figure 3.2. Image of a BVS during mechanical testing with markers to track local displacement to determine local strains (a). Outer diameter of a BVS cultured under cyclic pressure application (32.5mmHg ± 7.5mmHg, rate of one cycle per minute) and no axial stretching (b). Data were collected once per minute for 96 hours. (scale bar 500μm)

The discontinuity occurring around 50 hours is due to removal of the culture chamber from the incubator and media exchange in the reservoir. While we concede that a four day culture is not considered “long-term”, we have currently cultured vessels for up to 14 days without contamination. 14 days was the end point of our experiments, however, we feel that the vessels could have remained longer if desired.

Wall thickness measurements are accomplished using ultrasonic techniques. One sample digitized waveform is shown in Figure 3.3a. To determine the peaks from this waveform, (which represent the interfaces between the vessel and the medium), the waveform is subjected to an algorithm which includes cross-correlation and a Hilbert transform. After the raw data is processed as shown in Figure 3.3b, the peaks can be easily determined using a simple peak search algorithm. Sequential waveforms can be processed in the same manner allowing thickness measurements to be determined throughout the course of the test or culture. The thickness measurements for one pressurization cycle (0 – 150 – 0mmHg) can be seen in Figure 3.3c.

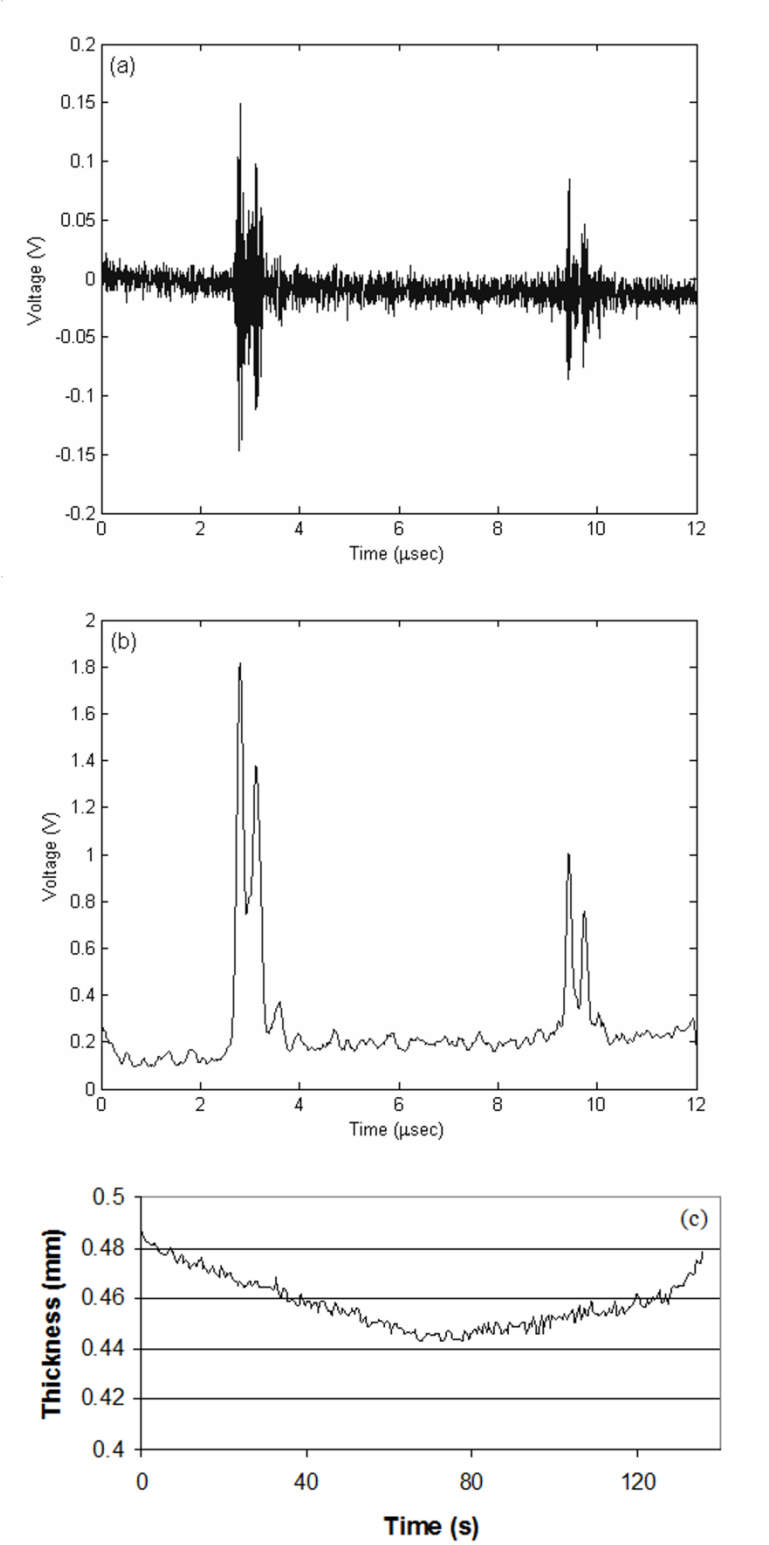

Figure 3.3. Ultrasound measurement results showing the collected waveform (a), manipulated waveform (b), and thickness measurements for one pressurization cycle (0 – 150 – 0mmHg) (c).

3.4.2 Loading Control

To demonstrate pressure-flow independence, two experiments were performed. The first was a low pressure/high flow test where pressure was held constant at 20 mmHg while maintaining a constant flow rate of 350 mL/min). The second was a high pressure and low flow was demonstrated by holding pressure constant at 100 mmHg and flow at 50 mL/min. There is no variation in both pressure (range 3 mmHg) and flow (range 10 mL/min) during low pressure/high flow testing (Figure 3.4). Likewise, there is little deviance in both pressure and flow during high pressure/low flow conditions. The likely cause of the slight fluctuations in the pressure and flow are a result of the nature of the peristaltic pump. While the dampener can't eliminate all pulsitility, the amount is small and within the noise level of the transducers.

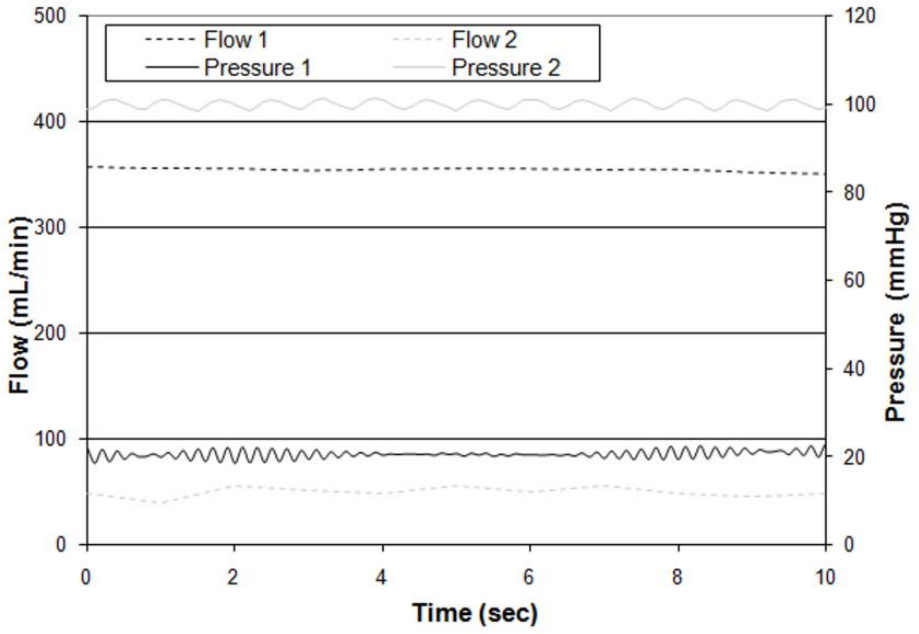

Figure 3.4. Loading results demonstrating independence of pressure and flow with constant low pressure of 20 mmHg and high flow of 350 mL/min (black lines), constant high pressure of 100 mmHg and low flow, 50 mL/min (grey lines).

To illustrate the independence between the four bioreactors, two bioreactors were set with mean pressures of 50 and 100 mmHg and ranges 20 mmHg and 40 mmHg, respectively, while two bioreactors were set to hold constant pressures of 20 and 40 mmHg. All four reactors are under constant axial stretch and no flow. Due to the independent design of the pressure control system, all four bioreactors are capable of operating in parallel without adverse effects (Figure 3.5).

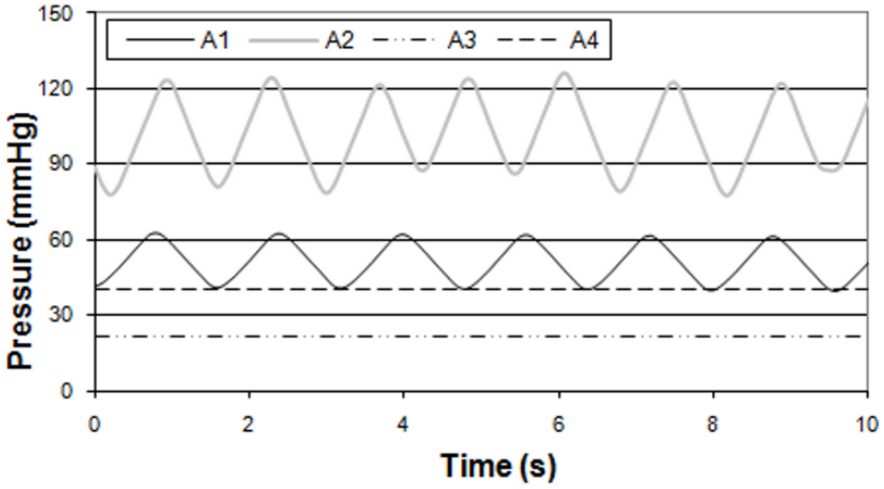

Figure 3.5. Independent pressure loading patterns of four bioreactors (A1 – A4) operating simultaneously from one control system.

3.4.3 Biomechanical Testing

Loading and unloading curves from statically cultured BVS demonstrate the cylindrical biaxial biomechanical testing capabilities of our device. These results, generated from a single BVS, provide representative data regarding the capabilities of our device. As previously described, a standard testing protocol consists of three pressure cycles from 0 – 120 - 0mmHg at a constant axial stretch. During this cycle, we monitor

outer diameter as well as axial force; these results are shown in Figure 3.6a and b, respectively. Axial force-length curves, generated at three constant pressures, exemplify typical viscoelastic materials as seen by the hysteresis occurring between the loading and unloading phases (Figure 3.6c). Not surprisingly, strain rate dependence has been observed to affect hysteresis; all samples *P-d* tests were pressurized and depressurized at a rate of 2mmHg/sec.

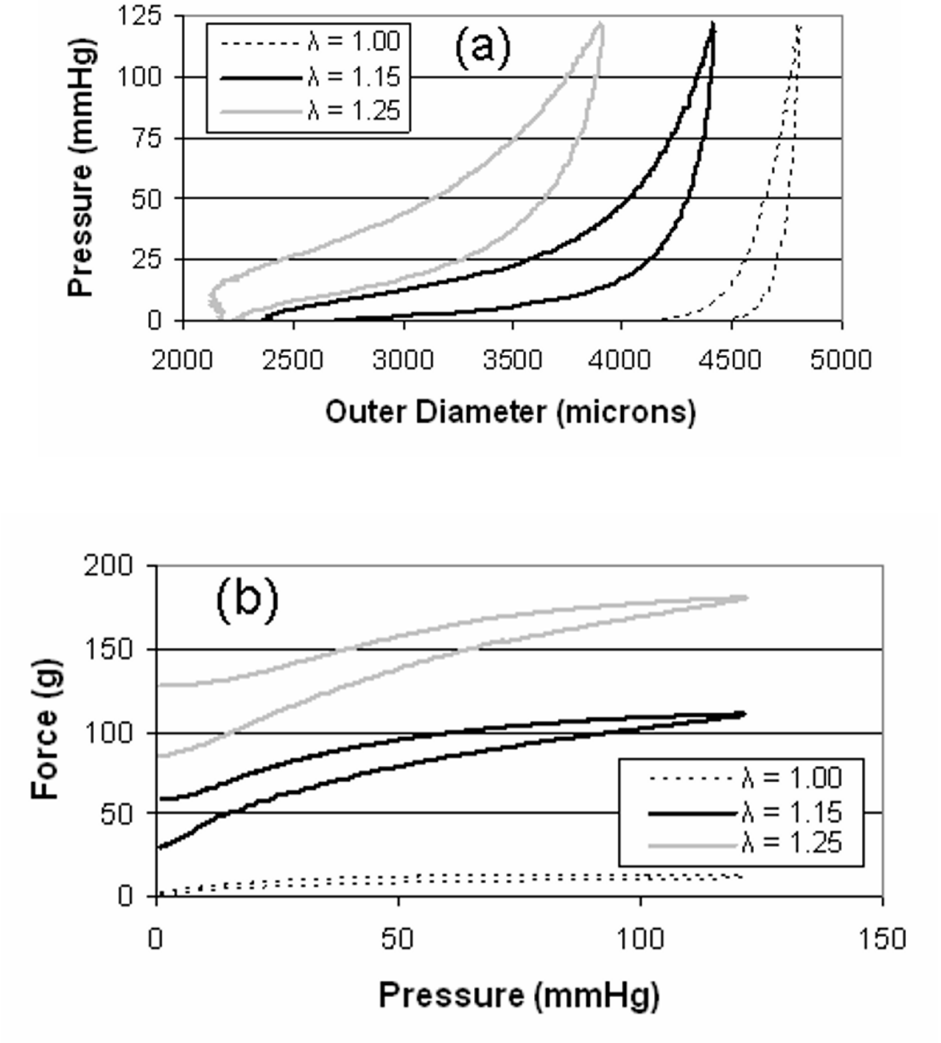

Figure 3.6. Loading and unloading pressure-diameter (a) and axial force-pressure (b) curves at three axial stretches generated during biomechanical testing on a statically cultured BVS. Loading and unloading axial force-length results at three constant pressures (c). Note the hysteresis typical of viscoelastic materials.

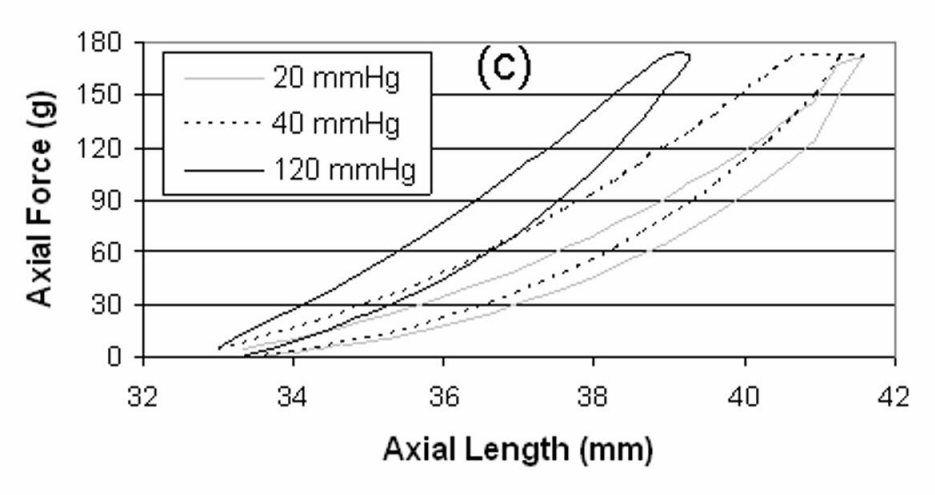

Figure 3.6 continued

These data combined with ultrasound thickness data can be used to generate mean axial and circumferential stress-strain curves, as well as perform stress analysis; see Equations (4.11) & (4.12). Biomechanical tests were also performed on two day statically cultured collagen gels. These data were generated from a single collagen construct and provide representative capabilities of the device. At just two days after gelling, these vessels are very fragile. Given the fragility of these vessels, it was clear that they would not exhibit high burst strength at these early culture times. Thus, we conducted a testing protocol that gradually increases the cyclic testing pressure from 0-10 mmHg, to 0-20 mmHg, and so forth (see Figure 3.7a). We were able to successfully mount and mechanically load these vessels and conduct pressure-diameter and axial force-length tests, as shown in Figure 3.7a and b, respectively. This protocol allows for the collection of several loading and unloading curves for stress analyses prior to rupture.

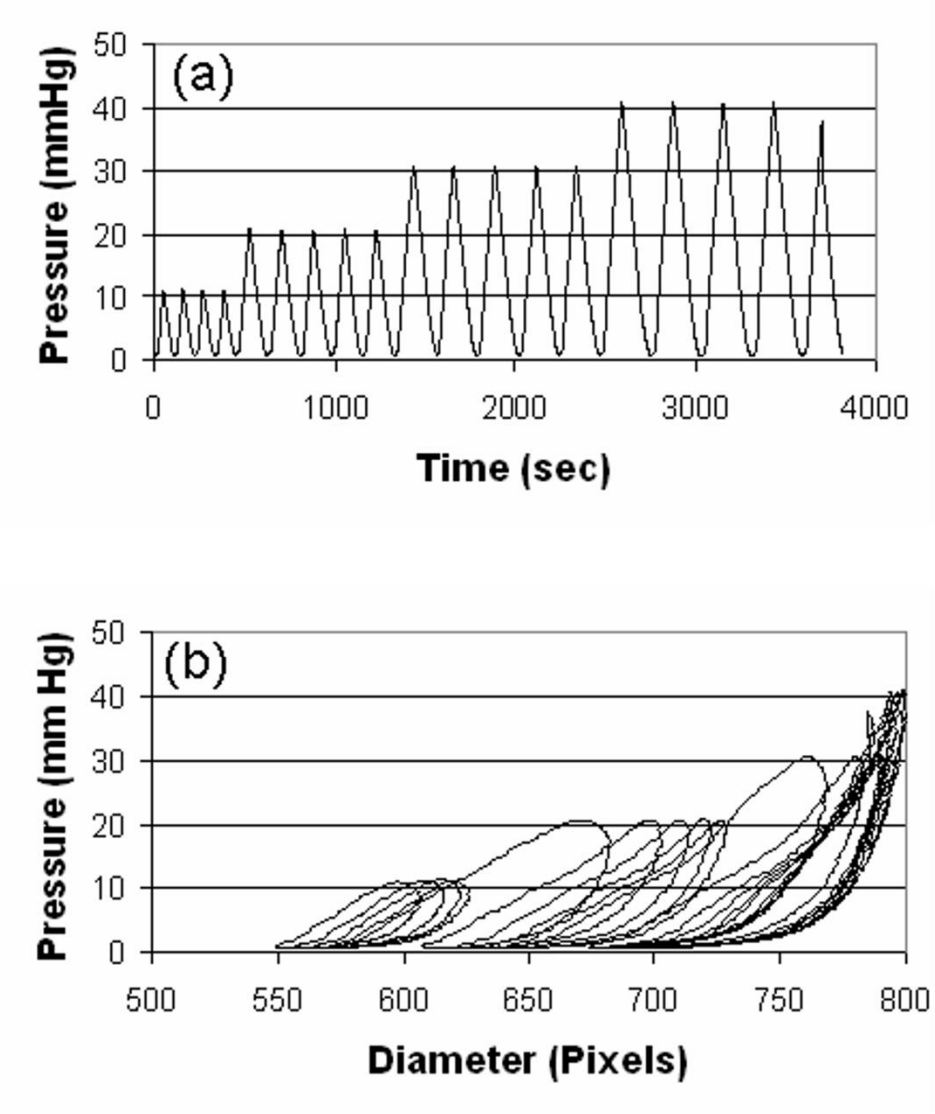

Figure 3.7. Cyclic biomechanical testing performed on cell-seeded collagen gel TEBV showing the loading history (a), Pressure-diameter (b), and axial force-pressure data (c).

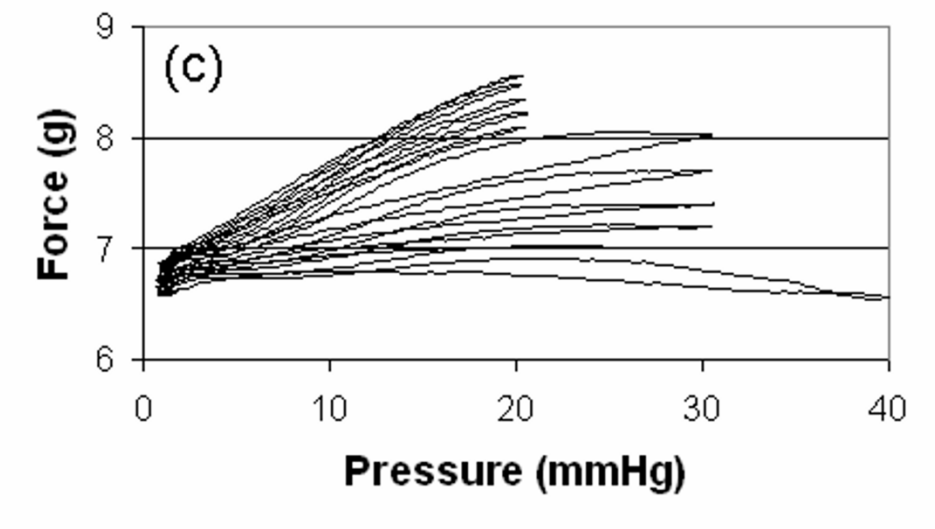

Figure 3.7 continued

3.4.4 Confocal Imaging

In multiple loaded configurations, collagen fibers of a TEVA were imaged using confocal microscopy. With a single TEVA mounted in the bioreactor, two successive images were taken at the same location within the vessel in two different loading scenarios: unloaded (Figure 3.8a) and loaded to 20 mmHg (Figure 3.8b). These images are located approximately 50 microns in from the abluminal surface. Densely arranged large and small bundles of collagen fibers can be seen. Quantification of these fibers at the various loading conditions will provide information relating fiber kinematics to the whole tissue kinematics as well as information on the evolution of fiber content, orientation, and kinematics with tissue growth and remodeling to more accurately generate microstructurally motivated biomechanical and growth and remodeling models.

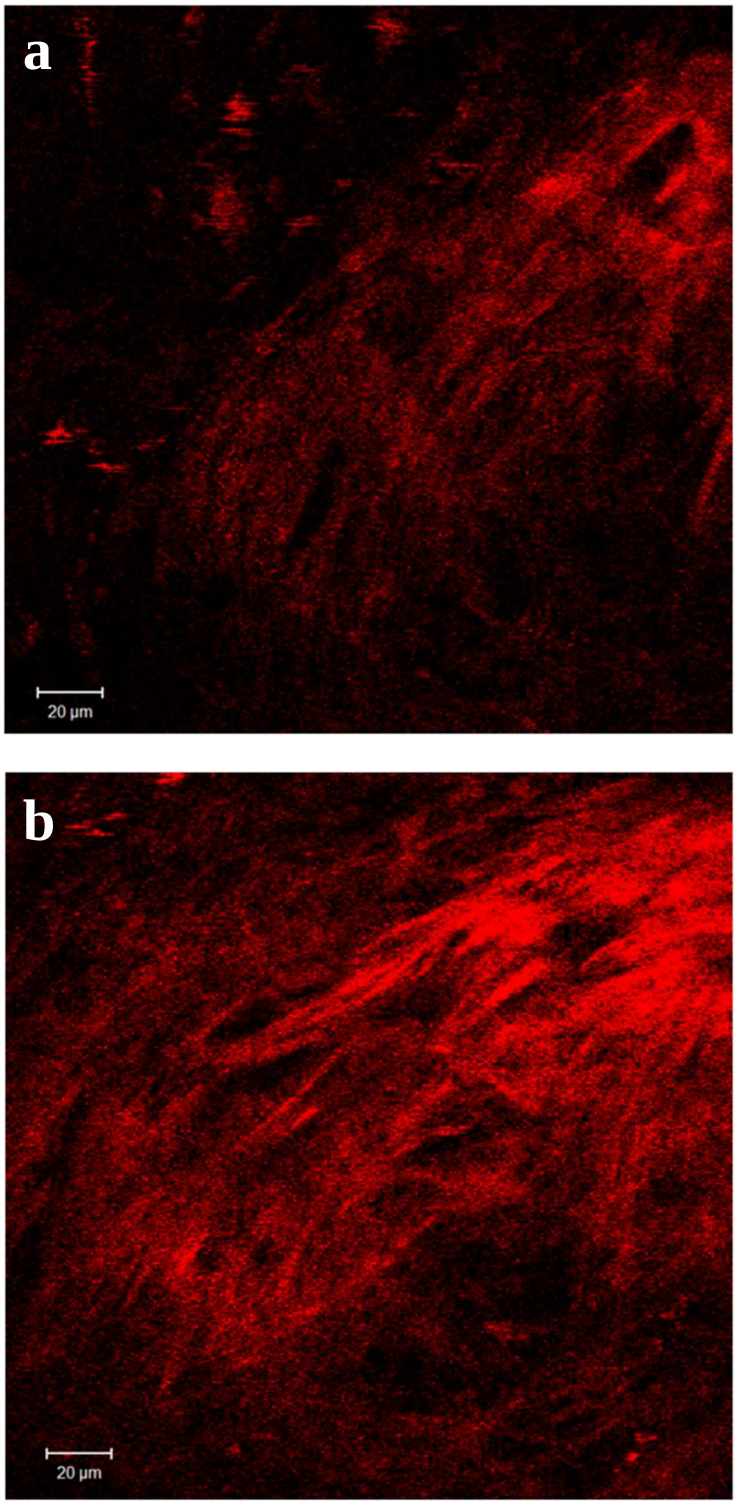

Figure 3.8. Collagen fibers on a statically cultured TEVA imaged using multiphoton confocal microscopy in the bioreactor. Two distinct loading scenarios, unloaded (a) and 20 mmHg (b), demonstrate the versatility of the bioreactor. Distinct fibers are formed during culture (scale bar 20 µm).

While Figure 3.8 simply demonstrates the ability of our system to image a vessel under various loading conditions, a representative sample of the microstructure would have to be determined using multiple images of the same vessel at random locations. Comparing the imaged length (255μm) to the total unloaded length (30 – 40mm), there is sufficient vascular length to attain multiple samples from different locations on the same vessel. In addition, photobleaching much be considered when imaging for longer time points. Multiple algorithms have been developed to detect fiber angle from images for use across a wide variety of mediums.[56, 57] Additionally these algorithms have been used to quantify structural information from biologics.[58-61] These algorithms will be sufficient to extract the quantitative structural information required for microstructurally motivated biomechanical models.

3.5 Discussion

Many techniques have been developed for constructing cellularized TEBVs, including gel-, polymer scaffold-, and self assembly-derived approaches. Common to all of these techniques is the opportunity to subject these vessels to mechanical loads. It has been shown that gel and polymer based approaches respond to cyclic circumferential stimulation in a manner which increases their mechanical strength.[19, 21, 49] Our goal was to develop a system that is capable of long term culture under multiaxial mechanical stimulation with the ability to monitor geometry, structural organization and vascular responses throughout the course of culture.

Many bioreactors have been designed to study the role of mechanical stimulation on TEBVs. Perhaps the most popular approach is to culture the TEBV on a distensible

tube, which allows for cyclic circumferential distension to be applied to the construct.[19, 21, 49] The advantage of such devices is the capability to deliver precise cyclic circumferential displacements. In addition, given that the distensible tube is impermeable to fluid, this tube also prevents leakage; a particularly significant challenge for polymeric scaffold- and gel-derived constructs at very early time-points in culture. There are, however, several disadvantages with these devices as it relates to quantifying mechanically-mediated remodeling of TEBVs. First, whereas the change in circumferential distension (i.e., change in inner diameter) is known, the true circumferential strain is not known and likely changes throughout culture. Consider the circumferential component of Green strain, $E_{\theta\theta} = (\lambda_\theta^{\,2} - 1)/2$, where $\lambda_\theta(r) = \pi r/(\Theta_o R)$ (in 3D) where r and R are radial locations in the current and stress-free configurations, respectively, and Θ_o is the opening angle (see Chuong and Fung, [62]) or $\lambda_\theta = d/D$ (in 2D) if we neglect variations across the vessel wall. In both the 3D and the 2D case, even though this device carefully controls d, since the stress-free diameter D of the vessel can change during culture, via growth and plasticity, the circumferential strain can change. In 3D, these changes are more pronounced, for example as the vessel thickens or compacts, or as the opening angle changes with growth and remodeling. Second, although the pressure applied to the distensible sleeve in known, the transmural pressure applied across the TEBV wall is not known; thus, the circumferential stress cannot be calculated. Third, in most cases the vessels are unconstrained and free to retract axially and, of course, given the distensible sleeve, wall shear stress cannot be applied along the luminal surface; thus multiaxial stimulation is not possible.

Another bioreactor which has multiaxial loading capabilities was designed by McCulloch *et al.*[63] This design allows for vascular pressurization as well as axial strain induction, however, this device is not capable of monitoring vascular geometry during culture which restricts the ability to perform stress analyses or quantify growth kinetics. In addition to McCulloch's device, it should be noted that there are several multiaxial organ culture devices that offer some of the same capabilities [40, 52, 64] and cylindrical biaxial mechanical testing devices for TEBV.[65] Whereas these devices offer the capability to quantify the tissue level biomechanical response, none of these devices have the ability to perform multiphoton confocal microscopy on the same (live) vessel at multiple time-points in culture.

One issue not addressed in this report is functional testing capabilities. Due to the non-contractile phenotype of cells used in the vascular equivalents, functional testing was not performed. However, as shown by Gleason *et al*., the design of this type of system permits functional tests.[53] As previously described, the structural hierarchy of a blood vessel controls its mechanical properties. Grenier *et al.* has shown significantly improved contractility of tissue engineered vascular media (TEVM) when human vascular smooth muscle cells (VSMC) were aligned circumferentially.[30] Because these vessels were created using the self-assembly method, alignment of VSMCs was accomplished by induced strain on two-dimensional tissue cultures prior to TEVM formation. The nature of the self-assembly method lends itself to pre-alignment while other approaches such as collagen gel or polymer scaffold will require remodeling of the three dimensional structure. Our device will allow for quantification of functionality intermittently during

culture. Additionally, because our device allows for microstructural imaging, we will be able to quantitatively relate structural organization to functional response.

In summary, we have developed a novel computer controlled bioreactor capable of long term culture subjected to external mechanical stimulation, intermittent cylindrical biaxial mechanical testing, functional testing, and confocal imaging of small diameter vascular tissue engineered grafts. This experimental device promises to provide new insights towards mechanically induced growth and remodeling of TEBVs. Using experimental results, theoretical models can be developed to mathematically describe these complex processes. Additionally, intermittent biomechanical testing in combination with microstructural imaging will allow us to gain further insights into both microstructure influence on tissue level biomechanics as well as constituent production, removal and reorganization in response to mechanical stimuli. Furthermore, these theoretical models will guide future experiments in an effort to optimize mechanical culture conditions to develop TEBV with adequate mechanical strength and functionality which can ultimately be used as an *in vivo* vascular graft. We have described capabilities for the system and shown performance data. This system allows users to gain further insights into mechanically induced growth and remodeling of TEBV.

CHAPTER IV

BIAXIAL BIOMECHANICS OF SA-TEBV

4.1 Introduction

Mismatched biomechanical properties between the graft and native surrounding tissue are commonly cited as a cause of graft failure, as noted in Chapter I. Given these observations, we submit that design criterion that minimize mechanically-induced restenosis in vascular grafts include, (i) matching the inner diameter of the host and the graft at physiological pressure and axial stretch, (ii) matching the compliance of the host and graft over the cardiac cycle, (iii) matching the axial force imposed by the graft on the host vessel under physiological loading, and (iv) matching the local circumferential and axial wall stresses of the graft to near homeostatic values of the native vasculature. The latter criteria will ensure that there are no significant changes in geometry or material properties after implant due to plasticity, fatigue or remodeling. From a practical perspective, these values would likely have to be matched to average values within a patient's grouping.

A constitutive model describing the mechanical response of the tissue to applied loads is required to predict the diameter, compliance, axial force, and local distribution of stresses across the vessel wall for a native or engineered blood vessel given a particular applied load (e.g., physiological loading). The goal of the current study is to characterize the biaxial biomechanical behavior of the tissue layers that comprise SA-TEBVs and identify a predictive constitutive model. Using a novel bioreactor and biomechanical testing device [66], biaxial biomechanical characterization of tissue engineered vascular

media (TEVM), tissue engineered vascular adventitia (TEVA), and two-layer tissue engineered vascular media-adventitia (TEVMA) was performed. These data were used to identify material parameters for TEVM and TEVA using the constitutive model of Baek *et al*. [67] We found that the compliances of the TEVM, TEVA, and TEVMA were within the range of values reported for coronary arteries taken from the literature. In addition, these vessels are pseudo-elastic and nearly incompressible over physiological loading. Identified material parameters for TEVM and TEVA provide a good fit to experimental data and predict the mechanical response of TEVMA well. Such predictive models can serve as a tool to quantify deformation to applied loads and local stresses and perform design analyses to indentify new fabrication strategies to control the SA-TEBV mechanical response.

4.2 Theoretical Framework

Initial biomechanical testing data suggests that finite elasticity is an appropriate framework to model the pseudo-elastic response of these tissues. Thus, these tissue engineered vessels will be modeled as a non-linear, elastic, anisotropic, incompressible solid which experience large deformations. The TEVM and TEVA are assumed to be homogeneous, as is each layer of the TEVMA. The kinematics and constituent strain energy functions for each layer are distinct due to differences in the stress-free reference state and material response of each layer [68]; we shall follow this approach.

For inflation and extension of a two-layer, axisymmetric tube, with each layer possessing residual-stress in the traction free state, one typically considers four configurations when performing stress analyses: a current (loaded) configuration (β_t), the traction free, unloaded configuration (β_u) and a (nearly) stress free configurations of each

layer (β_o^M and β_o^A, Figure 4.1). Thus, we must specify the stress free configuration for the media (R_o^M, R_i^M, Λ^M, and Θ_o^M) and the stress free configuration for the adventitia (R_o^A, R_i^A, Λ^A, and Θ_o^A), where R_o^J is the outer radius, R_i^J is the inner radius, Λ^J is the axial stretch and Θ_O^J is the opening angle (J= M or A, denoting media and adventitia, respectively). Note that Θ_o^M and Θ_o^A are one measure of the opening angle which occurs when a single radial cut is imposed in a vessel ring in the unloaded configuration.

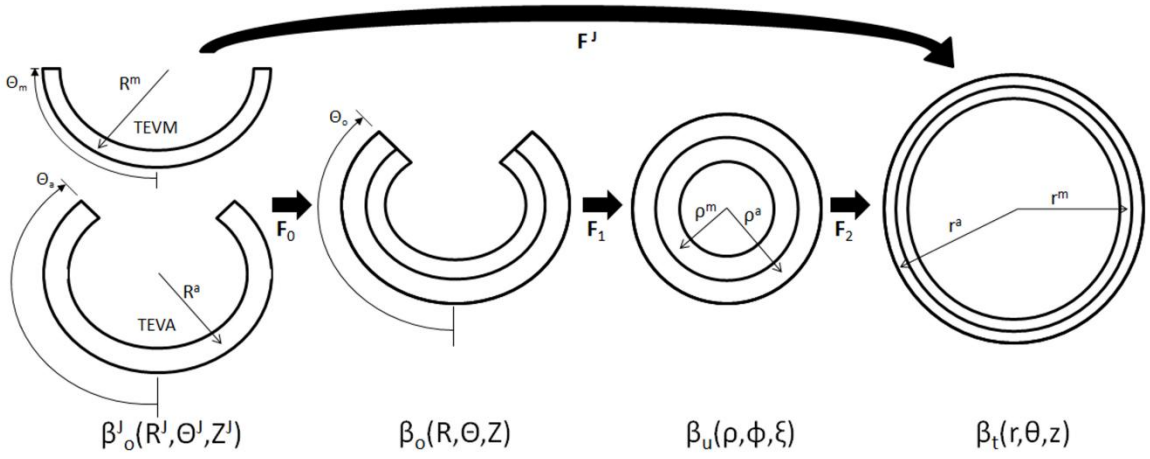

Figure 4.1. Kinematics for inflation and extension of a two layer elastic cylinder.

The deformation gradients, $\mathbf{F}^M$ and $\mathbf{F}^A$, are the gradient of the map that takes points from an appropriate stress free configuration (β_o^M and β_o^A, respectively) to the loaded configuration (β_t); the components of $\mathbf{F}^J$ and $\mathbf{C}^J$, the right Cauchy-Green deformation tensor, are diagonal matrices, given as,

$$[\mathbf{F}^J] = diag\left\{\frac{\partial r}{\partial R^J}, \frac{\pi r}{\Theta_o^J R^J}, \lambda_z \Lambda^J\right\} \tag{4.1}$$

$$[\mathbf{C}^J] = diag\left\{\left(\frac{\partial r}{\partial R^J}\right)^2, \left(\frac{\pi r}{\Theta_o^J R^J}\right)^2, \left(\lambda_z \Lambda^J\right)^2\right\} \tag{4.2}$$

where λ_z and Λ^J are axial stretches for the motion from β_u to β_t and β_o^J to β_u, respectively. Finally, given the incompressibility assumption, $\det[\mathbf{F}^J] = 1$; thus

$$\frac{\partial r}{\partial R^J} = \frac{\Theta_o^J R^J}{\pi r \lambda_z \Lambda^J} \quad \text{and} \quad r = \sqrt{r_o^2 - \frac{\Theta_o^J}{\pi \lambda_z \Lambda^J}\left(\left(R_o^J\right)^2 - (R^J)^2\right)} \tag{4.3}$$

where r_o is the outer radii of the vessel in β_t and r and R^J are the radius of interest in β_o^J and β_t (Figure 4.1). In the framework of finite elasticity, the Cauchy stress is defined as $\mathbf{T} = -p\mathbf{I} + \mathbf{2} \cdot \mathbf{F}^J \cdot (dW^J/d\mathbf{C}^J) \cdot (\mathbf{F}^J)^T$, where $\mathbf{I}$ is the identity tensor and W^J is the strain energy density function for material J and p is the Lagrange multiplier that arises due to the incompressibility constraint.

The equations of equilibrium for a two-layer vessel may be written as,

$$P = \int_{r_i}^{r_{MA}} \left(\hat{T}_{\theta\theta}^M - \hat{T}_{rr}^M\right)\frac{dr}{r} + \int_{r_{MA}}^{r_o} \left(\hat{T}_{\theta\theta}^A - \hat{T}_{rr}^A\right)\frac{dr}{r} \tag{4.4}$$

$$f = \pi \int_{r_i}^{r_{MA}} \left(2\hat{T}_{zz}^M - \hat{T}_{rr}^M - \hat{T}_{\theta\theta}^M\right) r dr + \int_{r_{MA}}^{r_o} \left(2\hat{T}_{zz}^A - \hat{T}_{rr}^A - \hat{T}_{\theta\theta}^A\right) r dr \tag{4.5}$$

where r_{MA} is the radial location of the media-adventitia interface in the loaded configuration (β_t) and $\hat{T}_{ii}^J = 2 \cdot \left(F_{ii}^J\right)^2 \left(dW^J/dC_{ii}^J\right)$, where $i = r, \theta, or\ z$. Note that f in Equation (4.5) is adjusted for the axial force generated from end-cap pressure existing in all in vitro biaxial testing devices

For single layer vessels (i.e., TEVM and TEVA) Equations (4.4) & (4.5) reduce to

$$P = \int_{r_i}^{r_o} \left(\hat{T}_{\theta\theta}^J - \hat{T}_{rr}^J\right) \frac{dr}{r} \tag{4.6}$$

$$f = \pi \int_{r_i}^{r_o} \left(2\hat{T}_{zz}^J - \hat{T}_{rr}^J - \hat{T}_{\theta\theta}^J\right) r dr \tag{4.7}$$

where $J = M$ for TEVM and $J = A$ for TEVA.

Constitutive Model. We used the strain energy function of Baek et al. [67], which is a simple extension of the model of Holzapfel et al. [69] for each layer. This strain energy function is

$$W^J = b^J\left(I_C^J - 3\right) + \sum_{k=1,2,3,4} \frac{b_{1k}^J}{4b_{2k}^J} \left\{ exp\left[b_{2k}^J \left(\left(\lambda_k^J\right)^2 - 1 \right)^2 \right] - 1 \right\} \tag{4.8}$$

where b^J, b_{1k}^J, and b_{2k}^J are material parameters, $I_C^J = tr(\mathbf{C}^J) = C_{rr}^J + C_{\theta\theta}^J + C_{zz}^J$ is the first invariant of $\mathbf{C}^J$, $\left(\lambda_k^J\right)^2 = C_{\theta\theta}^J \sin^2\left(\alpha_k^J\right) + 2C_{\theta z}^J \sin\left(\alpha_k^J\right)\cos\left(\alpha_k^J\right) + C_{zz}^J \cos^2\left(\alpha_k^J\right)$ is

the stretch of the k^{th} fiber family, and α_k^J is the associated angle between the axial and fiber directions. For inflation and extension tests (given appropriate material symmetry), $C_{\theta z}^J = 0$, so that $\left(\lambda_k^J\right)^2 = C_{\theta\theta}^J \sin^2\left(\alpha_k^J\right) + C_{zz}^J \cos^2\left(\alpha_k^J\right)$, We considered four fiber families with $\alpha_1^J = 0^o$, $\alpha_2^J = 90^o$, $\alpha_3^J = -\alpha_4^J = \alpha^J$.

Parameter Identification. Material parameters were determined for TEVM and TEVA via a nonlinear regression technique that minimized the error between measured values of P and f and calculated values of P and f from Equations (4.6) & (4.7) given measured values of outer diameter and length under these measured values of P and f and the measured stress free configuration. We seeked to identify material parameters via nonlinear regression that minimize the error function

$$error = \frac{1}{n}\left[\sum_{i=1}^{n}\left(\frac{P_{meas}(i) - P_{model}(i)}{P_{max}}\right)^2 + \sum_{i=1}^{n}\left(\frac{f_{meas}(i) - f_{model}(i)}{f_{max}}\right)^2\right] \quad (4.9)$$

which quantifies the difference between experimental data and modeling predictions for *n* data points. P_{max} and f_{max} are the maximum pressure and axial force in their respective data set. Calculations were performed in MatLab using the *lsqnonlin* subroutine which allows the prescription of upper and lower limits on the parameter values. The lower and upper limits of the parameters were prescribed as $b^J \in [10^2, 10^8]$, $b_{1k}^J \in [10^{-5}, 10^8]$, kPa, $b_{2k}^J \in [10^{-5}, 10^3]$, and $\alpha^J \in [0^o, 90^o]$.

Evaluate Predictive Capability of Model. Using the material parameters determined for the TEVM and TEVA, the mechanical response of a two-layer TEVMA was predicted using this constitutive model. Namely, the unloaded geometry and pressure

from the experimental data were used to calculate the outer diameter and axial force via Equations (4.4) & (4.5). The model predictions were compared to experimental data from the TEVMA using a standard R^2 value to evaluate the predictive capability of the model and material parameters.

4.3 Methods and Materials

4.3.1 Cell Isolation and Construct Fabrication

Human dermal fibroblasts (hDF) were isolated from a human skin biopsy as previously described.[33] Briefly, the dermis was separated from the epidermis by incubation in thermolysin (Sigma, Oakville, ON, Canada). hDF were enzymatically dissociated from the dermis using collagenase H (Roche, Indianapolis, IN), centrifuged, plated in tissue culture flasks and cultured in Dulbecco-Vogt modified Eagle medium (DMEM; Invitrogen, Burlington, ON, Canada) supplemented with 10% fetal bovine serum (FBS; Hyclone, Logan, UT) and antibiotics (penicillin (100U/ml, Sigma, Oakville, ON, Canada), gentamicin (25ug/ml, Schering, Pointe-Claire, QC, Canada)). Smooth muscle cells were isolated from a human umbilical cord (hUSMC). An umbilical cord was obtained from a healthy newborn and processed immediately. The umbilical vein was rinsed with phosphate buffered saline (PBS), opened longitudinally and pinned to a dissection board with the lumen facing upward. Endothelial cells (EC) were gently scraped from the underlying basement membrane using a scalpel blade without grossly damaging the subendothelial layer. Bands of the thin underlying media layer were then collected, cut into smaller pieces and placed in a gelatin-coated Petri dish to allow the outgrowth cells to attach to the gelatin. Explants were cultured in Dulbecco-Vogt modified Eagle medium with Ham's F12 (ratio 3:1; Invitrogen, Burlington, ON, Canada)

supplemented with 10% fetal bovine serum and antibiotics until cells migrated out of the biopsy samples. Freshly isolated cells were frozen for long term storage and subsequent use. Cells between passage 3 and 7 were used for tissue production.

The tissue-engineered vascular constructs were developed as previously described.[33] Briefly, human umbilical smooth muscle cells (hUSMC) or human dermal fibroblasts (hDF) were seeded at a density of $1x10^4$ cells/cm^2 in tissue culture flasks and cultured in DMEM supplemented with 10% FBS. Antibiotics were added to DMEM and sodium L-ascorbate (50 μg/ml, Sigma, Oakville, ON, Canada) was added to the culture medium of vascular constructs to stimulate ECM synthesis. Cells were cultured 28 for days until their neosynthesized ECM proteins had self-assembled into an adherent living tissue sheet, which was then gently detached from the culture flask using fine forceps. The tissue sheet was rolled onto a polystyrene tubular support of 4.5mm in diameter and maintained in culture in DMEM-Ham (3:1) supplemented with 10% bovine Fetal Clone II serum (HyClone), antibiotics and 50 μg/ml of sodium ascorbate. TEVM were developed by wrapping sheets formed from hUSMCs. TEVA were developed by wrapping tissue sheets formed from hDF.

The production of the TEVMA utilized a new and original technique allowing the fabrication of the TEVMA in a single step assembly (ssTEVMA). SMC and DF were seeded in two distinct compartments of a tissue culture plate (Corning, Lowell, MA) separated by a custom designed spacer. The spacer was removed 24 hours following cell seeding in order to allow cell adhesion to the underlying tissue culture plastic. The two cell types migrate toward each other to form a continuous sheet of tissue with two distinct areas containing SMC and DF with an integrated region at their interface.[70] The spacer

was placed in the center of the tissue culture flask to maintain a ratio of media to adventitia thickness of 0.5. All vascular constructs were maintained for a 14-day-culture period on the tubular support at 37ºC in a humidified incubator containing 8% CO_2. The culture medium was changed three times per week. Note, that vessels were grown and fabricated in the Laboratoire d'Organogénèse Expérimentale (LOEX) in Quebec City, Quebec, Canada. Two weeks after the tissue sheets were wrapped around the tubular mandrel, the vessels were shipped overnight to the Georgia Institute of Technology in Atlanta, GA, USA for biomechanical testing.

4.3.2. Biaxial Biomechanical Testing

Rings sections, approximately 2mm wide, were cut from the construct prior to biomechanical testing to determine if the traction free configuration contained residual stress, With the vessel still on the mandrel, a scalpel was used to remove a 4mm section from the end of the vessel and discarded. The ring section was subsequently cut from the remaining length of the construct. These sections were gently removed from the mandrel using forceps and placed into a tissue culture dish containing culture media at 37°C. Each ring was imaged on an inverted microscope (Zeiss, Axiovert 40C) equipped with a digital camera. With minimal movement of the sample, fine scissors were used to impose a radial cut in the ring while suspended in the culture media. An image of the cut section was taken on the same device and opening angle information was processed in MATLAB (MathWorks, Inc.).

Cylindrical biaxial biomechanical testing was performed on the vascular constructs using a custom built bioreactor.[66] Each construct was mounted to the cannula using silicon o-rings and submerged in the same formulation of culture media in

which the tissue sheets were grown. After the TEBV was mounted in the device and placed in the incubator, a minimum of 30 minutes was given for the TEBV and culture medium to equilibrate to the incubator environment. Immediately prior to testing, 3 preconditioning cycles to 50 mmHg were performed. Following preconditioning, the vessel length was measured as the distance between each o-ring using a digital caliper; this was defined as the unloaded length. The testing protocol consisted of 3 inflation/deflation cycles to 150mmHg at a rate of 2 mmHg/sec at fixed axial stretches of λ_z = 1.0, 1.1, 1.2 and 1.3 for the TEVA and TEVMA and λ_z = 1.0, 1.1 and 1.2 for the TEVM, while monitoring the outer diameter and axial force in real time. The axial stretch is defined as $\lambda_z = l/L_o$ where l is the loaded length and L_o is the unloaded length. An ultrasound probe was used to measure the vessel wall thickness.

4.3.3. Stress-strain response

With measured values of the axial force, transmural pressure, axial stretch, outer diameter, and wall thickness, stress analyses may be performed. The circumferential Green strain

$$E_{\theta\theta} = \frac{1}{2}\left({\lambda_\theta}^2 - 1\right) \tag{4.10}$$

was used, where λ_θ represents the circumferential stretch ratio. The circumferential stretch is defined as $\lambda_\theta = d/D_o$ with d as the loaded midwall diameter and D_o the unloaded midwall diameter. Note that unlike linearized measures of strain, the Green

strain is an appropriate strain measure for large deformations. The mean circumferential stress ($\bar{\sigma}_\theta$) and mean axial stress ($\bar{\sigma}_z$) are,

$$\overline{\sigma}_{\theta} = \frac{Pa}{h} \tag{4.11}$$

$$\overline{\sigma}_{z} = \frac{f}{\pi h(2a + h)} \tag{4.12}$$

respectively, where P is the transmural pressure, f is the axial force, a the lumen radius and h is the thickness of the vessel wall. For all three vessel types, incompressibility was assumed for the stress analysis; thus, $\det(\mathbf{F}) = 1$. Compliance over the physiological pressure range may be defined through the relation

$$C\Delta P = \Delta\varepsilon = \frac{r_m^{sys} - r_m^{dys}}{\bar{r}_m} \tag{4.13}$$

where C is compliance, ΔP is the pressure difference between systolic pressure and diastolic pressure, $\Delta\varepsilon$ is the local linearized cyclic strain experienced over ΔP, r_m^{sys} is the midwall radius at systolic pressure, r_m^{dys} is the midwall radius at diastolic pressure, $\bar{r}_m$ is the midwall radius at mean pressure.

4.4 Results

4.4.1. Pseudoelastic response and Incompressibility

Three inflation/deflation cycles were performed at each axial stretch to ensure consistency of the sample response. Between cycles 1 and 2, there was a slight shift of the pressure-diameter curve of approximately 40μm at 150mmHg (Figure 4.2a) for a representative TEVA. However, there were negligible differences in the pressure-diameter curves (<10μm at 150mmHg) between cycle 2 and all subsequent cycles. Not only was there a shift at the maximum pressure tested, there is also a notable shift throughout the pressure range. There was more hysteresis occurring during the first cycle than in the other two cycles. These same trends were seen with the axial force (Figure 4.2b) as a 0.12N shift occurs at 150 mmHg between cycles 1 and 2, while all subsequent cycles had a much smaller shift (<0.05N). This plot also provided insight into the energy dissipation of the vascular construct between loading and unloading. Only a small degree of hysteresis is observable following the first loading/unloading cycle; thus, finite elasticity is an appropriate framework for stress analysis of these so-called pseudo-elastic materials. This response is not limited to the TEVA, but is also seen in TEVM and TEVMA.

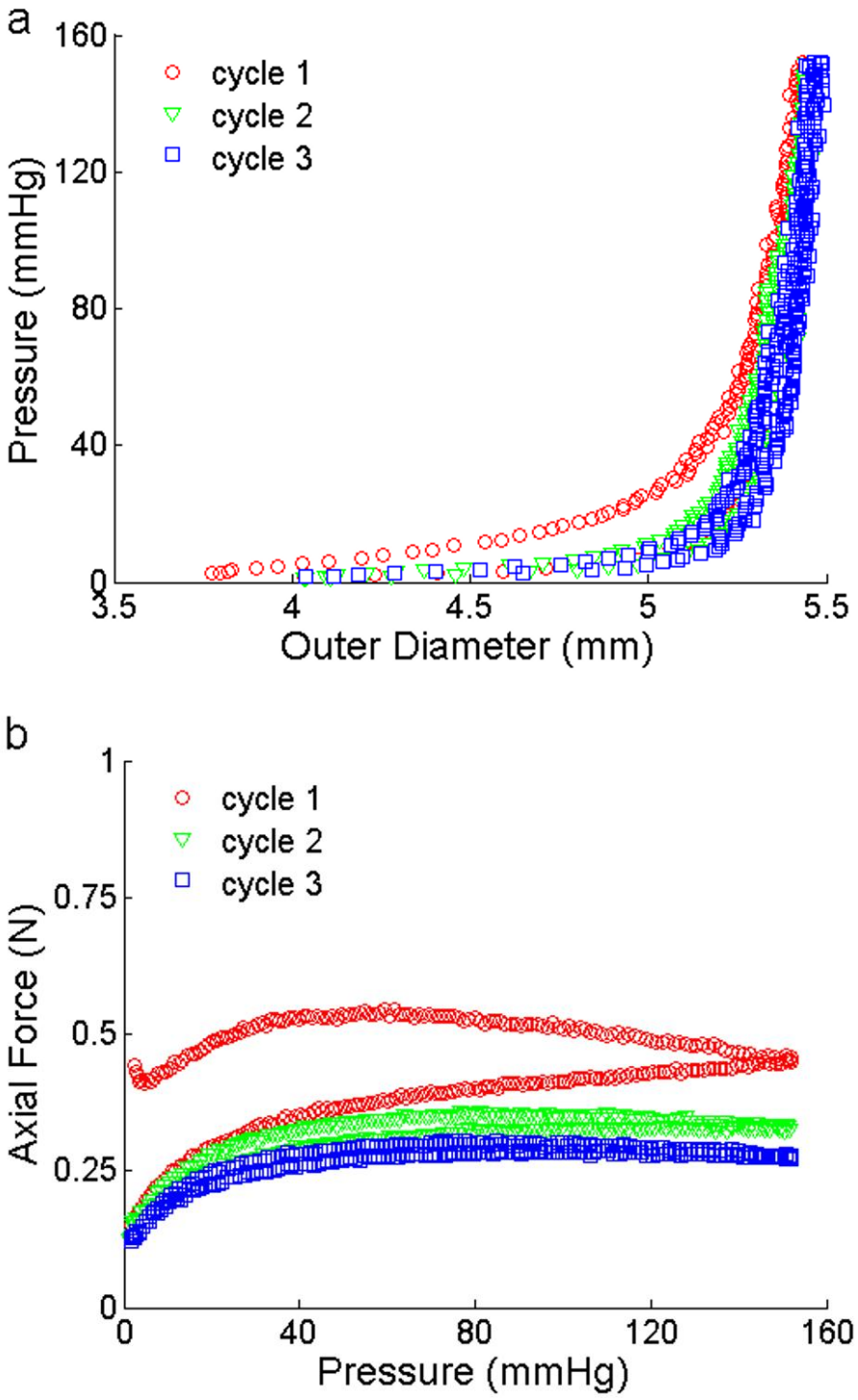

Figure 4.2. Biomechanical repeatability occurs after the first cycle for pressure-diameter (a) and axial force-pressure (b) responses of TEVA (shown at an axial stretch of 1.2). The repeatability is also seen in the other two construct types.

A negligible difference (<50μm) is observed when comparing the measured wall thickness of a TEVA to the predicted thickness assuming incompressibility with reference to the unloaded configuration, throughout the inflation/deflation cycle (not shown). Similar results were obtained with the TEVM and TEVMA.

4.4.2. Opening angle

A representative image of the opening angle of a TEVMA (Figure 4.3) indicates an angle of 107°. The experimental methods used to determine the opening angle for each vessel must be performed extremely carefully to avoid impacting the results. Table 4.1 shows the unloaded geometry as well as opening angle information for all of the vessels tested. Additionally, this table shows mean and standard deviations for each vessel type.

Table 4.1. Vascular geometry in the unloaded configuration as well as opening angle data (measured as arc length) for all construct types. Measured compliance over physiologic range (80-120mmHg) calculated using Equation (4.13).

Construct	Number	Opening Angle °	Unloaded OD (mm)	Unloaded Thickness (μm)	Unloaded Length (mm)	Compliance (MPa^{-1})
TEVA	1	n/a	5.35	518	24.45	2.90
	2	32.25	5.32	614	25.35	2.11
	3	44.5	5.36	574	26.11	3.55
	4	81.25	5.57	571	27.48	3.25
	5	107.0	5.43	498	28.40	2.97
	mean	66.25	5.41	555	26.36	2.96
	std. dev.	34.23	0.10	46.5	1.59	0.54
TEVM	1	0.0	4.92	400	16.5	2.64
	2	133.0	4.77	360	28.0	2.61
	3	9.0	5.03	429	25.1	2.52
	mean	47.33	4.91	397	23.2	2.59
	std. dev.	74.33	0.13	34.6	5.98	0.06
TEVMA	1	135.0	5.12	485	26.02	3.31
	2	0.0	5.04	515	27.50	2.90
	3	100.0	4.98	442	26.11	2.81
	4	10.0	4.98	396	24.38	1.90
	mean	61.25	5.03	459.5	26.00	2.73
	std. dev.	66.63	0.07	51.79	1.28	0.59

There was a large variability in the opening angle measurements. The large variation in the opening angle is a result of both variability in the vessels and the experimental method of cutting the construct. It should be noted that some constructs exhibited residual

stresses in other directions as indicated by a twisting of the ring in the circumferential direction; these deformations, however, were not quantified.

Figure 4.3. Representative image of opening angle for TEVA in culture media at 37ºC; taken from an inverted microscope. Results suggest residual stresses are developed in the vessel during maturation.

4.4.3. Biaxial Biomechanical Behavior

Representative results of pressure – outer diameter and axial force – pressure curves for TEVA (Figure 4.4a and b), TEVM (Figure 4.4c and d) and TEVMA (Figure 4.4e and f) indicate a difference between the 3 construct types. Differences were observed (though not statistical) when comparing the pressure - diameter curves and calculated compliance over the cardiac cycle for the three construct types. Over the pressure range tested, the TEVA was the most compliant construct while the TEVM was

the least compliant. The compliance of the TEVMA fell in between the compliance of the other two constructs, indicating contribution to mechanical integrity from both the TEVM and TEVA. With more constructs tested, we believe that a statistical difference would result. The biaxial biomechanical response of a human coronary artery at an axial stretch of $\lambda = 1.1$ is shown (Figure 4.4e and 4f) to compare the response of a native vasculature to that of a tissue engineered vessel. This response is generated from the model and material parameters determined by.[69] There was a definitive difference between the responses of two vascular constructs at lower pressures, however, the response became much more similar within the physiologic range.

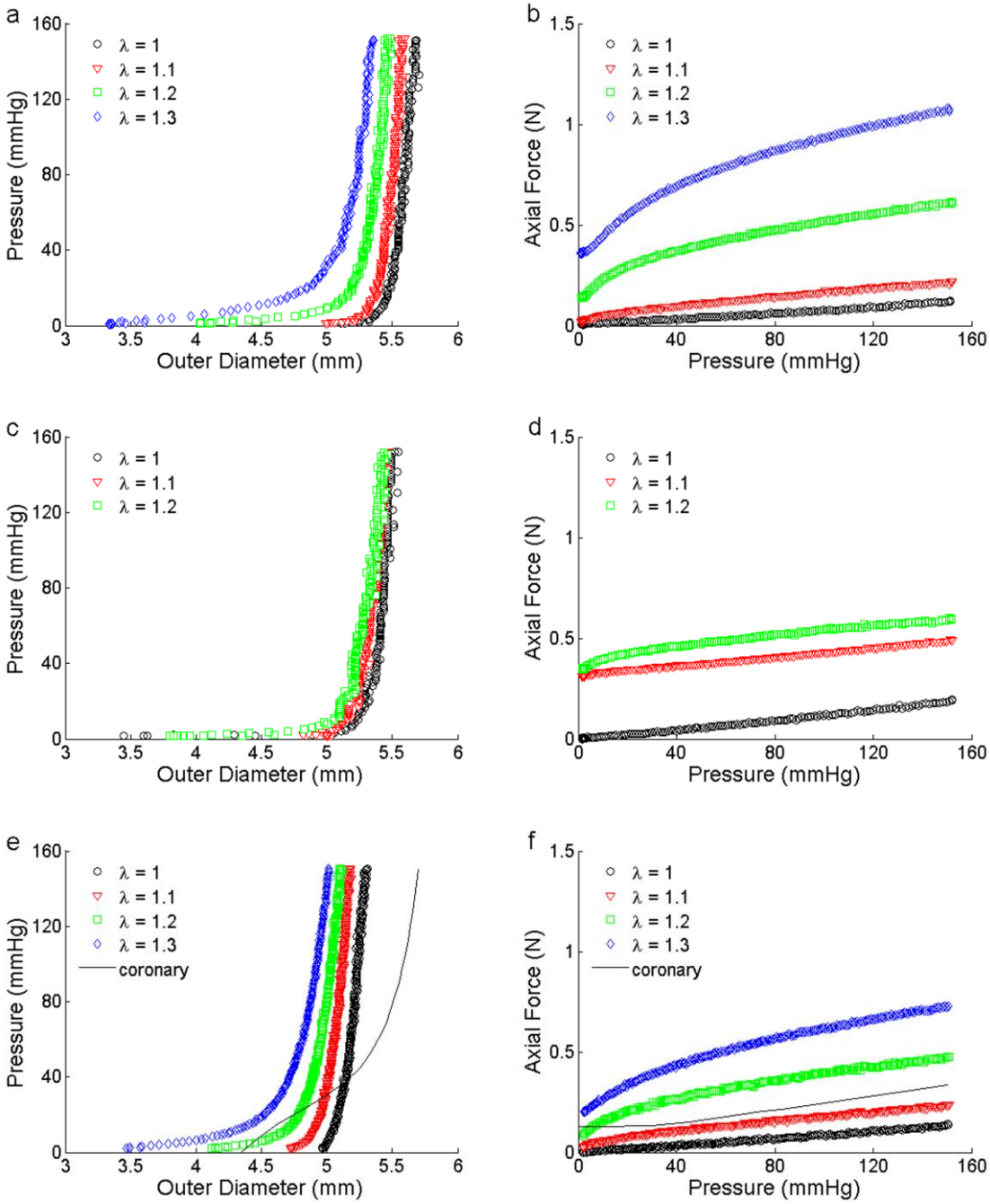

Figure 4.4. Representative biaxial biomechanical response of a TEVA (a,b), TEVM (c,d) and TEVMA with a representative coronary artery (e,f) using the constitutive model and material parameters of Holzapfel *et al*., 2007 [71] during standard cyclic inflation testing at fixed axial length.

Because the pressure-diameter response depends on both material properties and geometry, it is difficult to quantify differences in the material properties between different vessels from these plots. Stress-strain plots, however, only depend on material properties; thus, differences in the stress-strain response indicate differences in the material properties. Using Equations (4.11), (4.12) and the incompressibility assumption, mean circumferential Cauchy stress – circumferential Green strain plots were generated for a representative TEVA and TEVM (Figure 4.5a and b) for the fixed length inflation tests. There were distinct differences in the stress analysis between the two construct types further suggesting that there were differences in material properties.

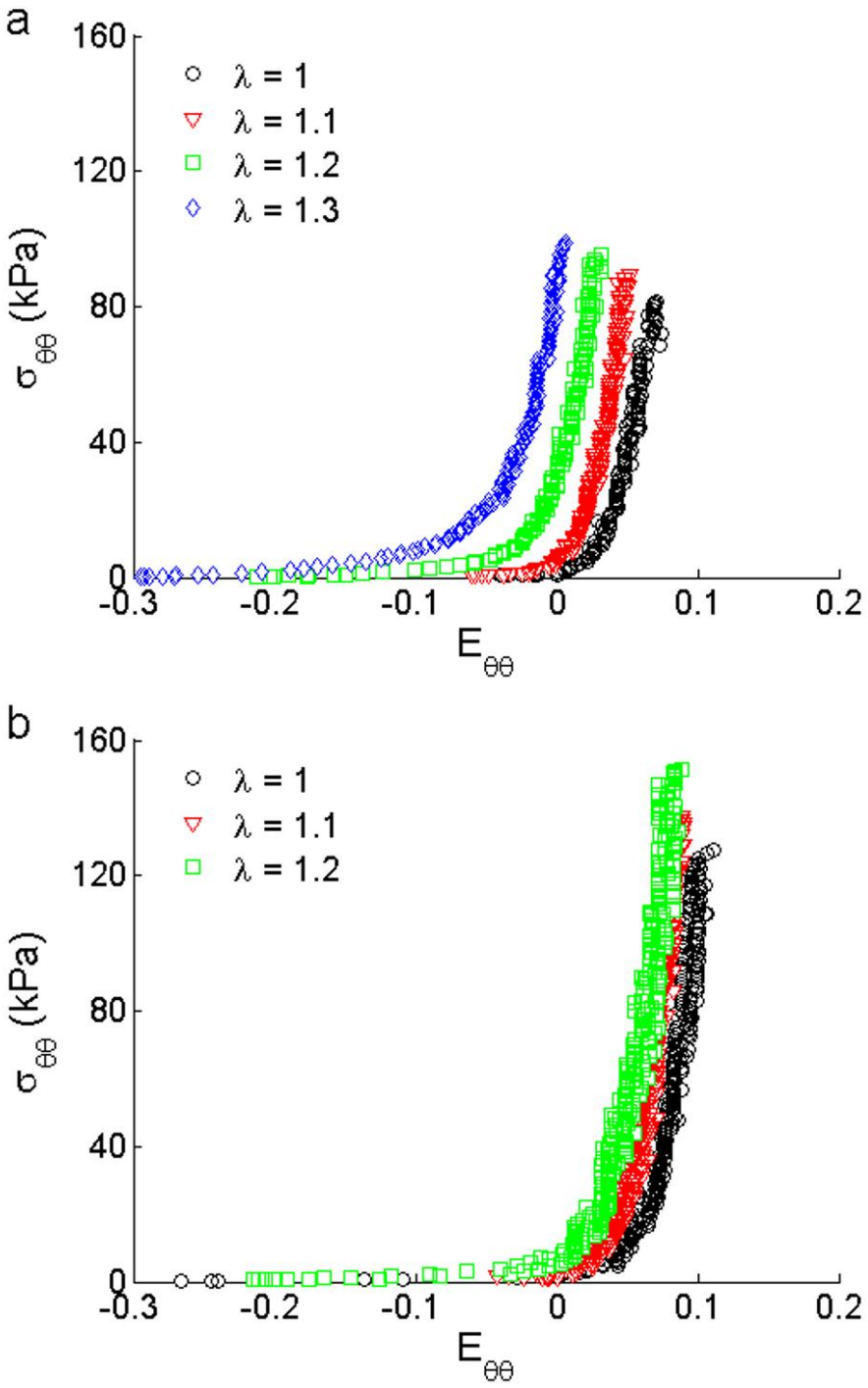

Figure 4.5. Mean circumferential Cauchy stress vs. circumferential Green strain for a representative TEVA (a) and TEVM (b) at fixed axial stretches.

4.4.4 Constitutive Modeling

Material parameters were identified for each TEVM and TEVA tested (Table 4.2). Final parameter values were insensitive to initial parameter values used in the nonlinear regression solver algorithm. The high R^2 values suggested that these parameters provided a good fit to data.

Table 4.2. Material parameters for TEVM and TEVA using constitutive Equation (4.8) by minimizing the error between experimental data and model predictions (Equation (4.9)) via non-linear regression.

Vessel	b^J (kPa)	b_{11}^J (kPa)	b_{21}^J	b_{12}^J (kPa)	b_{22}^J	b_{13}^J (kPa)	b_{23}^J	α^J	R^2
TEVM #1	0.10	56.82	29.84	2.38e-4	64.64	65.54	16.26	51.60	0.927
TEVM #2	65.02	64.86	19.68	24.09	1e-5	1.19e-6	100	19.06	0.866
TEVM #3	83.96	0.282	31.36	45.06	1e-5	0.159	27.84	66.54	0.811
mean	49.69	40.65	26.96	23.05	21.55	22.38	48.03	45.74	0.868
std. dev.	43.98	35.19	6.35	22.55	37.32	37.39	45.38	24.28	0.063
TEVA #1	0.10	20.43	5.212	24.87	1.33	59.71	32.11	57.83	0.922
TEVA #2	0.10	1.815	17.08	32.19	0.88	11.74	16.49	59.07	0.912
TEVA #3	0.10	10.07	19.17	26.23	1.78	35.62	10.95	45.90	0.942
TEVA #4	0.10	40.21	16.49	22.94	0.61	60.78	7.305	52.20	0.880
TEVA #5	0.10	39.13	22.60	49.40	0.12	34.75	8.391	45.09	0.931
mean	0.10	22.33	16.11	31.13	0.94	40.52	15.05	52.02	0.918
std. dev.	0.00	17.15	6.55	10.79	0.64	20.40	10.18	6.50	0.032

A representative example of the model fitting the experimental biaxial biomechanical properties can be seen in Figure 4.6a and b; these figures illustrate fitting for a

representative TEVA. The model fit TEVA constructs better than the TEVM as indicated by the higher R^2 value.

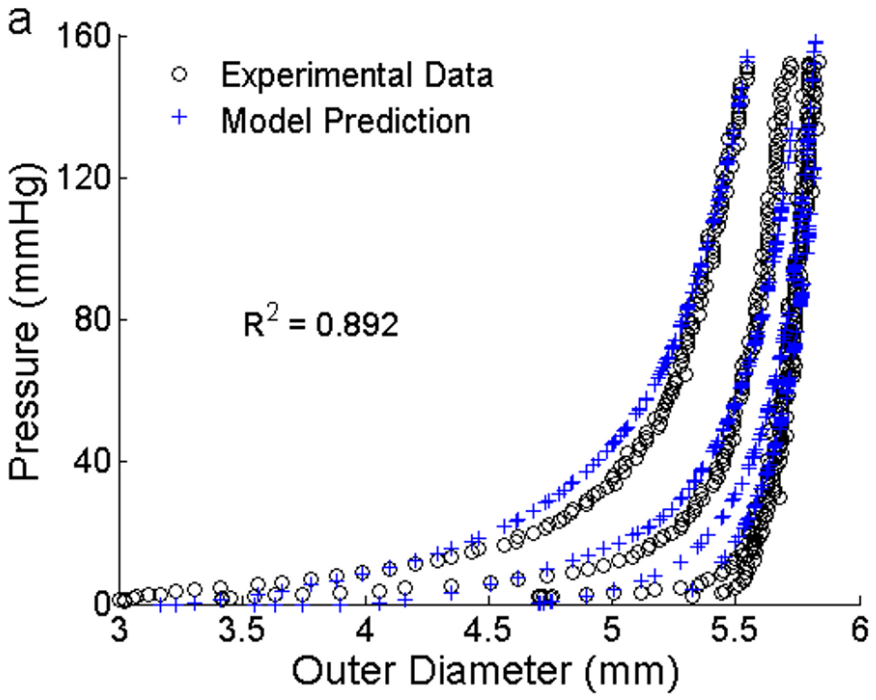

Figure 4.6. Pressure-diameter (a) and axial force-pressure (b) for TEVA#5 (black circles) and model predictions using the parameters for TEVA#5 from Table 4.2 (blue pluses).

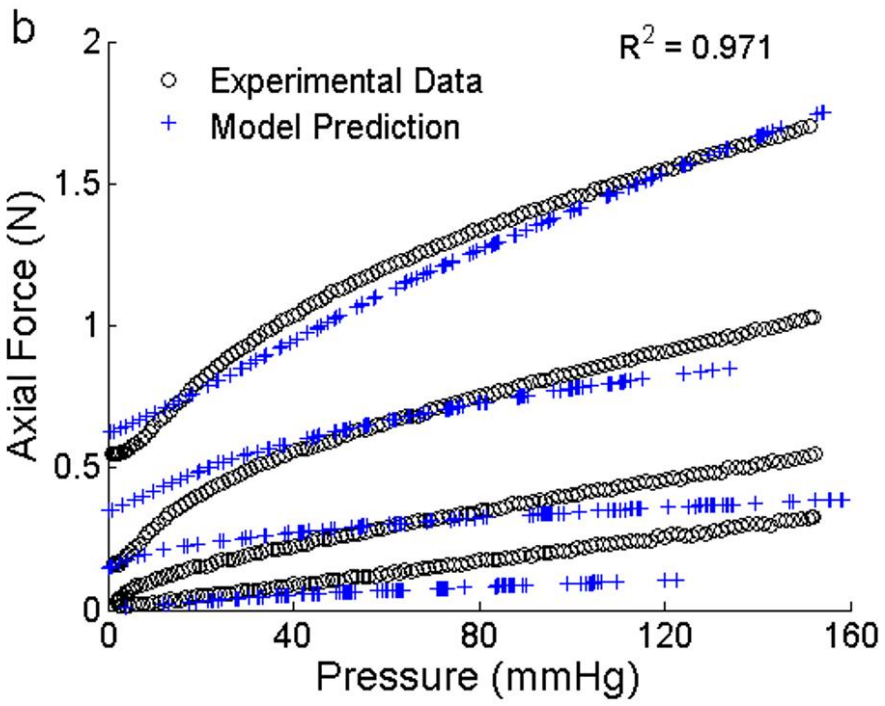

Figure 4.6 continued

The parameters identified for the TEVA and TEVM constructs were used to predict the biaxial response of the TEVMA. Comparing the experimental values to the predicted values, the model was a good predictor of the material response of the two layer construct; a representative example of the model's biaxial biomechanical predictive capabilities is seen in Figure 4.7a and b. Due to the deviations in the parameters within the TEVM (Table 4.2), using the mean values of these parameters in the two-layer model introduced large errors into the predictive model. Therefore, a combinatorial approach was taken to determine which TEVM, paired with the mean values for the TEVA produced the smallest mean error in predicting the TEVMA response. While all sets of parameters produced reasonably good fits, it was found that TEVM#1 could be used to best predict the two-layer response with an average R^2 value of 0.424.

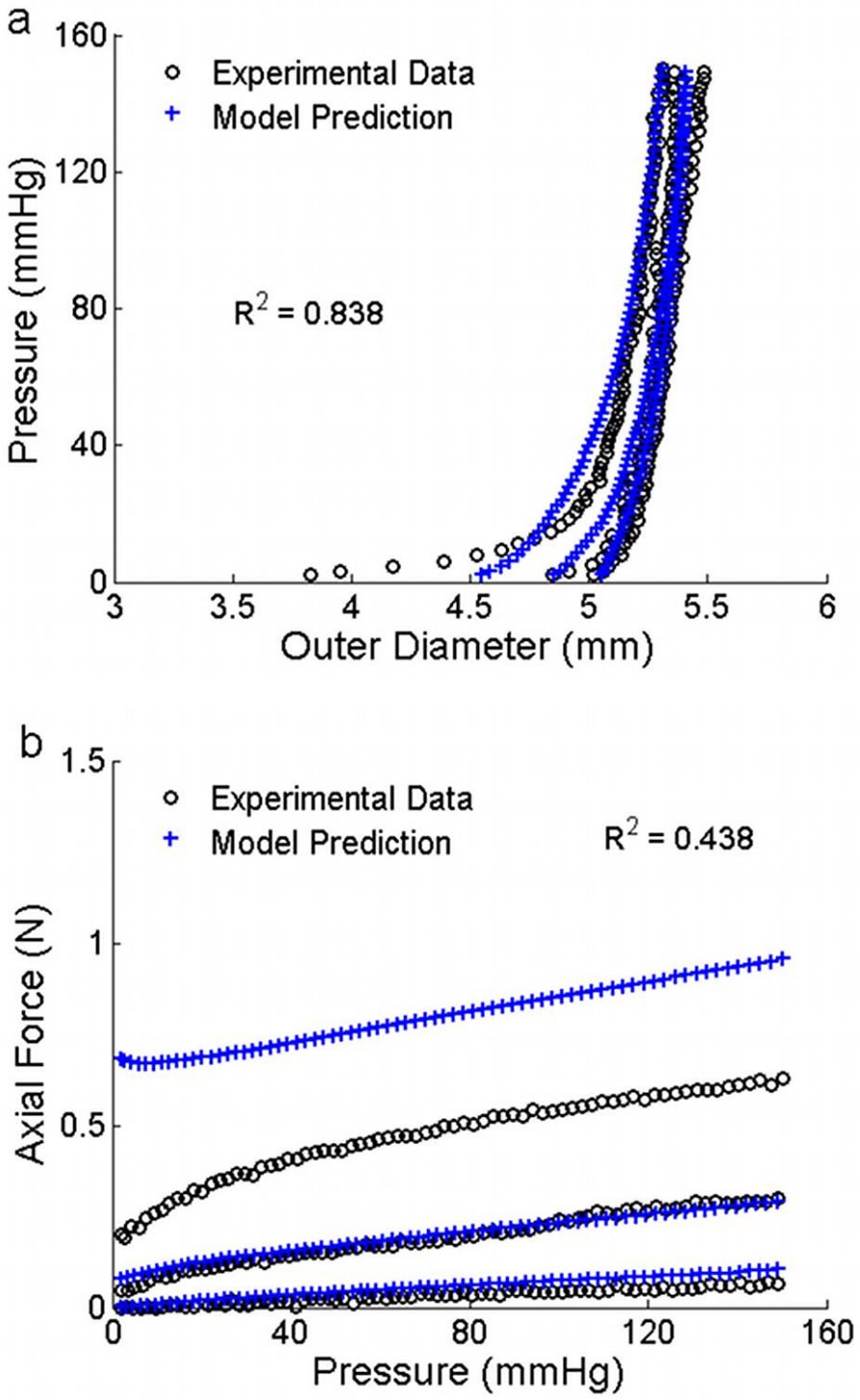

Figure 4.7. Predicted pressure-diameter (a) and axial force-pressure (b) of TEVMA (blue pluses) using the material parameters from Table 4.2 along with experimental measurements (black circles).

However, most of these errors are associated with a specific loading region; namely, discrepancies arise at low pressures and high axial stretches. This is likely due to the model predicting a less compliant response in the axial direction. The average R^2 value of the pressure-diameter plots alone is 0.673. These errors illustrate an important aspect of this model is that the exponential component restricts its use to only loading regions that the model was originally fit. Thus, the constitutive model (Equation (4.8)) with identified material parameters is suitable for subsequent mechanical design analysis to optimize fabrication strategies for self-assembly TEVMA.

4.5 Discussion

It has been long held belief that matching biomechanical properties between the native vasculature and a vascular graft is a necessary design target to achieve long term patency.[8] Although it is recognized that restenosis following vascular by-pass grafting is a multifactorial phenomenon, mechanically-mediated adaptations play a key role in restenosis. Traditionally, saphenous veins have been used for coronary by-pass grafting; in their native environment, these veins experience an order-of-magnitude lower shear stresses, much lower mean and cyclic pressures, and higher radius to thickness ratio when compared to coronary arteries. Thus, following implantation of the differences were observed saphenous vein into the arterial system, the shear stress increases along with the circumferential stress, while the cyclic pressure and cyclic strain dramatically increase. Typically, veins are implanted at a fairly low axial stretch, thus the axial stress likely decreases. These altered loads can induce significant remodeling in the graft vessel. Grafts derived from the arterial system (e.g., internal mammary artery (IMA) or radial artery) experience less dramatic, but still significantly, altered loading following implant.

Thus the IMA often grows in a tortuous fashion, indicating maladaptive remodeling due to insufficient axial loading.[7]

In addition to graft remodeling, the host vessel experiences significant changes in the local loads near the anastomosis, including altered cyclic strains due to compliance mismatch between the host and graft and altered hemodynamics due to diameter and compliance mismatch. Host tissues experience oscillatory shear stress and a significant reduction in cyclic strain; both mechanical stimuli are associated with intimal hyperplasia and plaque formation. Comparing autologous (compliant) to synthetic (non-compliant) grafts, it was found that the two year patency rate of compliant grafts was more than two times superior than the patency rate of non-compliant grafts.[8] This experiment however brings into question the resulting effect of synthetic graft biocompatibility. To eliminate synthetic materials from the experiment, Abbott *et al*. [9] chemically cross-linked arterial autografts with glutaraldehyde to decrease the compliance of the grafts prior to implantation. It was thus found that the 3 month patency was significantly greater in compliant (not cross-linked) grafts.

Specific mechanisms of failure as a result of compliance mismatch have been investigated. Intimal hyperplasia (IH) at and around the suturing point has been shown to cause significant intimal thickening with synthetic grafts (ePTFE) whereas IH with autologous grafts result in significantly less thickening.[10] To eliminate blood-synthetic material contact, [11] used autologous vein autografts externally stiffened with Dacron mesh to force compliance mismatch. It was found that significant IH occurred in compliance mismatched vessels while very little IH was observed in diameter mismatched vessels. Ballyk *et al*. [12] mathematically investigated compliance mismatch

and found that significantly increased transmural stresses develop near the vasculature-graft junction. This mathematical finding, along with experimental results of Matsumoto and Hayashi [13], further suggest a localized cellular response to an increased stress.

There are numerous reports of the mechanical properties of human coronary arteries. These properties vary significantly with age and from patient to patient. Gow *et al*. [72] and Gow and Hadfield [73] reported compliance (as defined in Equation (4.13)) of C =1.50 MPa^{-1} and C = 1.60 MPa^{-1} for the left coronary arteries (LCA) and right coronary arteries (RCA), respectively. Hayashi *et al*. [74] reported a compliance of C = 1.76 MPa^{-1} for the left circumflex. Purinia & Kas'ianov [75] reported cyclic strains of 5.3 ± 1.3% and 4.7 ± 0.2% over pressures of 60-140 mmHg in the LCA and RCA, respectively in patients between 40 and 59 years of age; these data correspond to compliances of C = 5.0 ± 1.2 MPa^{-1} and C = 4.4 ± 0.2 MPa^{-1} for the LCA and RCA, respectively. For patients above 60 years of age Purinya et al. reported cyclic strains of 5.1 ± 2.7% and 5.2 ± 2.5% over pressures of 60-140 mmHg, which is in keeping with compliances of C = 4.8 ± 2.5 MPa^{-1} and C = 4.9 ± 2.3 MPa^{-1} for the LCA and RCA, respectively. Holzapfel *et al.* [71] characterized a two-layer model for human left anterior descending (LAD) coronary artery; based on their constitutive model, material parameters, and stress free reference states for the media and adventitia, over the pressure range of 80-120 mmHg and an axial stretch of 1.1, this model predicts an inner radius of $r_i \in [4.9,5.1]$ mm, an outer radius of $r_o \in [6.0,6.1]$ mm, a cyclic strain of $\Delta\varepsilon$ = 2.6%, a compliance of C = 4.6 MPa^{-1}, and an axial force on the vessel wall of $f \in [0.15,0.18]$ N (Figure 4.4e and f).

We have shown that the average compliance of a TEVMA was 2.73 MPa^{-1}, which is within the range of those reported by [72] and [74], and in the same order of magnitude, albeit slightly lower than the compliance reported by [75] and [71]. Thus, these TEBVs exhibit compliances near or slightly lower than native human coronary arteries. The axial force for TEVMA under an axial stretch of $\lambda_z = 1.1$ was nearly identical to that of a representative native coronary artery (Figure 4.4f). Thus, upon implant of an end-to-end anastomosis, with the graft at an axial stretch of 1.1, the axial force (and thus, axial stress) imposed on the host vessel at the anastomosis will be equal to pre-graft values. Note that end-to-side anastomosis develops a more complicated stress field.[12]

Representative pressure-diameter and axial force-pressure curves are shown in Figure 4.4. From the understanding of the macro-structure, the biomechanical response of the TEVMA would be expected to be a composite of the two constituent layers. Qualitatively, pressure-diameter plots demonstrate that the TEVMA (Figure 4.4e) combines trends of both the TEVA (Figure 4.4a) and TEVM (Figure 4.4c). Visual inspection of these three figures revealed that the most compliant construct was the TEVA while the TEVM was the least compliant. While both curves had similar shapes, the TEVM curve had a much greater distension at lower pressures than the TEVA. During inflation of the TEVMA, the TEVA was restricting the TEVM from rapidly distending at low pressures. However, the inflation curve of the TEVMA did not precisely follow that of the TEVA since the adventia layer thickness in the TEVMA is only half of the full TEVA. The compliance of a TEVMA lies in between the other two construct types. This result was further confirmed quantitatively as shown in Table 4.1. A

similar result can be seen in the axial direction when comparing Figure 4.4b, d and f. As expected, in both the circumferential and axial directions it appears that such behavior was dominated by the TEVA.

All three vessel types displayed a large range in opening angle measurements. Because these vessels were developed individually in a tissue engineering laboratory, vessel to vessel variability can arise during the fabrication. For example, the process of wrapping the tissue sheets around the mandrel is performed manually and not automated. This can lead to different circumferential pre-stretch levels being imposed on the tubular construct while on the mandrel. Knowing that static stretching of SMCs induces remodeling [76], it is reasonable to believe that different circumferential static stretches while on the mandrel will lead to different remodeling rates and therefore different opening angles. In addition, the differences in stress between the stress-free and traction-free states of a vessel are very small. Using calculated parameters for a representative TEVA, a 5.434 mm outer diameter and 0.498 mm thickness vessel with an opening angle of 107º will have a $T_{\theta\theta} \in [-0.164, 2.806]$ kPa from the inner to outer radius, respectively, in the unloaded configuration. When comparing these values to those observed during inflation and extension (Figure 4.5a and b), there is an order of magnitude difference between the stresses observed in the traction free state and the mean stresses at physiological pressures. With these very small differences in stress, the experimental methods to determine opening angle could influence measurements. While these residual stresses are on the same order of magnitude as native vessels [62], the tissue engineered tissues display less consistent results. This could result from the axial

location from where the rings were taken since end effects or different contraction rates might cause different residual stresses.

These models are a valuable tool in understanding the biomechanical response of a TEVMA prior to development. Figure 4.7a and b indicate that the calculated material properties of the TEVM and TEVA can be used to develop a two-layer model which will predict the response of a TEVMA. For all TEVMA modeled, the predicted values for diameter over the physiologic range were slightly underestimated. There are a number of reasons why this would be the case. During the production of the TEVMA, the tissue sheet was developed as a co-culture. With two cell types being in the same cell culture media, there was the possibility of one cell type influencing the cellular processes of the other. This would lead to different material properties and therefore a different material response. One solution to develop more representative TEVA and TEVM would be to use conditioned culture medium from a TEVMA tissue sheet. In addition, unlike native vessels, once the TEVMA is formed, the media- and adventitia-like layers are indistinguishable; thus, these layers could not be separated to measure the individual opening angles of each layer. Rather, we assumed that the opening angle was similar to those measured from the single layers. Inaccuracies in the true stress-free state of each layer of the TEVMA could, at least in part, explain the slight differences between the prediction model and the experimental data.

It is well known that tissues grow and remodel in response to altered mechanical loading and these mechanisms appear to be aimed at restoring the local mechanical environment to a homeostatic state of stress (and/or strain). Whereas studies on native tissues suggest that the homeostatic circumferential and axial stresses are 50-150 kPa, the

homeostatic stresses for TEVM, TEVA, and TEVMA are not yet known. One advantage to understanding the stress distribution across the vascular wall is the knowledge of local mechanical influences on cellular responses. The predicted circumferential and axial stress in the media and adventitia of a TEVMA at 100 mmHg at an axial stretch of λ_z=1.1 were $T_{\theta\theta}^{M} \in [79.81,258.77]$ kPa, $T_{zz}^{M} \in [31.17,45.87]$ kPa, $T_{\theta\theta}^{A} \in [-7.29,3.03]$ kPa, and $T_{zz}^{A} \in [5.91,8.50]$ kPa (Figure 4.8b), which are considerably different when compared to the wall stresses of a human coronary artery as predicted by [69] (Figure 4.8a). The stress distribution in both the circumferential and axial directions across the native vasculature is relatively uniform compared to the large gradient seen in the media layer of the TEVMA.

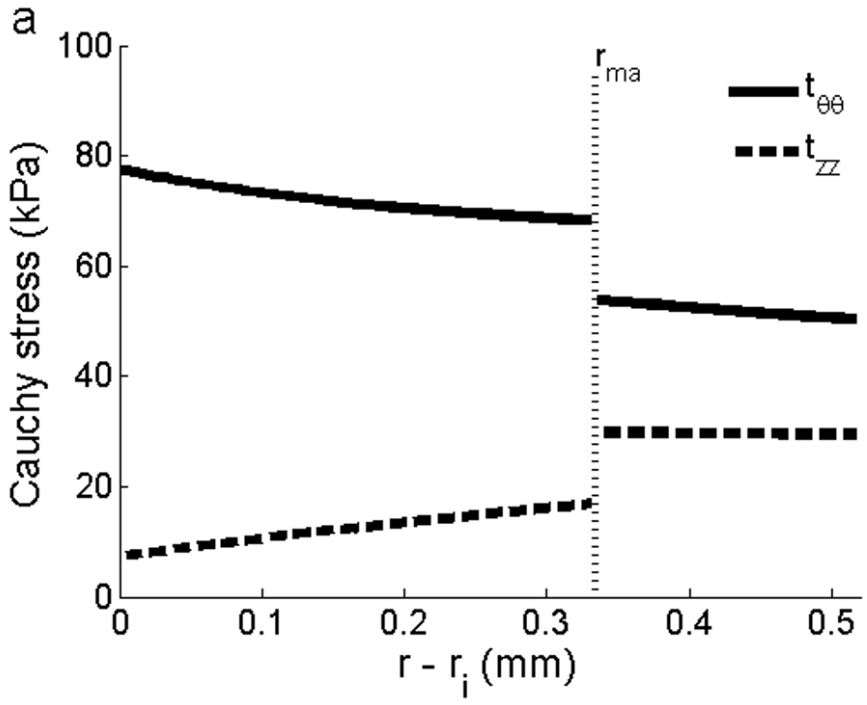

Figure 4.8. Predicted circumferential and axial stresses for a representative coronary artery (a) using the constitutive model and material parameters of Holzapfel et al., 2007 and for a TEVMA (b) using the material parameters from Table 4.2.

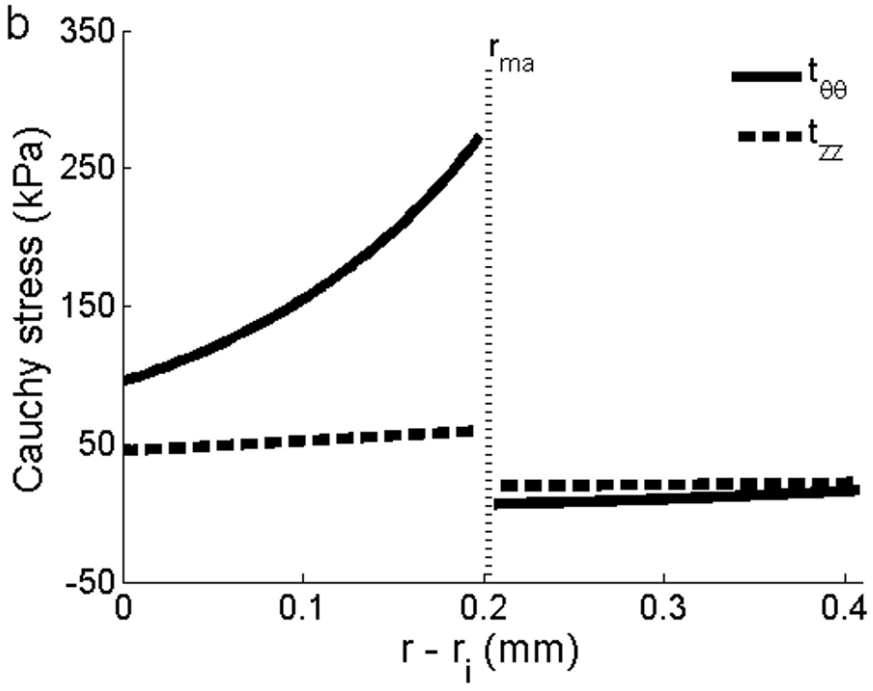

Figure 4.8 continued

Indeed, these results suggest that following implant, the TEVMA may experience significant stress-mediated growth and remodeling. For example, large stresses predicted in the media could result in significant local growth (or atrophy) and even intimal hyperplasia. Thus, although the overall biomechanical indicators such as compliance and axial force are similar between native coronary arteries and TEVMA, if the local mechanical environment deviates significantly from the homeostatic mechanical environment, maladaptive remodeling may ensue. For this reason, we submit that identification of a predictive constitutive model is critical to conduct design analysis that not only matches the global biomechanical response parameters (e.g., compliance), but also matches the local mechanical environment (i.e., local stresses) to minimize maladaptive remodeling. Such analysis can be used to motivate novel fabrication

strategies to achieve reasonable matches to both global and local mechanical targets. Note that the abrupt change in stress at the media-adventitia interface is due to the step-wise change in the material model; in reality, there is a narrow continuous transition between the stresses in the media and those in the adventitia.

While these models provide good insights into the local mechanical response as well as tissue level mechanics, they are not without limitations. The TEVMA was fully capable of loading beyond an axial stretch of 1.2, however because the TEVM was only capable of being tested to $\lambda = 1.2$, the two-layer model cannot be extrapolated to predict the response at higher axial stretches. Moreover, at an axial stretch of 1.2, the circumferential strains that were experienced by the TEVMA are considerably smaller than those experienced by the TEVM alone. Thus, the range of strains that the media-like layer of the TEVMA experienced over the experimental loading was different from the range of strains that the TEVM were exposed to during the same experimental loading. Since the material parameters were determined for the TEVM are only valid over the range of strains experienced by the TEVM, any extrapolation outside the range of strains will induce significant error; this is especially true for the chosen constitutive equation that incorporate exponential functions. The predictive capabilities of the model are quickly lost once strains outside of the tested range are introduced as this leads to negative or extremely large values for pressure and axial force. Therefore, one must use caution when using this model as a tool to predict the material response of the tissue engineered vasculature.

In summary, our *in vitro* biomechanical characterization has demonstrated that TEVMA displayed compliance on the same order of magnitude as native vessels when

subjected to the same physiologic loads. Previous studies have shown that TEVMA do possess the mechanical strength to be used as a viable graft [18, 77], but biomechanical properties at physiological loads had not been characterized until now. In order for these vessels to have the greatest chance of patency, their biomechanical properties would ideally match that of the surrounding vasculature. The results of these experiments demonstrate that the biomechanical response of the self-assembly tissue engineered constructs do not precisely match that of the native vasculature, but we have now developed a model to better understand the effect of different assembly strategies on the biaxial biomechanical response.

CHAPTER V

FIBROBLAST ALIGNMENT IN RESPONSE TO BIAXIAL STRETCHING

5.1 Introduction

As tissue engineering technologies progress, viable grafts must not only act as simple structural replacements, but must also possess the functionality and appropriate mechanical response of the native tissue. It is well established that the microstructural organization of tissues affect their functionality, as well as biomechanical properties.[78, 79] This has also been shown to be true of various engineered tissues.[19, 21, 30] To date, tissue engineered blood vessels (TEBV) constructed by self-assembly (SA-TEBV) have shown superior mechanical strength, biomechanical behavior, morphology, cell and extracellular matrix (ECM) organization, and vasomotor response compared to other TEBVs or autologous grafting tissues.[3, 28-31, 33, 34, 36, 80] The self assembly approach consists of culturing cells to form a tissue sheet composed of cells and self-assembled ECM, then rolling these sheets around a mandrel and culturing them to form a tubular structure[33]. Sheets or tubes made from different cell types (i.e. smooth muscle cells versus fibroblasts) can be combined to produce heterogeneous tissues that mimic the native vasculature in cell and ECM content. However, until recently, cells had only been grown on flat, rigid substrates, not allowing for control over the organization of the microstructure.

One often cited cause for graft failure is a mismatch of biomechanical properties between the graft and native surrounding tissue. As shown from biaxial material characterization of heterogeneous SA-TEBV, the tissue level biomechanics do not currently match that of a native artery.[81] In addition to matching 'global' mechanical properties (i.e. compliance) between the host and graft tissue, we submit that one must also match the 'local' mechanical environment (e.g., local stresses) to minimize local mechano-biological mechanisms that lead to maladaptive remodeling and stenosis. Mathematical analysis in Zaucha *et al*. also revealed a difference in local stress gradients as compared to the native artery.[81] Therefore, the ability to manipulate tissue mechanical properties would minimize one of the current weaknesses of the self-assembly strategy.

Present in most soft tissues, fibroblasts are responsible for maintaining and remodeling the ECM which is the structural support of soft tissue. Within blood vessels, fibroblasts play a critical role in the adventitial layer generating new, reorganizing existing and degrading collagen fibers. It has been established that fibroblasts perform these function in response to both chemical and mechanical stimuli. With regard to the latter, little is known about the exact mechanisms which dictate behavior; however, these cells *in vivo* are typically subjected to multiaxial loading. Experimental studies have shown that collagen orientation follows the alignment of the cells.[82] Therefore, if we wish to use mechanical stimulation to generate new engineered tissue, as in the self-assembly approach, we must better understand how cells reorient and align in response to multiaxial loading. *in vitro* studies have revealed that fibroblasts appear to align

perpendicular to the principle stretch direction.[83-87] However, a critical gap remains in the literature in regards to fibroblast orientation in response to biaxial stimulation.

In the present study, the motivation for using mechanical stimulation to alter the biomechanical properties of SA-TEBV is outlined. Experimentally, we subjected human dermal fibroblasts (hDF) to uniaxial and biaxial cyclic mechanical stimulation to understand its effects on cell orientation and alignment. A custom designed bioreactor [88] was used to subject a cell-seeded silicone tube to both cyclic axial and cyclic circumferential mechanical strain. This same device was used to subject a cell-seeded silicone tube to equibiaxial strain. Cell orientation and alignment was measured by two different imaging methods, both of which produced similar results. In both cases of uniaxial stretch, it was found that hDFs aligned perpendicular to the principle stretch direction. In the biaxial stretch group, hDFs aligned at an off-axis angle from both principle stretch directions. Statistical differences of all three stretch groups were found when measuring alignment of cells along these preferred directions. These findings can be used to scale up and extend the culture period until tissue sheets are generated with controlled ECM alignment, ultimately generating SA-TEBV with manipulated mechanical properties.

5.2 Methods and Materials

5.2.1 Culture of human dermal fibroblasts

Human dermal fibroblasts (hDF, from passage 6-8) were cultured in Dublecco's modified Eagles medium (DMEM, Mediatec, Inc., with 4500mg/L of D-glucose and L-glutamine) supplemented with 10% fetal bovine serum (Mediatec, Inc.), antibiotic (P/S,

Mediatec, Inc., 50 I.U./mL penicillin and 50 mg/mL streptomycin) and additional L-glutamine (Mediatec, Inc., 5000 g/L).

The silicone tube (Dow Corning Q7-4735) was prepared using a similar method to Asanuma *et al*.[76] Prior to seeding, the tube was rinsed in 10N sulfuric acid (VWR International) for 2 hours and then rinsed thoroughly in sterile water. Each tube was coated with a 1 mg/mL collagen type I (MP Biomedical, LLC) solution in 0.02N acetic acid (Ricca Chemical Company) through 5 dip/dry cycles, and rinsed once again with sterile water. Each tube was then placed under UV light for 30 minutes and subsequently placed in a sterile cryogenic freezing vial (NalgeNuc International). Cell seeding was accomplished by placing 1.8 mL hDF cell solution in the vial with the silicone tube. In a standard incubator at 37ºC, the vial was rotated 45 degrees every 8 minutes until a full rotation was achieved. Following seeding, the silicone tube was removed from the vial and placed in a 15mL tube with fresh medium. This approach achieved an initial seeding density of ~10,000 cells/cm^2. The cells were cultured for 24 hours prior to stretching experiments.

5.2.2 Cell stretching experiments

The device used to subject the cell seeded silicone tube to mechanical strain was previously described [88], with a slight modification. As shown in Figure 5.1, the pressure control system, as previous described, was replaced with a computer controlled pinch value to allow for the pressurization of the reservoir with a 5% CO_2/air gas mixture directly from the tank regulator. Approximately 2 psi was required to obtain a 5% circumferential stretch. The computer control program, from [88], was modified to also control the pinch value so as to ensure proper phasing with the cyclic axial extensions.

Four experimental groups were investigated: a control where no stretching was imposed, a cyclic axial extension of 5%, a cyclic circumferential extension of 5%, and an equibiaxial cyclic extension of 5% in both the circumferential and axial directions. All stretching studies were performed at 1Hz for 24 hours.

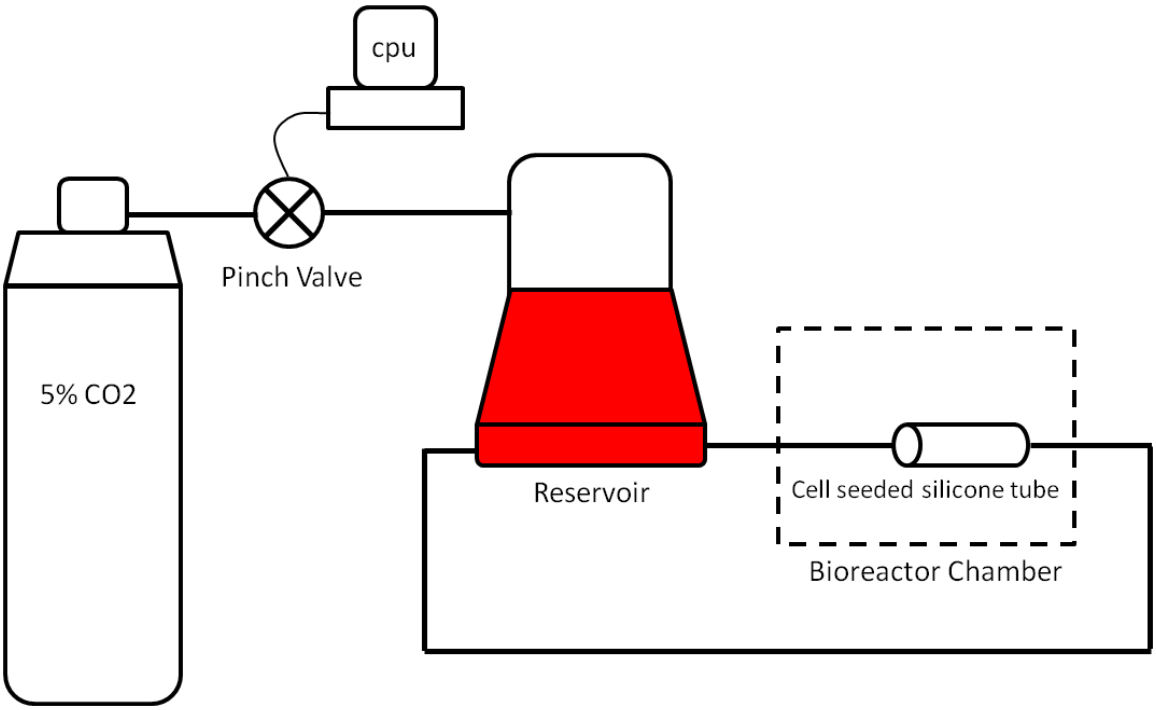

Figure 5.1. Experimental apparatus for cell stretching experiments showing modification to pressure control system. The bioreactor chamber is further described in Zaucha *et al.* [88]

5.2.3 Cell Staining and Confocal Imaging

After stretch experiments, the silicone tube was immediately placed in 10% buffered formalin acetate (Fisher Scientific) for 30 minutes and stored in 70% ethanol. To

stain F-actin fibers, the sample was first permeabilized in 0.05% Triton-X for 30 minutes at room temperature. After removal from the Triton-X , the sample was rinsed in PBS and then placed in a 1:50 phalloidin (Invitrogen, AlexaFluor 488):PBS solution for 30 minutes in a standard incubator at 37ºC. Prior to mounting, the silicone tube was again rinsed in PBS, cut axially, and laid flat on a glass slide. A DAPI mounting medium (Vector Laboratories, Inc.) was used to stain cell nuclei.

A Zeiss LSM 510 META inverted confocal microscope with Chameleon Ultra Ti:sapphire femtosecond laser (Coherent) was tuned to 750nm to excite DAPI and detect cell nuclei, while an argon 488 laser was used to excite phalloidin and detect F-actin . Using a 20x/0.8NA objective (Zeiss) in combination with a computer controlled motorized stage, each sample was imaged at 9 equally spaced locations (Figure 5.2) to gain a better representation of alignment throughout the entire sample.

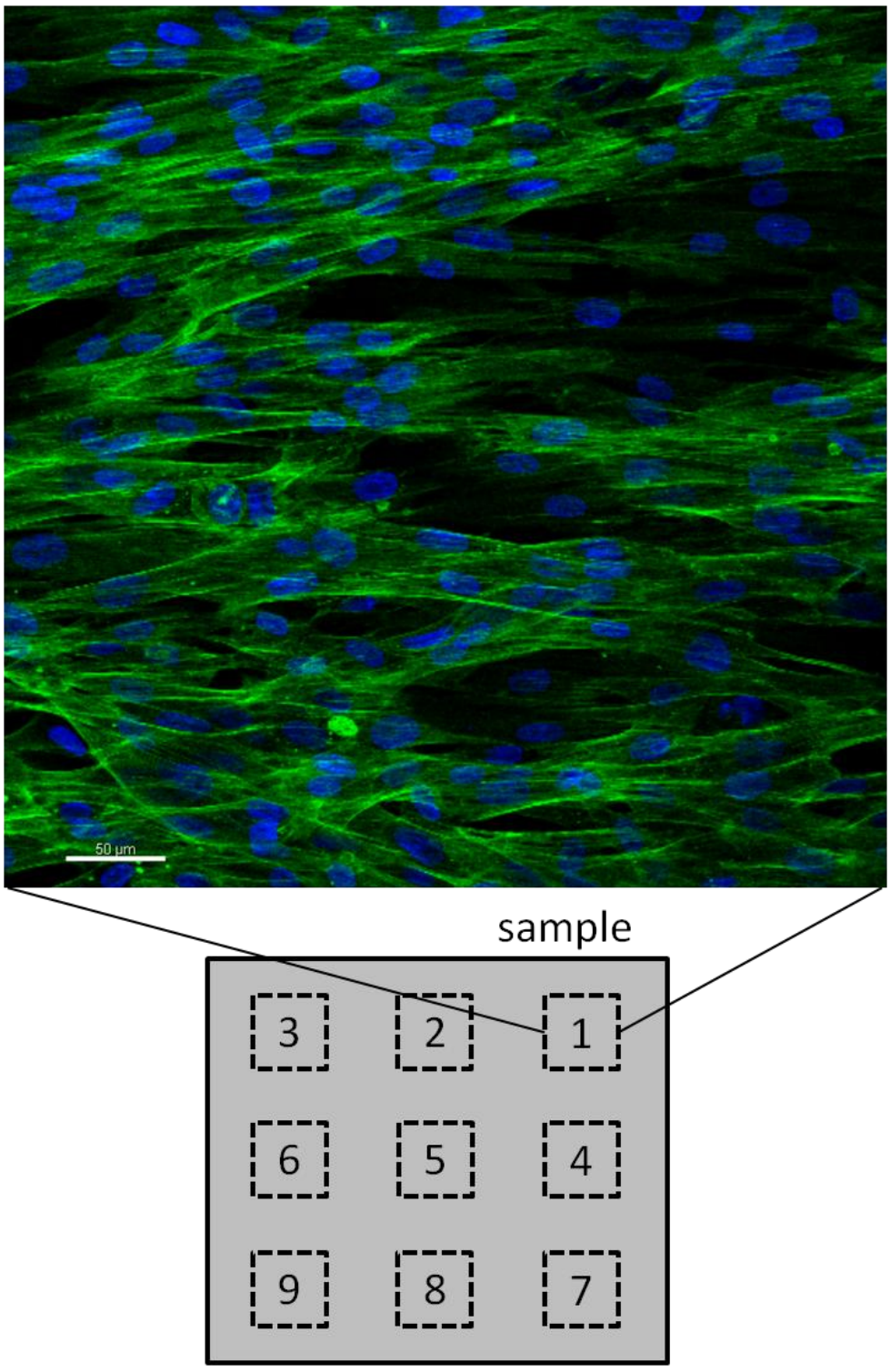

Figure 5.2. Nine equally spaced images were taken from each sample and combined to determine mean peak nucleus orientation and mean peak f-actin fiber orientation as well as alignment index (scale bar = 50 µm).

5.2.4 Image Processing

Images were processed via custom MATLAB (MathWorks, Inc.) scripts. Prior to processing, each image was decomposed into two images containing either F-actin fibers or cell nuclei (Figure 5.3). The F-actin fibers were processed to determine orientation similar to Ng *et al*.[89] Fast Fourier transform (FFT) analysis was used to determine the fiber orientation distribution within each image. The image was first imported into MATLAB as a square matrix and filtered using a circular averaging filter. To eliminate any intensity bias, the image was converted to binary using the built in threshold function. The image was then transformed to the power spectrum via two-dimensional FFT. Intensity frequencies were summed to develop a fiber distribution histogram.

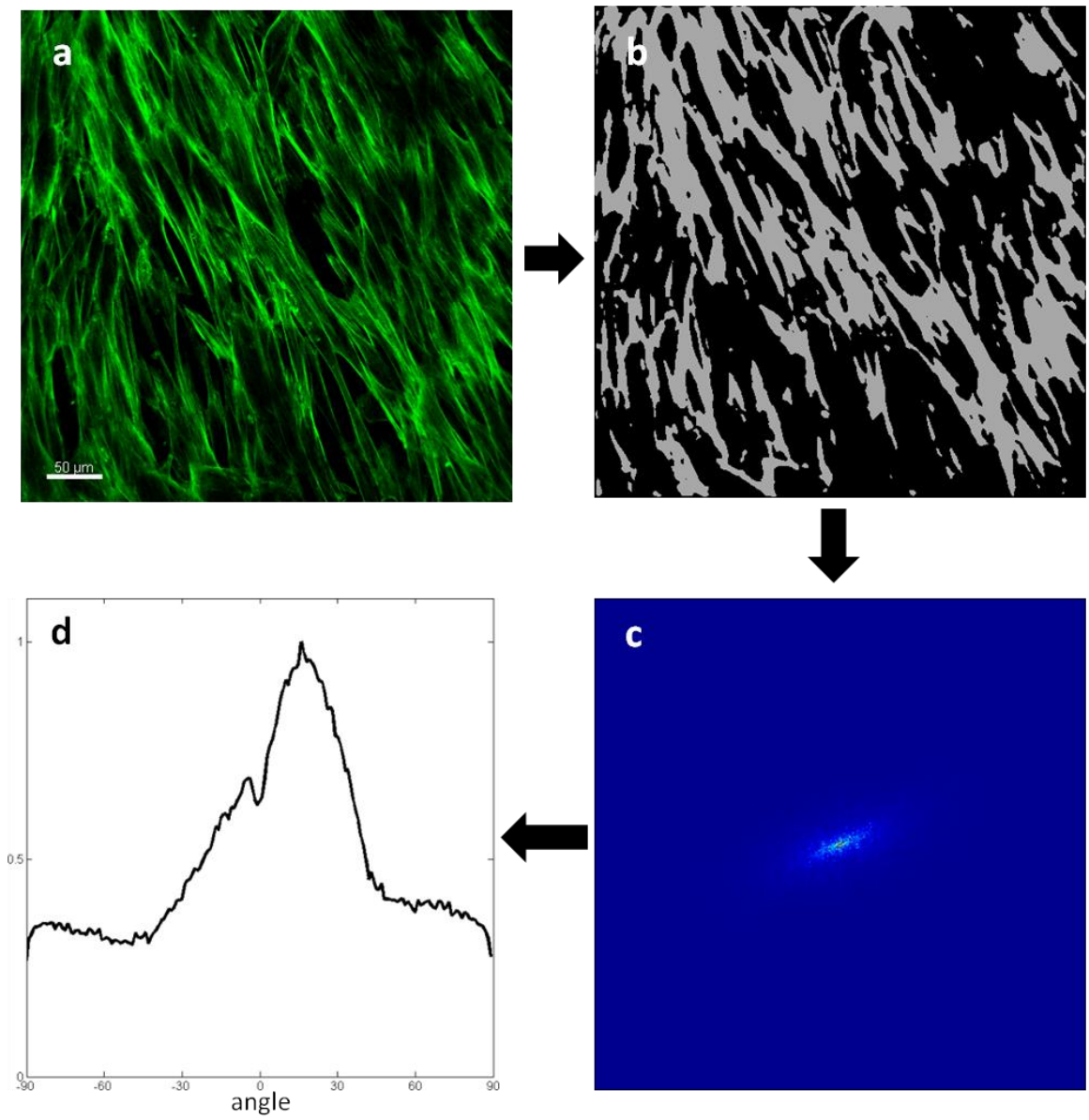

Figure 5.3. Process of quantifying the orientation and alignment from the original image (a) of f-actin fibers. The image is filtered and converted the binary (b) prior to being transformed into the power spectrum via FFT. From the transformed image, a distribution histogram (d) is generated. (scale bar = 50µm)

Cell nuclei orientations were determined by a different method. Each image was again imported, filtered and converted to binary in MATLAB using the same procedure as above. The transformed image was then viewed and individual nuclei were selected if the nuclei were not touching other nuclei, were mostly elliptical and not missing a major portion of the nucleus (Figure 5.4). MATLAB's built in functions were then used to calculate the major and minor axes, as well as the orientation from the x-axis of the image. A distribution histogram of nuclei orientations was developed with bin widths of 2º.

From F-actin and nuclei distribution histograms, a peak angle was determined. While the peak angle on the histogram might indicate directionality, this is not necessarily representative of the cell orientation. For example, a random orientation of cells/fibers will still have a peak but will be random and not necessarily representative of the distribution of cells. To give further meaning to the peak value, we have also calculated an alignment index (AI) as described by Ng *et al*. [89] and Timmins *et al*.[90] with slight modifications. The AI is calculated as the fraction of fibers that are ±15º from the peak as compared to all measureable fibers and normalized to the fraction of fibers that would lie in this region if it were a truly random distribution (i.e. 30/180 = 0.167). Hence, 1 would represent a fully random distribution while a higher number represents greater alignment.

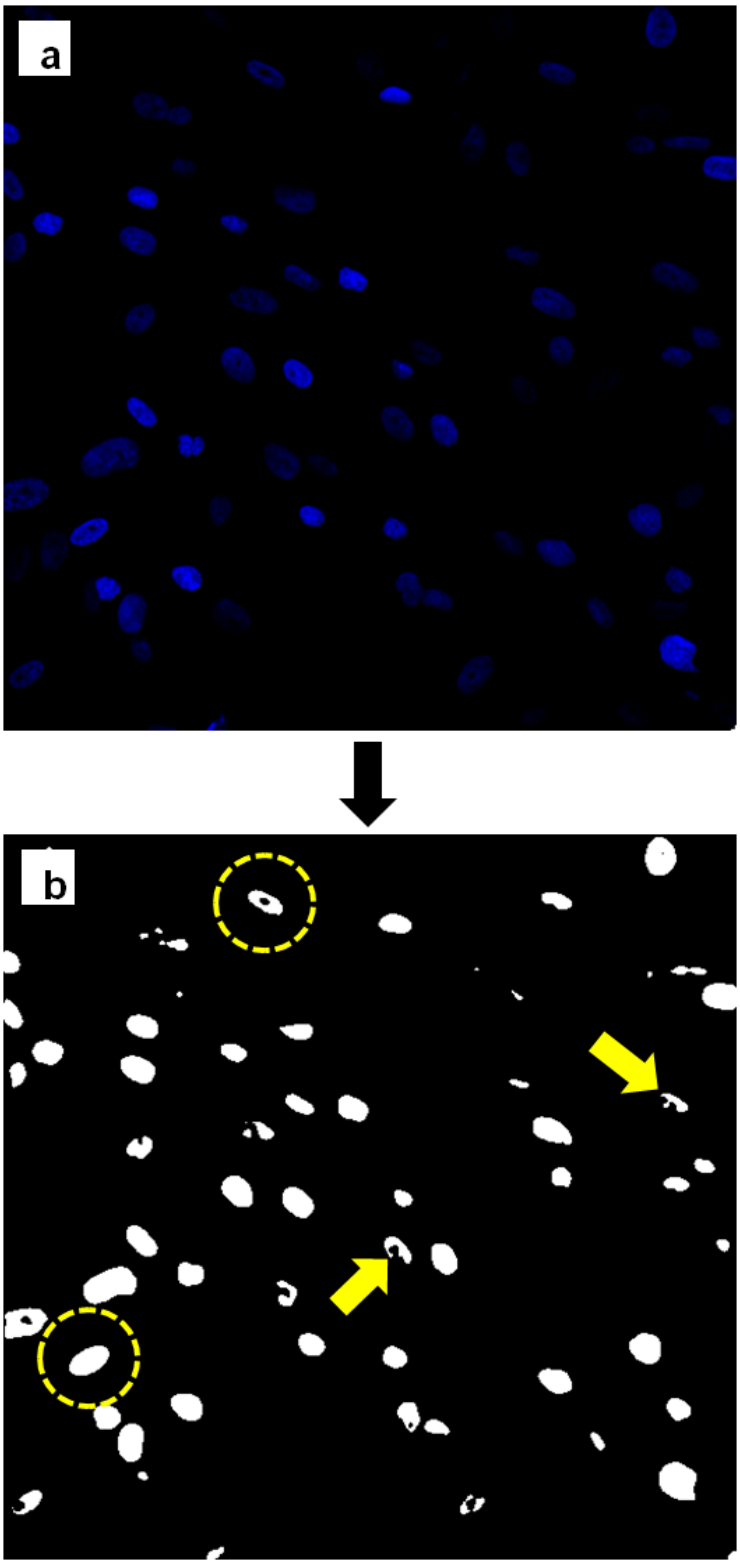

Figure 5.4. Process of converting (a) the original DAPI images to (b) binary and selecting appropriate nuclei based on the described criteria to be counted in the distribution histogram. Circles represent selected nuclei while arrows represent non-chosen nuclei

5.2.5 Statistical Analysis

Comparisons of three groups within the F-actin and nuclei were performed using and ANOVA with Tukey's post hoc test. Comparisons of the AI between the control and three experimentally stretched groups was performed using Student's t-test with verification of nearly equal variances using an F-test.

5.3 Results

F-actin fibers from the control group are much more randomly oriented than the three mechanically strained groups (Figure 5.5). As expected from studies reported in the literature [83-87], the cyclic circumferential and cyclic axial stimulation show fiber alignment in the direction perpendicular to the principle strain direction (arrows indicate stretch direction). The biaxial stimulated cells show fibers aligned at an off axis angle.

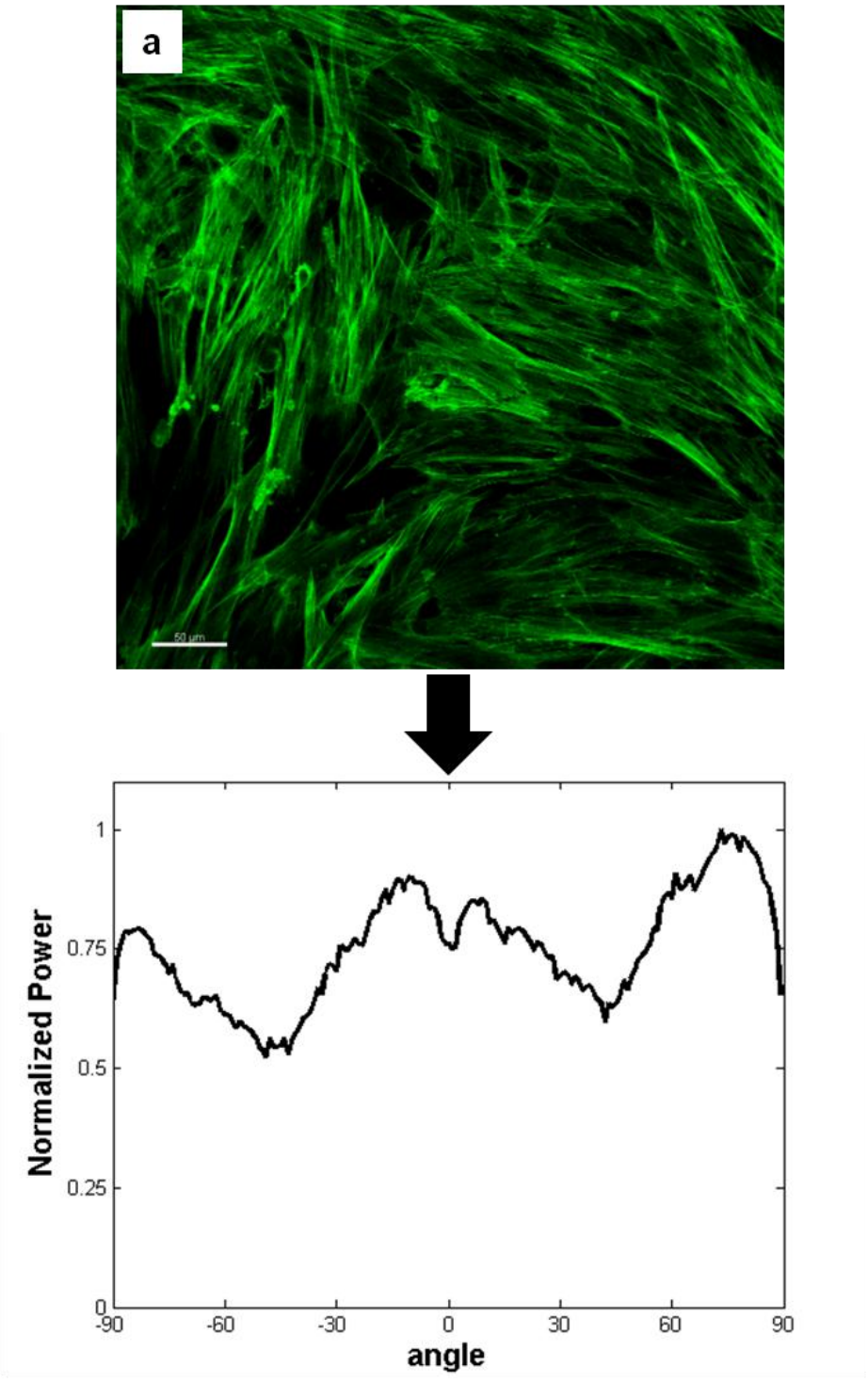

Figure 5.5. Representative images and distribution histograms of f-actin fibers showing a random distribution from the control (a) group, perpendicular alignment to strain with the circumferentially (b) and axially (c) stimulated groups, and off axis alignment from the biaxially (d) stimulated group. White arrows depict the principle stretch direction(s). (scale bar = 50 μm).

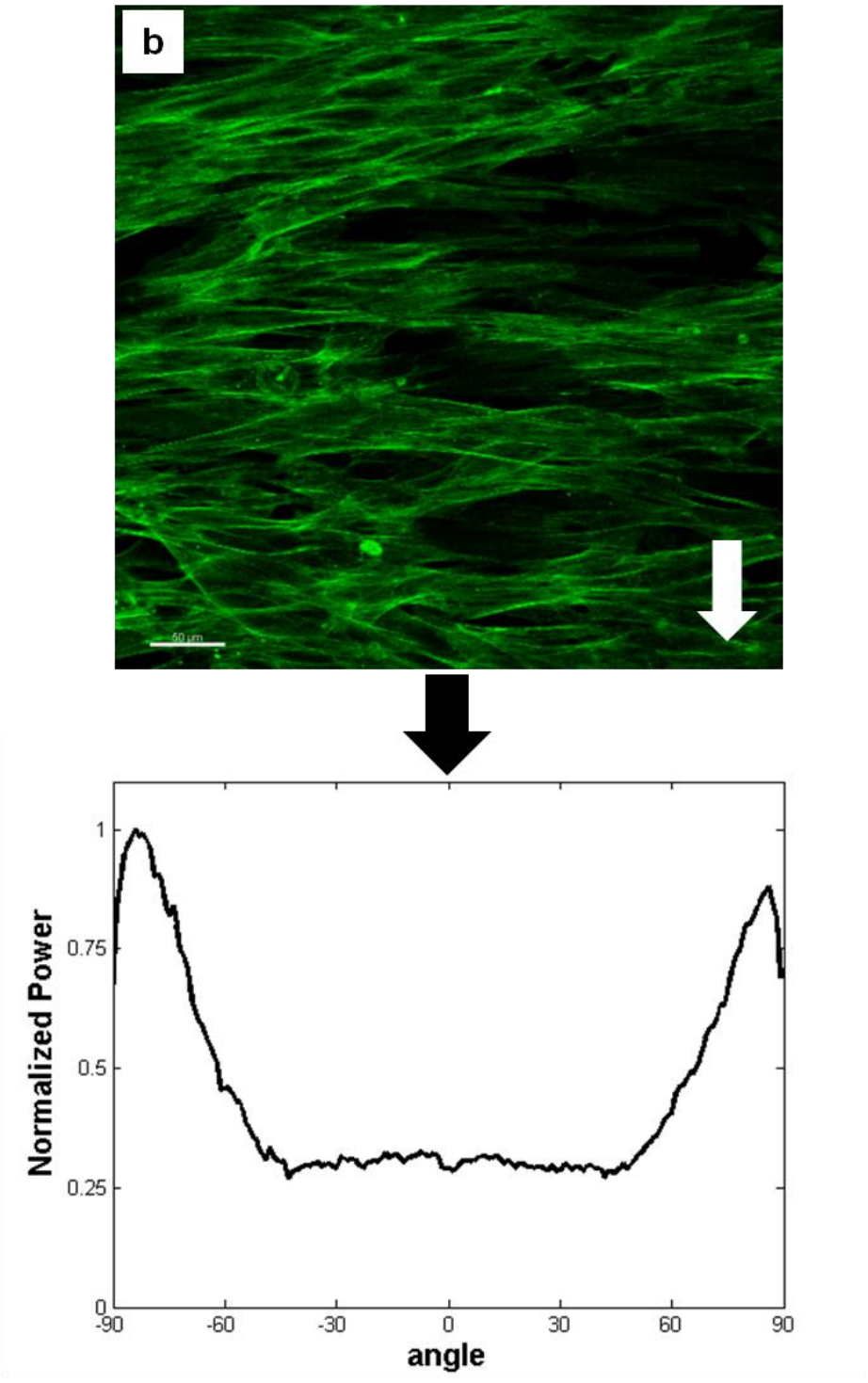

Figure 5.5 continued

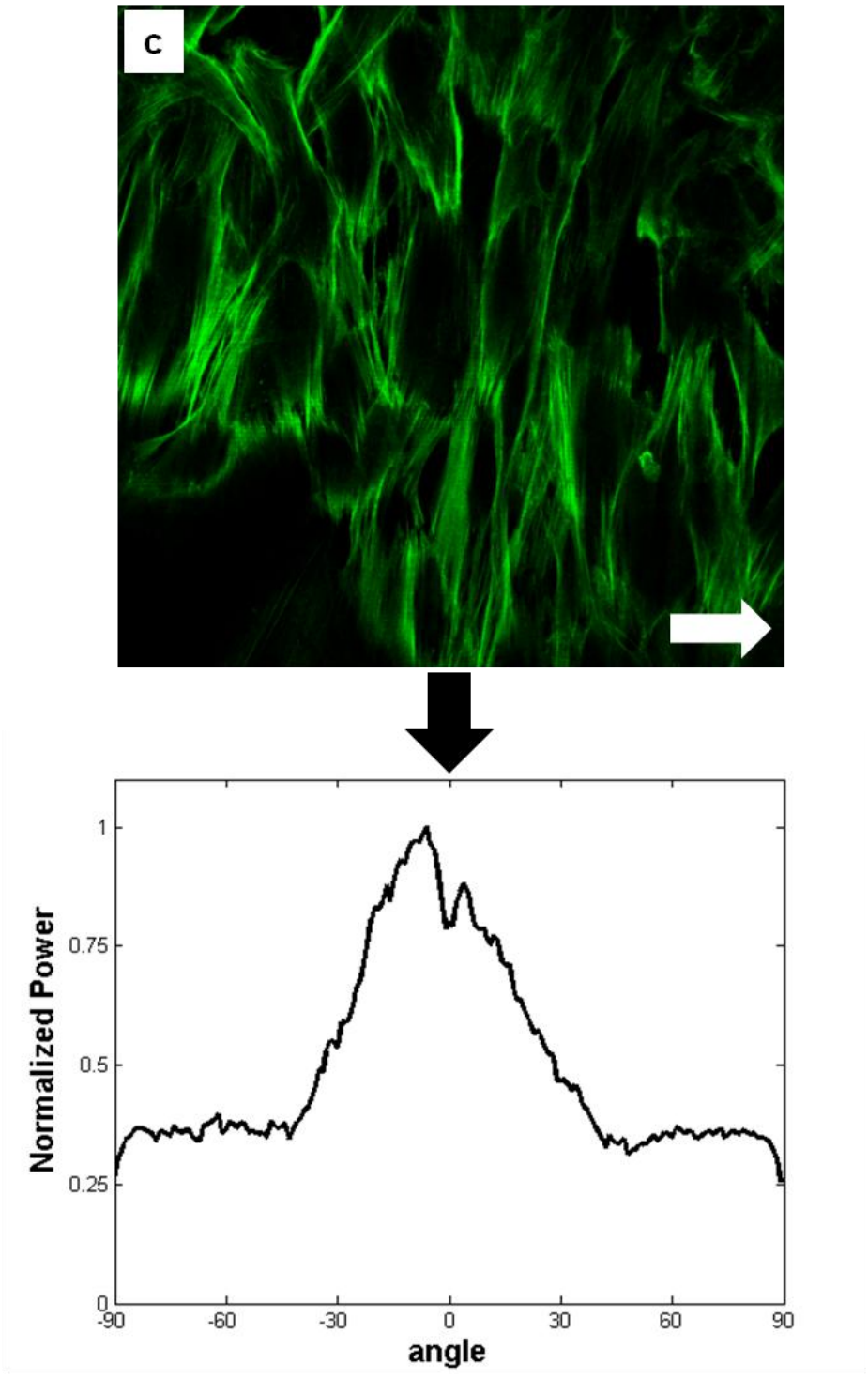

Figure 5.5 continued

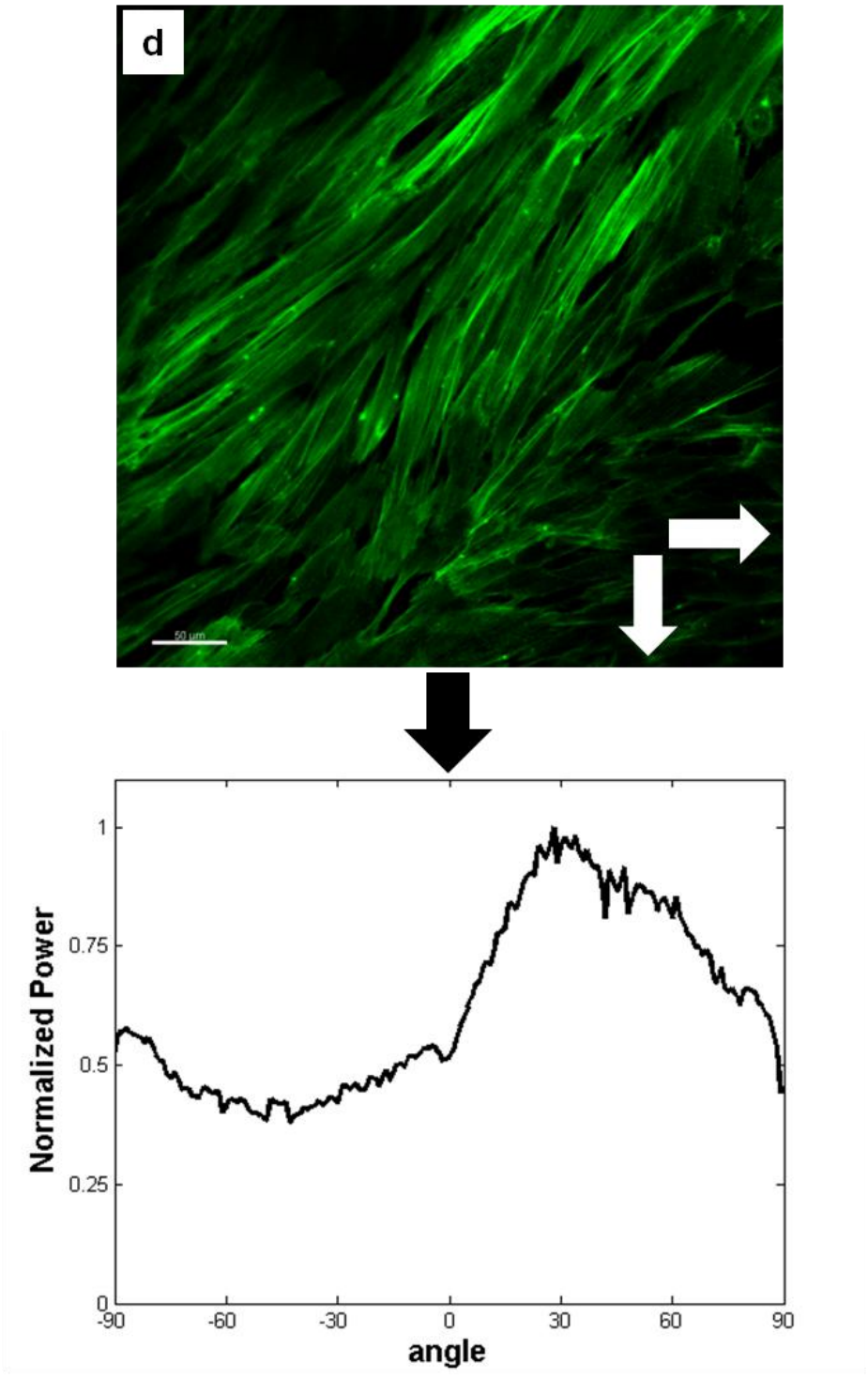

Figure 5.5 continued

These same trends are seen from the images of the cell nuclei. Representative distribution histograms of nuclei show that the control group has a generally equal cell count throughout the range of angles (Figure 5.6). As observed from the F-actin stain, the circumferentially and axially stimulated cells aligned perpendicular to the principle stretch direction, while the biaxial group has exhibited an off axis alignment peak and distribution. The shape of the three mechanically strained groups maintains a roughly normal distribution with near equal variances.

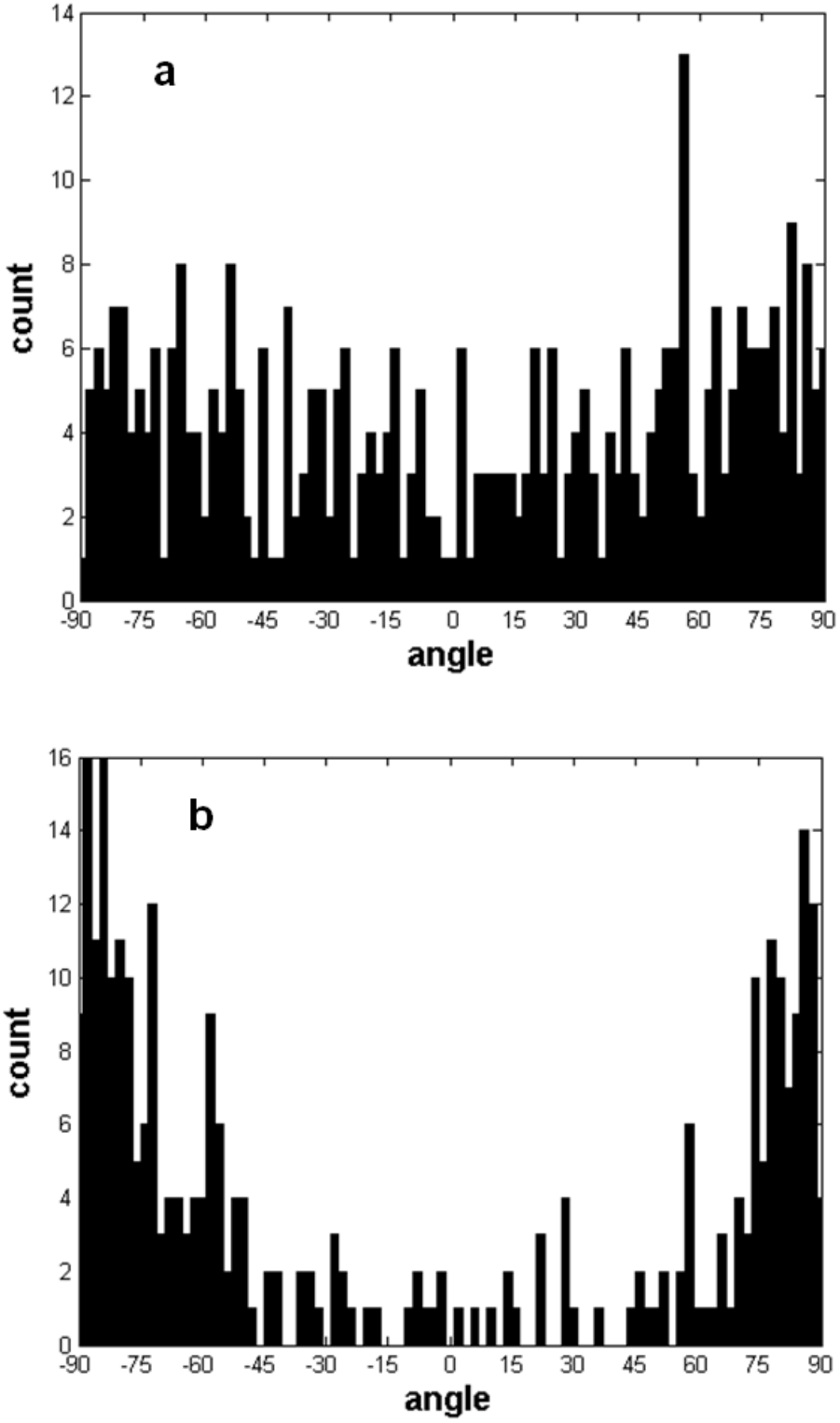

Figure 5.6. Representative distribution histograms of cell nuclei from the control group (a), circumferentially (b), axially (c) and biaxially (d) stimulated groups.

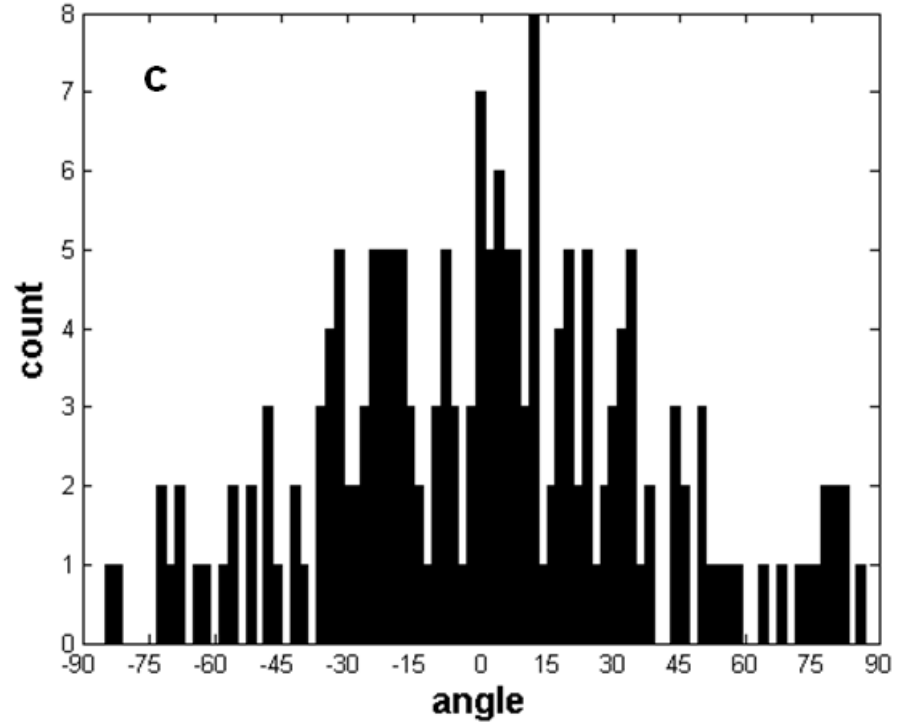

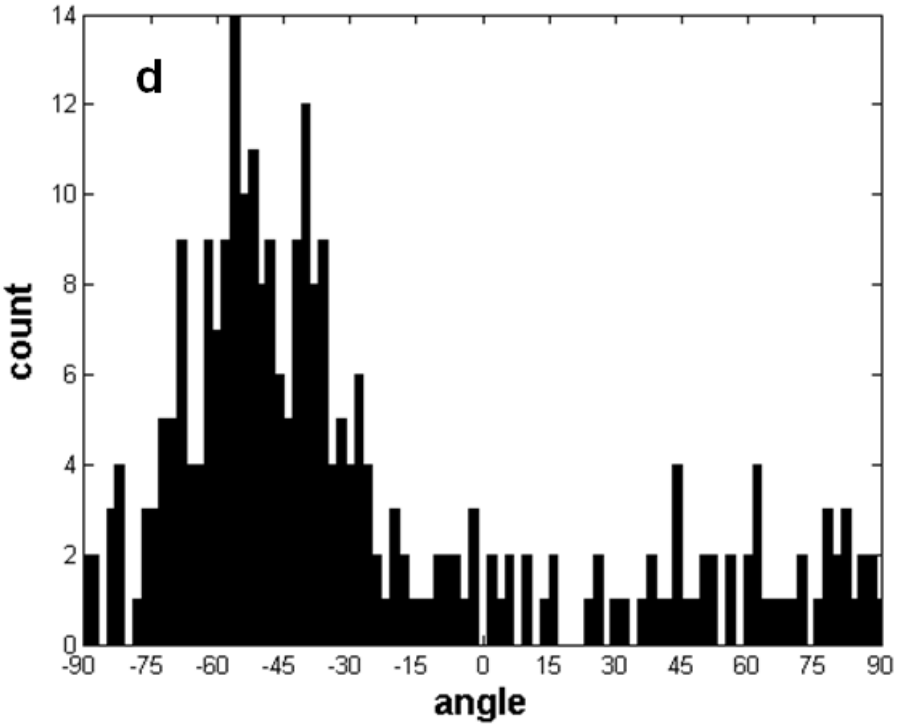

Figure 5.6 continued

The nuclei of the control group have a peak angle and deviation of -3±51 while the control group for the F-actin is -17±67 (note 0º refers to the circumferential direction). The standard deviation of the control groups was very large compared to the deviation of the axially stimulated group (Figure 5.7). The large deviations in both control cases indicate peaks are randomly found throughout the range of possible angles.

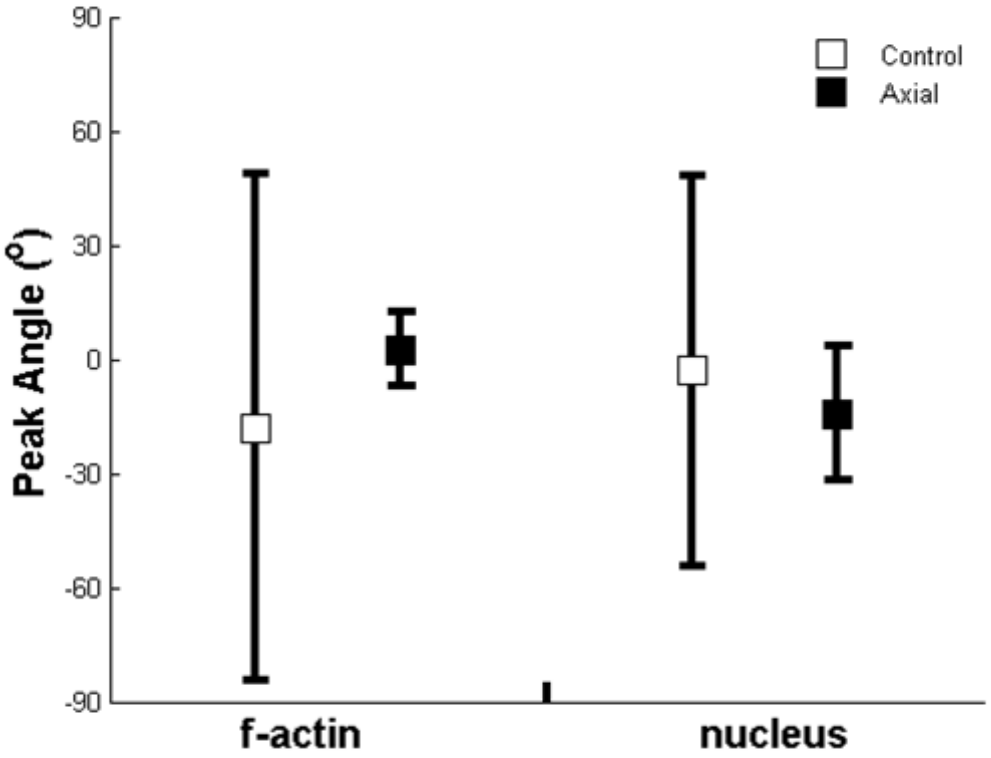

Figure 5.7. Peak angles of the distribution histogram for both the f-actin and nuclei. The large deviation in the control group indicates that peak angles are randomly distributed throughout the angular range.

In contrast, the peak angle for each stretch group of both the nuclei and F-actin fibers has much smaller deviations (Figure 5.8). The orientation angle of the nuclei in the biaxial (-58±6), circumferential (-74±11) and axial (-14±17) groups have much lower variance than the control indicating a more preferred alignment. In addition, statistical differences were observed between all three groups. Similar trends occur in the alignment of F-actin with slightly greater variances. The biaxial (-67±40), circumferential (-88±16) and axial (0±12) groups also have smaller deviations than the control group, however statistical difference only exist between the circumferential and axial groups. The large deviation in the biaxial group is mainly due to noise during processing of the images. When calculating the variations of peaks for those which are centered around or are near ±90º (i.e. circumferential and biaxial), the values were all made negative to reflect a more accurate variation. An example of this would be transforming a peak value of 80º to -100 º for the deviation calculation. This is still the same distance from the principle stretch direction and does not bias the results. This was only required for 2 values of the circumferential and 1 value for the biaxial within the F-actin image results.

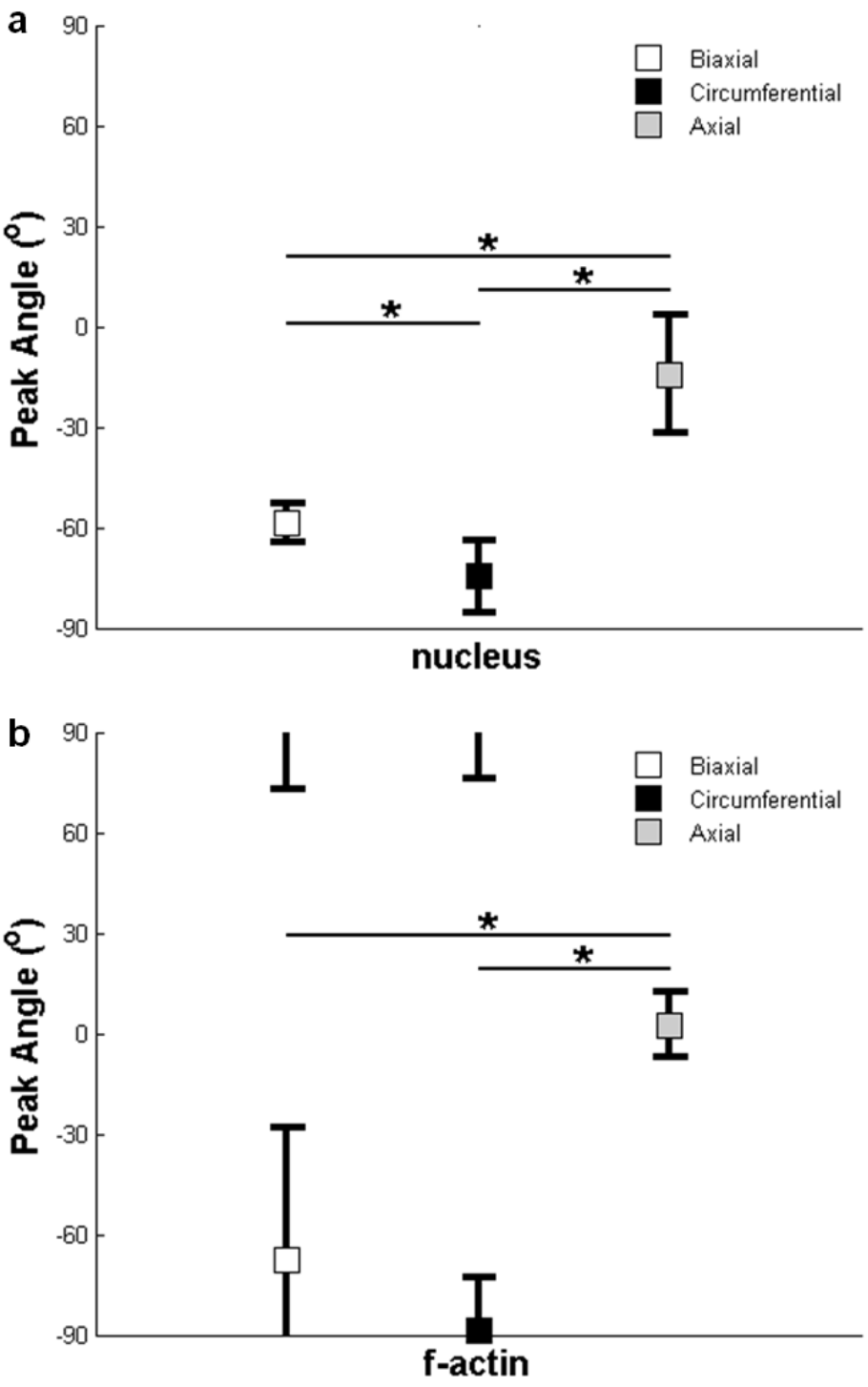

Figure 5.8. Peak angles of the distribution histogram for the cell nuclei (a) and f-actin (b). Statistical differences were observed between peak angle measurements (*$p<0.05$).

Another representation of alignment is the AI, which is a measure of the fraction of cells or fibers ±15° from the peak. Statistical differences were seen when comparing the AI of the nuclei between the control group and the biaxial, circumferential and axial groups (Figure 5.9a). F-actin fibers also showed significant differences between the control group and circumferential and axial groups (Figure 5.9b).

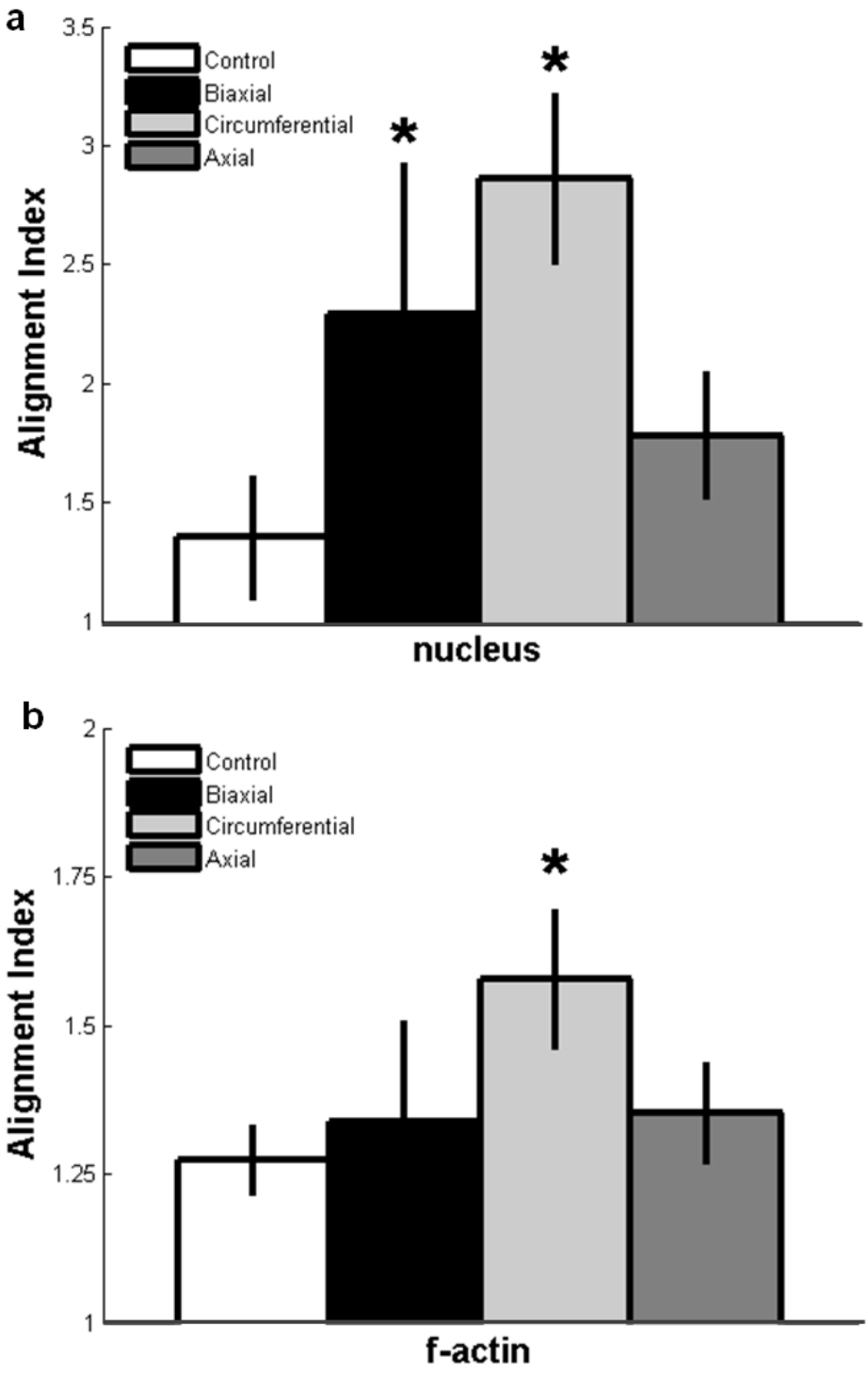

Figure 5.9. After 24 hours of substrate stretching, significant differences in AI were observed in the nuclei (a) between the control group and the three stretch groups. Significant differences were seen in f-actin (b) fibers between the control group and the circumferential and axial groups (*$p<0.05$, as compared to control).

5.4 Discussion

Composed of cells and extracellular matrix (ECM), a tissue's structural organization is determined by its function. For example, smooth muscle cells (SMC) located in the media of blood vessels are oriented circumferentially and actively contract and relax to dictate vascular tone. With regard to the adventitia, collagen fibers of the arterial adventitia have a bimodal distribution in their loaded configuration.[91] If we wish to design and construct TEBV which mimic the microstructure (and therefore biomechanics) of native blood vessels, we must understand how cells orient in response to various stimuli. Guillemette *et al*.[80] recently showed that surface topography (i.e. contact guidance) can be utilized to organize the first layer of human dermal fibroblasts (hDF) and endogenously produced collagen fibers. However, subsequent superficial layers of the tissue sheet were randomly aligned. If we wish to generate tissue sheets with alignment throughout, this method does not allow for any control beyond the initial layer.

Mechanical stain, on the other hand, is sensed by the cells throughout the entire tissue sample. Grenier *et al*.[30] found that a simple constraint imposed on the formed tissue sheet induces SMC alignment along the constrained direction. Once the tissue sheet was rolled, significant functionality of the resulting tissue engineered vascular media was observed. While this was imposed on a single tissue sheet, cyclic mechanical stain has also been shown to affect cells throughout engineered tissues. As compared to control groups, mechanically strained tissues show cellular alignment at various depths within the tissue.[92] Results from our experiments indicate cells will change alignment as a result of cyclic mechanical strain. Taken with other studies,[80, 82, 93] as the culture times are extended allowing for production of ECM, we anticipate collagen alignment to

follow cell orientation thus generating a tissue sheet that, once rolled, more closely resembles that of the native vasculature.

The levels of frequency and strain chosen in these experiments were based on previous studies. It has been shown that there is little stain magnitude dependence. Within the range of approximately 2-20% substrate stretch, fibroblasts will align perpendicular to the principle stretch direction. Below this range there was no statistical alignment of cells, while above this range apoptosis began to occur.[83] In addition to magnitude, frequency also dictates cell alignment. It was found that at frequencies below 0.1Hz, there was little significant cell alignment, while above this value, cells would consistently align perpendicular to the stretch direction.[87] The results from our uniaxial studies reinforce previous data found in literature.

Our group and others have developed constitutive models based on cell and ECM content and organization such as collagen fiber angle, distribution, and undulation.[67, 69, 81, 94-96] In these microstructurally-motivated models, tissue is modeled as a distribution of structural fiber (e.g., collagen) embedded in an amorphous solid mainly consisting of water and proteoglycans. The general functional form of the constitutive equation, postulated by Holzapfel *et al*. [69] and modified by our group and others, is given as:

$$W = b(I_c - 3) + \sum_{k=1}^{n} \frac{b_1^k}{b_2^k} \left\{ \exp\left[b_2^k \left(\left(\lambda_f\right)^2 - 1 \right)^2 \right] - 1 \right\}$$

In this equation b, b_1^k, and b_2^k are material parameters, λ_f^k is the stretch in the k^{th} fiber, which contains information on the orientation and undulation of the fiber and the deformation of this fiber, given tissue-level deformations; summation over all of the fiber

directions allows for the incorporation of fiber distribution functions. This model therefore ties into the current body of work in that we are attempting to control these fiber angles/distributions using mechanical stimulation.

A qualitative description of how fibers embedded within an amorphous solid influence the biaxial mechanical properties is shown in Figure 5.10. For the instance of tissue sheets generated by hDF, the primary fibers would be collagen. Changes in fiber orientation with respect to the principle stretch directions result in changes in tissue biomechanical behavior. For example, Figure 5.10a demonstrated that a tissue with fibers oriented solely in the "1" direction produce a stiffer response in the "1" direction, compared to the "2" direction. In contrast, when there are two principle fibers directions oriented along the two principle shear directions, the response in the "1" direction is identical to that in the "2" direction (Figure 5.10c). As the two principle fiber angles rotate relative to each other, the responses in the "1" and "2" directions diverge (Figure 5.10b). Thus, by controlling the orientation of these fibers within the solid, we are able to control the mechanical response of the tissue sheet.

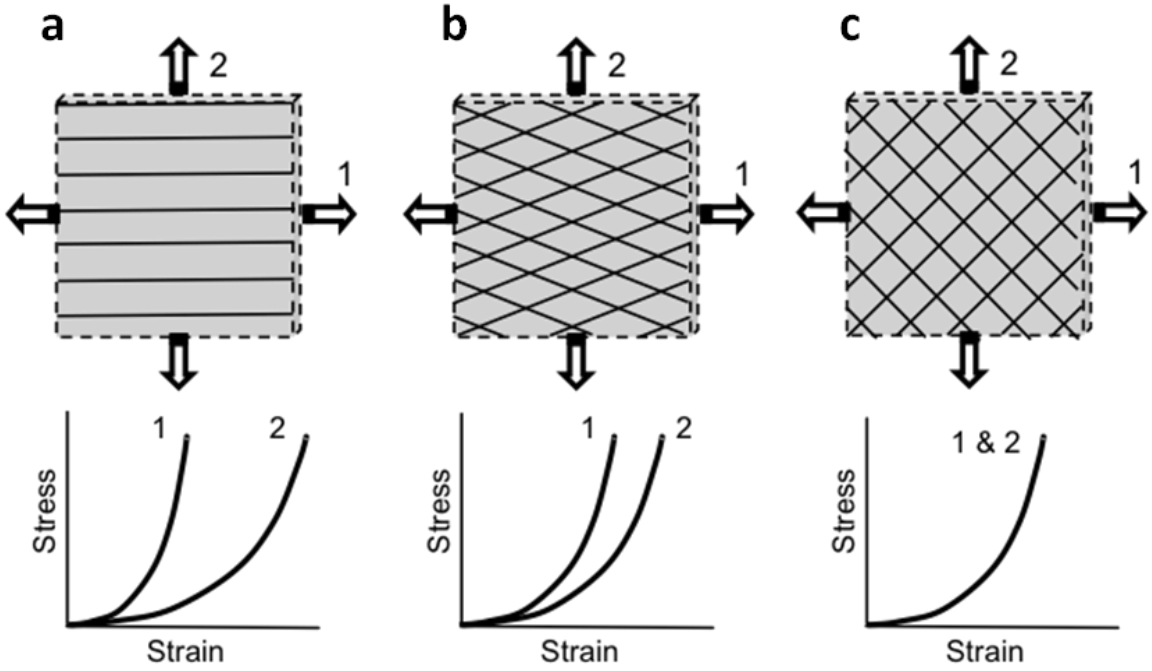

Figure 5.10. Illustration of the role of collagen fiber orientation in the biomechanical behavior of tissue sheets.

In addition to orientation of the fibers, undulation of the fibers within an amorphous solid affects the mechanical response. We know from studies of native tissue, that upon excision and mechanical unloading of the tissue, often collagen fibers are not straight or taut.[97] Changes in the degree of undulation in the unloaded state will affect the biomechanical response. For example, Figure 5.11a demonstrates that fibers oriented along the principle stretch direction and are straight in the unloaded state will have a stiffer response than a material where the fibers are undulating in the unloaded state (Figure 5.11b). This phenomena is a result of fiber engagement. While the fibers from Figure 5.11a are fully engaged from the onset of stretching and thus contribute to the mechanical integrity, the fibers from Figure 5.11b do not engage until a certain amount of

strain is applied; the specific amount required to engage the fibers depends on the degree of undulation in the unloaded state.

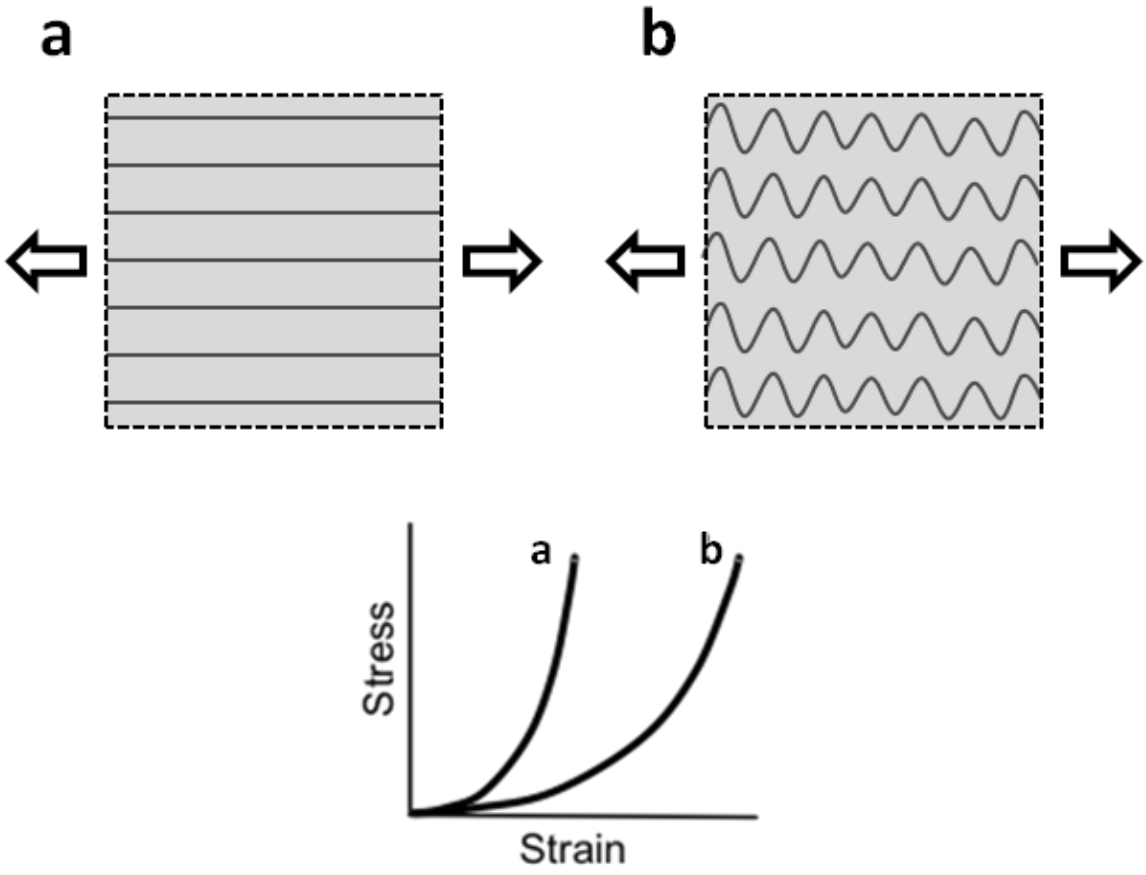

Figure 5.11. Qualitative illustration of the role of collagen fiber undulation in the role of mechanical response in tissue sheets.

It is the specific combination of fiber orientation, alignment and undulation that gives tissues their unique biomechanical response.

In the context of the self-assembly method, these tissue sheets are rolled into a tubular structure to make a SA-TEBV. In the mathematical modeling of a native artery with two distinct layers, the strain energy function of Holzapfel *et al*.[69] was split to account for different principle fiber angles and material properties between the media and adventitia. The specific combination of fiber angles and distributions between the layers influences the mechanical response of the artery. Therefore, we anticipate combining tissue sheets with different ECM organization (i.e., fiber angle, distribution and undulation), as well as different geometry and pre-strain, into SA-TEBVs one can control the mechanical properties to match target ranges of diameter, compliance, and transmural wall stresses. Thus we are able to 'tune' the mechanical response of the SA-TEBV to match that of the native healthy vasculature.

In summary, our *in vitro* culture of hDF subjected to biaxial mechanical stimulation has demonstrated that we are able to develop confluent cell sheets with a general off-axis alignment angle Taken with other studies that suggest ECM deposition follows cell orientation, we anticipate ECM fibers to also be aligned in this orientation. As the process of controlling the mechanical properties of SA-TEBV moves forward, similar experiments must be performed with SMCs to understand how they orient themselves under the influence of cyclic biaxial mechanical stimulation. Additionally, for both cell types individually and the co-culture, culture times must be extended to allow for ECM deposition and experimental quantification of ECM fiber alignment. While there is significantly more work to be performed before conclusively stating that control

of the biaxial mechanical properties of SA-TEBV using biaxial mechanical stimulation is possible, this paper is the first step towards achieving that goal.

CHAPTER VI

CONCLUSIONS AND FUTURE WORK

6.1 Summary

This thesis proposes a novel approach to studying the biaxial biomechanical properties of SA-TEBV, as well as understanding how biaxial mechanical stimulation can be used to manipulate the biaxial mechanical properties of mature SA-TEBV. Previous studies on the mechanical properties of SA-TEBV focused solely on single-axis properties (i.e. burst pressure, circumferential compliance, elastic modulus, ultimate tensile strength). However, once *in vivo*, these vessels will experience multiaxial loading (i.e. circumferential and axial distension, and flow induced shear). To better understand how SA-TEBV will response *in vivo*, biaxial mechanical characterization was performed. From this analysis, it was revealed that the mechanical response of the SA-TEBV did not match that of the native vasculature. Therefore, biaxial mechanical stimuli were also investigated as a means of controlling the mechanical properties of the SA-TEBV.

To accomplish these experimental goals, a custom bioreactor was designed and built with numerous capabilities and features:

- Perform long term culture of TEBV subjected to external mechanical stimulation
- Perform intermittent and end-point cylindrical biaxial mechanical testing
- Perform functional testing

- Perform confocal imaging of small diameter vascular tissue engineered grafts under various mechanical loads (i.e. pressure and axial stretch)
- Utilizes ultrasonic technologies to accurately measure wall thickness required for stress analysis
- Custom designed LABVIEW program controlling all accessories

Using the custom designed bioreactor, the biaxial biomechanical properties of the TEVA, TEVM and TEVMA were characterized and compared to that of a native coronary artery. Within this study, there were numerous significant contributions to the literature:

- The biomechanical response of the self-assembly tissue engineered constructs do not precisely match that of the native vasculature, but
- TEVMA displayed compliance on the same order of magnitude as native vessels when subjected to the same physiologic loads
- Material and structural properties in a 4-fiber constitutive model were identified for both the TEVA and TEVM
- A predictive mathematical model was development for the mechanical response of the TEVMA
- According to the constitutive model, the stress gradient across the vessel wall was significantly larger in the TEVMA than a native artery

The scope of this work fully characterized the mechanical properties of the single layer correlates as well as the bi-layer as they are currently produced.

The final portion of this research laid the groundwork for developing control over the mechanical properties of SA-TEBV. With the self-assembly approach, endogenously produced tissue sheets are rolled around a center mandrel to form a tubular vessel-like structure. Therefore, control over the microstructure of the tissue sheets will permit control over the mechanical response of the TEBV. Contributions from this study include:

- hDF subjected to cyclic uniaxial mechanical strain align themselves perpendicular to the principle stretch direction
- hDF subjected to cyclic biaxial mechanical strain has demonstrated that cells align at a general off-axis angle
- Significant differences in alignment index were seen in mechanically stimulated groups as compared to controls.

In summary, this body of work developed the tools for testing TEBV as well as establishing a baseline for comparison to future novel fabrication strategies and laying the groundwork for the next series of experiments.

6.2 Future Work

Based on the work presented in this thesis, there are a number of future directions for research. Studies with validated mathematical models have the advantage over experimental research in that individual parameters can be altered to understand how these individual components affect the overall function. In addition, the time and cost savings using mathematical models makes them significantly more valuable. With regard

to the characterization of material properties of the TEVM, TEVA and TEVMA (Aim 2), parametric mathematical studies can be performed to further understand how changes in vascular geometry (i.e. inner diameter, wall thickness and TEVM/TEVA ratio) will affect the biomechanical response of the TEVMA. In addition, changes in circumferential pre-stretch, which will influence the opening angle, can be performed to further understand how different combinations of opening angles between the TEVM and TEVA will influence the local stress gradient across the vascular wall. Lastly, different off-axis angles can be input into the constitutive model proposed in Chapter IV to understand how the fiber angle affects the tissue level biomechanical response.

With regard to the cell stretching experiments, the first obvious extension of this work would be to repeat the stretching experiments with hUSMCs or human vascular smooth muscle cells (hVSMC) to understand how SMCs align in response to biaxial stretching. Previous studies from literature have shown that SMCs also align perpendicular to the direction of principle stretch.[98-101] Therefore, it is reasonable to hypothesize that in response to biaxial stretching, SMCs would have a bimodal alignment distribution with the two peaks aligning along the principle shear directions. However, if the SMCs follow the same alignment pattern as hDFs, they may only align along one off-axis direction. Following the cell alignment studies, the culture times should be extended with supplemented (ascorbic acid) medium to permit formation of an endogenous ECM. Quantification of the ECM orientation must be performed as this is what dictates the biomechanical response of the formed tissue sheet and ultimately SA-TEBV. Previous studies indicate that the ECM will align along the same axes as the cells.[80, 82]

Beyond the single layer correlate studies, mechanical stretching of co-cultures should follow. The most recent technique for the development of TEVMA is to grow the hDF and hUSMC as a co-culture with distinct sections to permit better adhesion between TEVA and TEMV.[70] Therefore, if we wish to replicate this fabrication process in combination with mechanical stretching, a co-culture system will need to be developed. What remains to be seen is how the presence of the two cell type will influence the align properties of the individual cells.

While the information and knowledge of the biaxial stretching studies is important, the ultimate goal of this body of work is to create a functional, usable blood vessel suitable for implantation. Therefore, all of these tissue sheets will need to be rolled into TEBVs. This will first require a scaling-up of the equipment currently in use for cell stretching studies; thus a new bioreactor will need to be developed. Secondly while we have shown that we can induce off-axis alignment of cells, we have not achieved a bimodal distribution as is seen in native arteries.[91] One proposed solution to this is shown in Figure 6.1. We have shown it is possible to develop an off-axis alignment; therefore, if two tissue sheets overlaid with symmetric fiber alignment, we can achieve a bimodal distribution upon rolling. The resulting microstructure should provide a closer biomechanical response to the native vasculature.

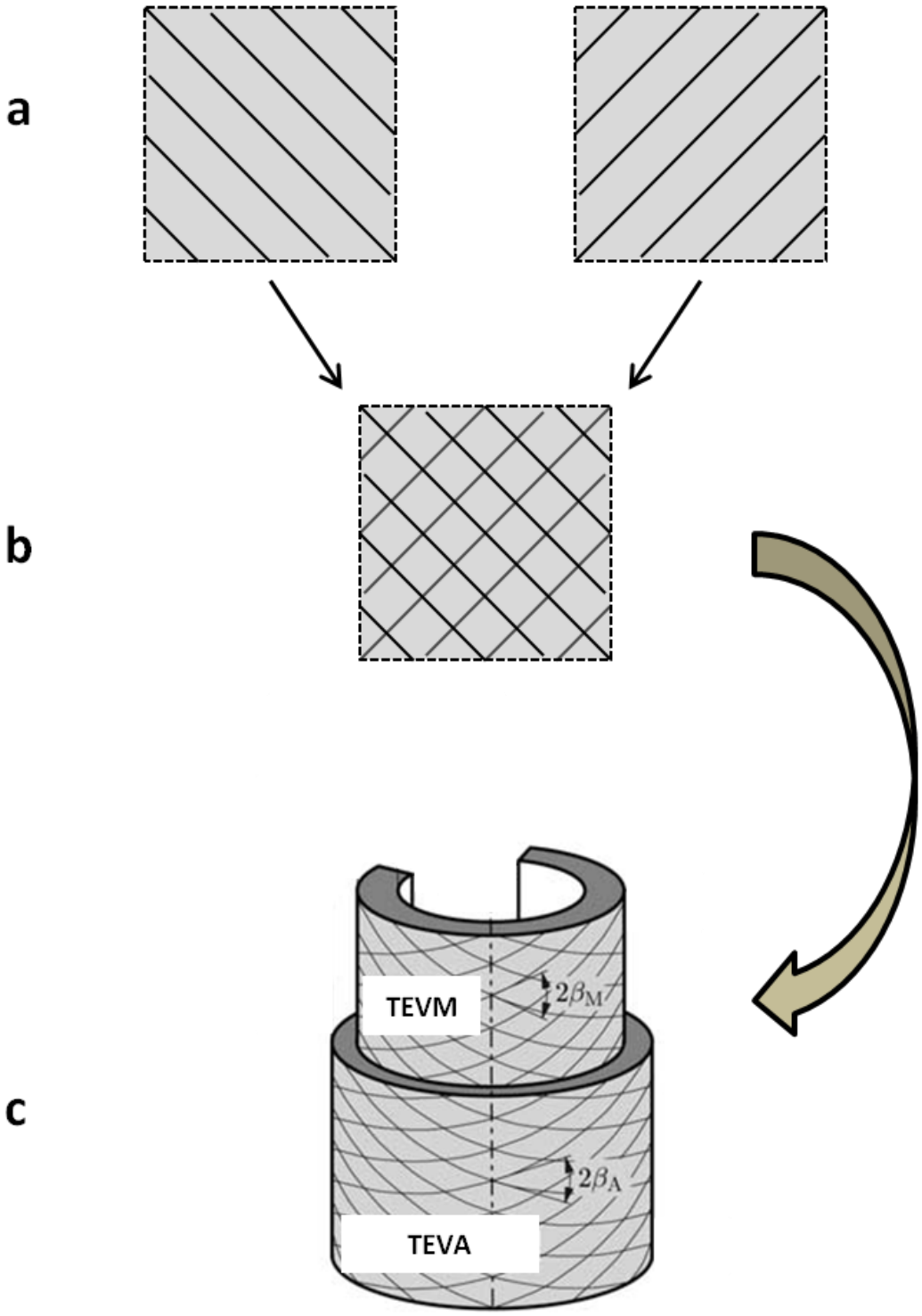

Figure 6.1. With the ability to develop tissue sheets with an off-axis fiber alignment (a) and overlapping them (b), it will be possible to achieve a bimodal fiber distribution once the sheets are rolled into a TEBV (c). ((c) adapted from [69])

REFERENCES

[1] Thom, T., Haase, N., Rosamond, W., Howard, V. J., Rumsfeld, J., Manolio, T., Zheng, Z. J., Flegal, K., O'Donnell, C., Kittner, S., Lloyd-Jones, D., Goff, D. C., Jr., Hong, Y., Adams, R., Friday, G., Furie, K., Gorelick, P., Kissela, B., Marler, J., Meigs, J., Roger, V., Sidney, S., Sorlie, P., Steinberger, J., Wasserthiel-Smoller, S., Wilson, M., and Wolf, P., 2006, "Heart disease and stroke statistics--2006 update: a report from the American Heart Association Statistics Committee and Stroke Statistics Subcommittee," Circulation, 113(6), pp. e85-151.

[2] Humphrey, J. D., 2002, Cardiovascular Solid Mechanics; Cells, Tissues, and Organs. Springer-Verlag New York, Inc. New York, NY.

[3] Laflamme, K., Roberge, C. J., Grenier, G., Remy-Zolghadri, M., Pouliot, S., Baker, K., Labbe, R., D'Orleans-Juste, P., Auger, F. A., and Germain, L., 2006, "Adventitia contribution in vascular tone: insights from adventitia-derived cells in a tissue-engineered human blood vessel," FASEB J, 20(8), pp. 1245-1247.

[4] Beranova, P., Schott, C., Chalupsky, K., Kleschyov, A. L., Stoclet, J. C., and Muller, B., 2005, "Role of the adventitia in the cyclic GMP-mediated relaxant effect of N-hydroxy-L-arginine in rat aorta," J Vasc Res, 42(4), pp. 331-336.

[5] Gonzalez, M. C., Arribas, S. M., Molero, F., and Fernandez-Alfonso, M. S., 2001, "Effect of removal of adventitia on vascular smooth muscle contraction and relaxation," Am J Physiol Heart Circ Physiol, 280(6), pp. H2876-2881.

[6] Rhodin, J., 1979, Architecture of the vessel wall. In: Handbook of Physiology, Section 2, Vol. 2. (RM Berne, ed.). American Physiology Society.

[7] Jackson, Z. S., Gotlieb, A. I., and Langille, B. L., 2002, "Wall tissue remodeling regulates longitudinal tension in arteries," Circ Res, 90(8), pp. 918-925.

[8] Walden, R., L'Italien, G. J., Megerman, J., and Abbott, W. M., 1980, "Matched Elastic Pproperties and Successful Arterial Grafting," Archives of Surgery, 115(10), pp. 1166-1169.

[9] Abbott, W. M., Megerman, J., Hasson, J. E., L'Italien, G., and Warnock, D. F., 1987, "Effect of Compliance Mismatch on Vascular Graft Patency," Journal of Vascular Surgery, 5(2), pp. 376-382.

[10] Bassiouny, H., White, S., Glagov, S., Choi, E., Giddens, D., and Zarins, C., 1992, "Anastomotic intimal hyperplasia: mechanical injury or flow induced," Journal of vascular surgery: official publication, the Society for Vascular Surgery [and]

International Society for Cardiovascular Surgery, North American Chapter, 15(4), p. 708.

[11] Trubel, W., Schima, H., Moritz, A., Raderer, F., Windisch, A., Ullrich, R., Windberger, U., Losert, U., and Polterauer, P., 1995, "Compliance mismatch and formation of distal anastomotic intimal hyperplasia in externally stiffened and lumen-adapted venous grafts," European Journal of Vascular & Endovascular Surgery, 10(4), pp. 415-423.

[12] Ballyk, P. D., Walsh, C., Butany, J., and Ojha, M., 1998, "Compliance mismatch may promote graft-artery intimal hyperplasia by altering suture-line stresses," Journal of Biomechanics, 31(3), pp. 229-237.

[13] Matsumoto, T., and Hayashi, K., 1996, "Stress and strain distribution in hypertensive and normotensive rat aorta considering residual strain," J Biomech Eng, 118(1), pp. 62-73.

[14] Isenberg, B. C., Williams, C., and Tranquillo, R. T., 2006, "Small-diameter artificial arteries engineered in vitro," Circ Res, 98(1), pp. 25-35.

[15] Nerem, R. M., and Seliktar, D., 2001, "Vascular tissue engineering," Annu Rev Biomed Eng, 3, pp. 225-243.

[16] Guilak, F., Butler, D. L., Goldstein, S. A., and Mooney, D. J., 2003, Functional tissue engineering, pp. 258-267. Springer, New York :.

[17] Weinberg, C. B., and Bell, E., 1986, "A blood vessel model constructed from collagen and cultured vascular cells," Science, 231(4736), pp. 397-400.

[18] L'Heureux, N., Dusserre, N., Konig, G., Victor, B., Keire, P., Wight, T. N., Chronos, N. A., Kyles, A. E., Gregory, C. R., Hoyt, G., Robbins, R. C., and McAllister, T. N., 2006, "Human tissue-engineered blood vessels for adult arterial revascularization," Nat Med, 12(3), pp. 361-365.

[19] Niklason, L. E., Gao, J., Abbott, W. M., Hirschi, K. K., Houser, S., Marini, R., and Langer, R., 1999, "Functional arteries grown in vitro," Science, 284(5413), pp. 489-493.

[20] Swartz, D. D., Russell, J. A., and Andreadis, S. T., 2005, "Engineering of fibrin-based functional and implantable small-diameter blood vessels," Am J Physiol Heart Circ Physiol, 288(3), pp. H1451-1460.

[21] Seliktar, D., Black, R. A., Vito, R. P., and Nerem, R. M., 2000, "Dynamic mechanical conditioning of collagen-gel blood vessel constructs induces remodeling in vitro," Ann Biomed Eng, 28(4), pp. 351-362.

[22] Seliktar, D., Nerem, R. M., and Galis, Z. S., 2001, "The role of matrix metalloproteinase-2 in the remodeling of cell-seeded vascular constructs subjected to cyclic strain," Ann Biomed Eng, 29(11), pp. 923-934.

[23] Boerboom, R. A., Rubbens, M. P., Driessen, N. J., Bouten, C. V., and Baaijens, F. P., 2008, "Effect of strain magnitude on the tissue properties of engineered cardiovascular constructs," Ann Biomed Eng, 36(2), pp. 244-253.

[24] Crapo, P. M., Gao, J., and Wang, Y., 2008, "Seamless tubular poly(glycerol sebacate) scaffolds: high-yield fabrication and potential applications," J Biomed Mater Res A, 86(2), pp. 354-363.

[25] Gao, J., Crapo, P. M., and Wang, Y., 2006, "Macroporous elastomeric scaffolds with extensive micropores for soft tissue engineering," Tissue Eng, 12(4), pp. 917-925.

[26] Sales, V. L., Engelmayr, G. C., Jr., Johnson, J. A., Jr., Gao, J., Wang, Y., Sacks, M. S., and Mayer, J. E., Jr., 2007, "Protein precoating of elastomeric tissue-engineering scaffolds increased cellularity, enhanced extracellular matrix protein production, and differentially regulated the phenotypes of circulating endothelial progenitor cells," Circulation, 116(11 Suppl), pp. I55-63.

[27] Liu, Y., Ji, Y., Ghosh, K., Clark, R. A., Huang, L., and Rafailovich, M. H., 2009, "Effects of fiber orientation and diameter on the behavior of human dermal fibroblasts on electrospun PMMA scaffolds," J Biomed Mater Res A, 90(4), pp. 1092-1106.

[28] Diebolt, M., Laflamme, K., Labbe, R., Auger, F. A., Germain, L., and Andriantsitohaina, R., 2007, "Polyphenols modulate calcium-independent mechanisms in human arterial tissue-engineered vascular media," J Vasc Surg, 46(4), pp. 764-772.

[29] Grenier, G., Remy-Zolghadri, M., Bergeron, F., Guignard, R., Baker, K., Labbe, R., Auger, F. A., and Germain, L., 2006, "Mechanical loading modulates the differentiation state of vascular smooth muscle cells," Tissue Eng, 12(11), pp. 3159-3170.

[30] Grenier, G., Remy-Zolghadri, M., Larouche, D., Gauvin, R., Baker, K., Bergeron, F., Dupuis, D., Langelier, E., Rancourt, D., Auger, F. A., and Germain, L., 2005, "Tissue reorganization in response to mechanical load increases functionality," Tissue Eng, 11(1-2), pp. 90-100.

[31] Laflamme, K., Roberge, C. J., Labonte, J., Pouliot, S., D'Orleans-Juste, P., Auger, F. A., and Germain, L., 2005, "Tissue-engineered human vascular media with a functional endothelin system," Circulation, 111(4), pp. 459-464.

[32] Laflamme, K., Roberge, C. J., Pouliot, S., D'Orleans-Juste, P., Auger, F. A., and Germain, L., 2006, "Tissue-engineered human vascular media produced in vitro by the self-assembly approach present functional properties similar to those of their native blood vessels," Tissue Eng, 12(8), pp. 2275-2281.

[33] L'Heureux, N., Paquet, S., Labbe, R., Germain, L., and Auger, F. A., 1998, "A completely biological tissue-engineered human blood vessel," FASEB J, 12(1), pp. 47-56.

[34] L'Heureux, N., Stoclet, J. C., Auger, F. A., Lagaud, G. J., Germain, L., and Andriantsitohaina, R., 2001, "A human tissue-engineered vascular media: a new model for pharmacological studies of contractile responses," FASEB J, 15(2), pp. 515-524.

[35] Auger, F. A., D'Orleans-Juste, P., and Germain, L., 2007, "Adventitia contribution to vascular contraction: hints provided by tissue-engineered substitutes," Cardiovasc Res, 75(4), pp. 669-678.

[36] Remy-Zolghadri, M., Laganiere, J., Oligny, J. F., Germain, L., and Auger, F. A., 2004, "Endothelium properties of a tissue-engineered blood vessel for small-diameter vascular reconstruction," J Vasc Surg, 39(3), pp. 613-620.

[37] Clark, J. M., and Glagov, S., 1979, "Structural integration of the arterial wall. I. Relationships and attachments of medial smooth muscle cells in normally distended and hyperdistended aortas," Lab Invest, 40(5), pp. 587-602.

[38] Han, H. C., Ku, D. N., and Vito, R. P., 2003, "Arterial wall adaptation under elevated longitudinal stretch in organ culture," Ann Biomed Eng, 31(4), pp. 403-411.

[39] Vorp, D. A., Peters, D. G., and Webster, M. W., 1999, "Gene expression is altered in perfused arterial segments exposed to cyclic flexure ex vivo," Ann Biomed Eng, 27(3), pp. 366-371.

[40] Clerin, V., Nichol, J. W., Petko, M., Myung, R. J., Gaynor, J. W., and Gooch, K. J., 2003, "Tissue engineering of arteries by directed remodeling of intact arterial segments," Tissue Eng, 9(3), pp. 461-472.

[41] Kamiya, A., and Togawa, T., 1980, "Adaptive regulation of wall shear stress to flow change in the canine carotid artery," Am J Physiol, 239(1), pp. H14-21.

[42] Ng, C. P., and Swartz, M. A., 2006, "Mechanisms of interstitial flow-induced remodeling of fibroblast-collagen cultures," Ann Biomed Eng, 34(3), pp. 446-454.

[43] Gleason, R. L., and Humphrey, J. D., 2005, "Effects of a sustained extension on arterial growth and remodeling: a theoretical study," J Biomech, 38(6), pp. 1255-1261.

[44] Gleason, R. L., Wilson, E., and Humphrey, J. D., 2007, "Biaxial biomechanical adaptations of mouse carotid arteries cultured at altered axial extension," J Biomech, 40(4), pp. 766-776.

[45] Engelmayr, G. C., Jr., Sales, V. L., Mayer, J. E., Jr., and Sacks, M. S., 2006, "Cyclic flexure and laminar flow synergistically accelerate mesenchymal stem cell-mediated engineered tissue formation: Implications for engineered heart valve tissues," Biomaterials, 27(36), pp. 6083-6095.

[46] Vunjak-Novakovic, G., and Kaplan, D. L., 2006, "Tissue engineering: the next generation," Tissue Eng, 12(12), pp. 3261-3263.

[47] Engelmayr, G. C., Jr., Soletti, L., Vigmostad, S. C., Budilarto, S. G., Federspiel, W. J., Chandran, K. B., Vorp, D. A., and Sacks, M. S., 2008, "A novel flex-stretch-flow bioreactor for the study of engineered heart valve tissue mechanobiology," Ann Biomed Eng, 36(5), pp. 700-712.

[48] Webb, A. R., Macrie, B. D., Ray, A. S., Russo, J. E., Siegel, A. M., Glucksberg, M. R., and Ameer, G. A., 2007, "In vitro characterization of a compliant biodegradable scaffold with a novel bioreactor system," Ann Biomed Eng, 35(8), pp. 1357-1367.

[49] Isenberg, B. C., and Tranquillo, R. T., 2003, "Long-term cyclic distention enhances the mechanical properties of collagen-based media-equivalents," Ann Biomed Eng, 31(8), pp. 937-949.

[50] Bilodeau, K., Couet, F., Boccafoschi, F., and Mantovani, D., 2005, "Design of a perfusion bioreactor specific to the regeneration of vascular tissues under mechanical stresses," Artif Organs, 29(11), pp. 906-912.

[51] Iwasaki, K., Kojima, K., Kodama, S., Paz, A. C., Chambers, M., Umezu, M., and Vacanti, C. A., 2008, "Bioengineered three-layered robust and elastic artery using hemodynamically-equivalent pulsatile bioreactor," Circulation, 118(14 Suppl), pp. S52-57.

[52] Vorp, D. A., Severyn, D. A., Steed, D. L., and Webster, M. W., 1996, "A device for the application of cyclic twist and extension on perfused vascular segments," Am J Physiol, 270(2 Pt 2), pp. H787-795.

[53] Gleason, R. L., Gray, S. P., Wilson, E., and Humphrey, J. D., 2004, "A multiaxial computer-controlled organ culture and biomechanical device for mouse carotid arteries," J Biomech Eng, 126(6), pp. 787-795.

[54] Stegemann, J. P., and Nerem, R. M., 2003, "Altered response of vascular smooth muscle cells to exogenous biochemical stimulation in two- and three-dimensional culture," Exp Cell Res, 283(2), pp. 146-155.

[55] Zoumi, A., Yeh, A., and Tromberg, B. J., 2002, "Imaging cells and extracellular matrix in vivo by using second-harmonic generation and two-photon excited fluorescence," Proceedings of the National Academy of Sciences of the United States of America, 99(17), pp. 11014-11019.

[56] Gowayed, Y., Schreibman, D. V., and Roberts, M., 1996, "Surface inspection of textile composite materials using image analysis techniques," Journal of Composites Technology & Research, 18(1), pp. 3-14.

[57] Chaudhuri, B. B., Kunda, P., and Sarkar, N., 1993, "Detection and gradation of oriented texture," Pattern Recognition Letters, 14, pp. 147-153.

[58] Courtney, T., Sacks, M. S., Stankus, J., Guan, J., and Wagner, W. R., 2006, "Design and analysis of tissue engineering scaffolds that mimic soft tissue mechanical anisotropy," Biomaterials, 27(19), pp. 3631-3638.

[59] Karlon, W. J., Covell, J. W., McCulloch, A. D., Hunter, J. J., and Omens, J. H., 1998, "Automated measurement of myofiber disarray in transgenic mice with ventricular expression of ras," Anat Rec, 252(4), pp. 612-625.

[60] Lee, C. H., Shin, H. J., Cho, I. H., Kang, Y. M., Kim, I. A., Park, K. D., and Shin, J. W., 2005, "Nanofiber alignment and direction of mechanical strain affect the ECM production of human ACL fibroblast," Biomaterials, 26(11), pp. 1261-1270.

[61] Sacks, M. S., 2003, "Incorporation of experimentally-derived fiber orientation into a structural constitutive model for planar collagenous tissues," J Biomech Eng, 125(2), pp. 280-287.

[62] Chuong, C. J., and Fung, Y. C., 1986, "On residual stresses in arteries," J Biomech Eng, 108(2), pp. 189-192.

[63] McCulloch, A. D., Harris, A. B., Sarraf, C. E., and Eastwood, M., 2004, "New multi-cue bioreactor for tissue engineering of tubular cardiovascular samples under physiological conditions," Tissue Eng, 10(3-4), pp. 565-573.

[64] Matsumoto, T., Okumura, E., Miura, Y., and Sato, M., 1999, "Mechanical and dimensional adaptation of rabbit carotid artery cultured in vitro," Med Biol Eng Comput, 37(2), pp. 252-256.

[65] Wagenseil, J. E., Elson, E. L., and Okamoto, R. J., 2004, "Cell orientation influences the biaxial mechanical properties of fibroblast populated collagen vessels," Ann Biomed Eng, 32(5), pp. 720-731.

[66] Zaucha, M. T., Raykin, J., Wan, W., Gauvin, R., Auger, F. A., Germain, L., Michaels, T. E., and Gleason, R., 2009, "A novel cylindrical biaxial computer controlled bioreactor and biomechanical testing device for vascular tissue engineering," Tissue Eng Part A.

[67] Baek, S., Gleason, R. L., Rajagopal, K. R., and Humphrey, J. D., 2007, "Theory of small on large: Potential utility in computations of fluid-solid interactions in arteries," Computer Methods in Applied Mechanics and Engineering, 196(31-32), pp. 3070-3078.

[68] Rachev, A., 1997, "Theoretical study of the effect of stress-dependent remodeling on arterial geometry under hypertensive conditions," J Biomech, 30(8), pp. 819-827.

[69] Holzapfel, G. A., Gasser, T. C., and Ogden, R. W., 2000, "A new constitutive framework for arterial wall mechanics and a comparative study of material models," Journal of Elasticity, 61, pp. 1-48.

[70] Gauvin, R., Ahsan, T., Larouche, D., Levesque, P., Dube, J., Auger, F. A., Nerem, R. M., and Germain, L., 2010, "A novel single-step self-assembly approach for the fabrication of tissue-engineered vascular constructs," Tissue Eng Part A, 16(5), pp. 1737-1747.

[71] Holzapfel, G. A., Sommer, G., Auer, M., Regitnig, P., and Ogden, R. W., 2007, "Layer-specific 3D residual deformations of human aortas with non-atherosclerotic intimal thickening," Ann Biomed Eng, 35(4), pp. 530-545.

[72] Gow, B. S., Schonfeld, D., and Patel, D. J., 1974, "The dynamic elastic properties of the canine left circumflex coronary artery," J Biomech, 7(5), pp. 389-395.

[73] Gow, B. S., and Hadfield, C. D., 1979, "The elasticity of canine and human coronary arteries with reference to postmortem changes," Circ Res, 45(5), pp. 588-594.

[74] Hayashi, K., Igarashi, Y., and Takamizawa, K., 1986, New Approaches in Cardiac Mechanics, (ed. Kazuo) pp. 285-294. Taylor & Francis, US.

[75] Purinia, B. A., and Kas'ianov, V. A., 1977, "[Biomechanical porperties of the human coronary arteries]," Kardiologiia, 17(11), pp. 108-111.

[76] Asanuma, K., Magid, R., Johnson, C., Nerem, R. M., and Galis, Z. S., 2003, "Uniaxial strain upregulates matrix-degrading enzymes produced by human vascular smooth muscle cells," Am J Physiol Heart Circ Physiol, 284(5), pp. H1778-1784.

[77] Konig, G., McAllister, T. N., Dusserre, N., Garrido, S. A., Iyican, C., Marini, A., Fiorillo, A., Avila, H., Wystrychowski, W., Zagalski, K., Maruszewski, M., Jones, A. L., Cierpka, L., de la Fuente, L. M., and L'Heureux, N., 2009, "Mechanical properties of completely autologous human tissue engineered blood vessels compared to human saphenous vein and mammary artery," Biomaterials, 30(8), pp. 1542-1550.

[78] Gilbert, T. W., Wognum, S., Joyce, E. M., Freytes, D. O., Sacks, M. S., and Badylak, S. F., 2008, "Collagen fiber alignment and biaxial mechanical behavior of porcine urinary bladder derived extracellular matrix," Biomaterials, 29(36), pp. 4775-4782.

[79] Liao, J., Yang, L., Grashow, J., and Sacks, M. S., 2005, "Molecular orientation of collagen in intact planar connective tissues under biaxial stretch," Acta Biomater, 1(1), pp. 45-54.

[80] Guillemette, M. D., Cui, B., Roy, E., Gauvin, R., Giasson, C. J., Esch, M. B., Carrier, P., Deschambeault, A., Dumoulin, M., Toner, M., Germain, L., Veres, T., and Auger, F. A., 2009, "Surface topography induces 3D self-orientation of cells and extracellular matrix resulting in improved tissue function," Integr Biol (Camb), 1(2), pp. 196-204.

[81] Zaucha, M. T., Gauvin, R., Auger, F. A., Germain, L., and Gleason, R. L., 2011, "Biaxial biomechanical properties of self-assembly tissue-engineered blood vessels," J R Soc Interface, 8(55), pp. 244-256.

[82] Wang, J. H., Jia, F., Gilbert, T. W., and Woo, S. L., 2003, "Cell orientation determines the alignment of cell-produced collagenous matrix," J Biomech, 36(1), pp. 97-102.

[83] Boccafoschi, F., Bosetti, M., Gatti, S., and Cannas, M., 2007, "Dynamic fibroblast cultures: response to mechanical stretching," Cell Adh Migr, 1(3), pp. 124-128.

[84] Yost, M. J., Simpson, D., Wrona, K., Ridley, S., Ploehn, H. J., Borg, T. K., and Terracio, L., 2000, "Design and construction of a uniaxial cell stretcher," Am J Physiol Heart Circ Physiol, 279(6), pp. H3124-3130.

[85] Carver, W., Nagpal, M. L., Nachtigal, M., Borg, T. K., and Terracio, L., 1991, "Collagen expression in mechanically stimulated cardiac fibroblasts," Circ Res, 69(1), pp. 116-122.

[86] Carano, A., and Siciliani, G., 1996, "Effects of continuous and intermittent forces on human fibroblasts in vitro," Eur J Orthod, 18(1), pp. 19-26.

[87] Jungbauer, S., Gao, H., Spatz, J. P., and Kemkemer, R., 2008, "Two characteristic regimes in frequency-dependent dynamic reorientation of fibroblasts on cyclically stretched substrates," Biophys J, 95(7), pp. 3470-3478.

[88] Zaucha, M. T., Raykin, J., Wan, W., Gauvin, R., Auger, F. A., Germain, L., Michaels, T. E., and Gleason, R. L., Jr., 2009, "A novel cylindrical biaxial computer-controlled bioreactor and biomechanical testing device for vascular tissue engineering," Tissue Eng Part A, 15(11), pp. 3331-3340.

[89] Ng, C. P., Hinz, B., and Swartz, M. A., 2005, "Interstitial fluid flow induces myofibroblast differentiation and collagen alignment in vitro," J Cell Sci, 118(Pt 20), pp. 4731-4739.

[90] Timmins, L. H., Wu, Q., Yeh, A. T., Moore, J. E., Jr., and Greenwald, S. E., 2010, "Structural inhomogeneity and fiber orientation in the inner arterial media," Am J Physiol Heart Circ Physiol, 298(5), pp. H1537-1545.

[91] Holzapfel, G. A., 2003, Structural and Numerical Models for the (Visco)elastic Response of Arterial Walls with Residual Stresses, Springer, Wien, New York.

[92] Rubbens, M. P., Driessen-Mol, A., Boerboom, R. A., Koppert, M. M., van Assen, H. C., TerHaar Romeny, B. M., Baaijens, F. P., and Bouten, C. V., 2009, "Quantification of the temporal evolution of collagen orientation in mechanically conditioned engineered cardiovascular tissues," Ann Biomed Eng, 37(7), pp. 1263-1272.

[93] den Braber, E. T., de Ruijter, J. E., Ginsel, L. A., von Recum, A. F., and Jansen, J. A., 1998, "Orientation of ECM protein deposition, fibroblast cytoskeleton, and attachment complex components on silicone microgrooved surfaces," J Biomed Mater Res, 40(2), pp. 291-300.

[94] Holzapfel, G. A., Sommer, G., Gasser, C. T., and Regitnig, P., 2005, "Determination of layer-specific mechanical properties of human coronary arteries with nonatherosclerotic intimal thickening and related constitutive modeling," Am J Physiol Heart Circ Physiol, 289(5), pp. H2048-2058.

[95] Sacks, M. S., and Sun, W., 2003, "Multiaxial mechanical behavior of biological materials," Annu Rev Biomed Eng, 5, pp. 251-284.

[96] Wicker, B. K., Hutchens, H. P., Wu, Q., Yeh, A. T., and Humphrey, J. D., 2008, "Normal basilar artery structure and biaxial mechanical behaviour," Comput Methods Biomech Biomed Engin, 11(5), pp. 539-551.

[97] Wan, W., Yanagisawa, H., and Gleason, R. L., Jr., "Biomechanical and microstructural properties of common carotid arteries from fibulin-5 null mice," Ann Biomed Eng, 38(12), pp. 3605-3617.

[98] Houtchens, G. R., Foster, M. D., Desai, T. A., Morgan, E. F., and Wong, J. Y., 2008, "Combined effects of microtopography and cyclic strain on vascular smooth muscle cell orientation," J Biomech, 41(4), pp. 762-769.

[99] Kim, B. S., Nikolovski, J., Bonadio, J., and Mooney, D. J., 1999, "Cyclic mechanical strain regulates the development of engineered smooth muscle tissue," Nat Biotechnol, 17(10), pp. 979-983.

[100] Liu, B., Qu, M. J., Qin, K. R., Li, H., Li, Z. K., Shen, B. R., and Jiang, Z. L., 2008, "Role of cyclic strain frequency in regulating the alignment of vascular smooth muscle cells in vitro," Biophys J, 94(4), pp. 1497-1507.

[101] Standley, P. R., Cammarata, A., Nolan, B. P., Purgason, C. T., and Stanley, M. A., 2002, "Cyclic stretch induces vascular smooth muscle cell alignment via NO signaling," Am J Physiol Heart Circ Physiol, 283(5), pp. H1907-1914.